Conductivity Structure of the Weathered Zone at Number Four Tank, Cobar, NSW

Mark Tingay, B.Sc.

This thesis is submitted as partial fulfilment of the
Honours Degree of Bachelor of Science in Geophysics

November 1998

The University of Adelaide
Department of Geology and Geophysics

Abstract

The Number Four Tank region, near Cobar in central New South Wales, is covered by a deep, conductive weathered zone. Schlumberger vertical electric soundings, in-loop SIROTEM soundings and dipole-dipole resistivity show an approximately layered earth conductivity structure over most of the region. The conductive weathered zone can be simplified as one layer of approximately 70 metres thickness and a resistivity of 25 Ohm-m. The Schlumberger soundings also reveal a 3.3 metre thick layer of resistive alluvium overlying the weathered zone.

A weathering trough is located at the base of the conductive weathered zone. Dipole-dipole resistivity was inverted to reveal a 100 metre wide weathering trough with an underlying 150 metre wide conductive zone. In-loop SIROTEM soundings detected the deep conductor, which strikes approximately north-south. Stripping and decay curve analysis reveal a less than 200 metre wide conductor with a 0.45 millisecond decay constant.

Table of Contents

1.0 Introduction

The Cobar Basin in central New South Wales, is one of the oldest mining areas in Australia and currently has three mines still operating. The Number Four Tank region is located 55 kilometres north-northwest of the Cobar township (figure 1).

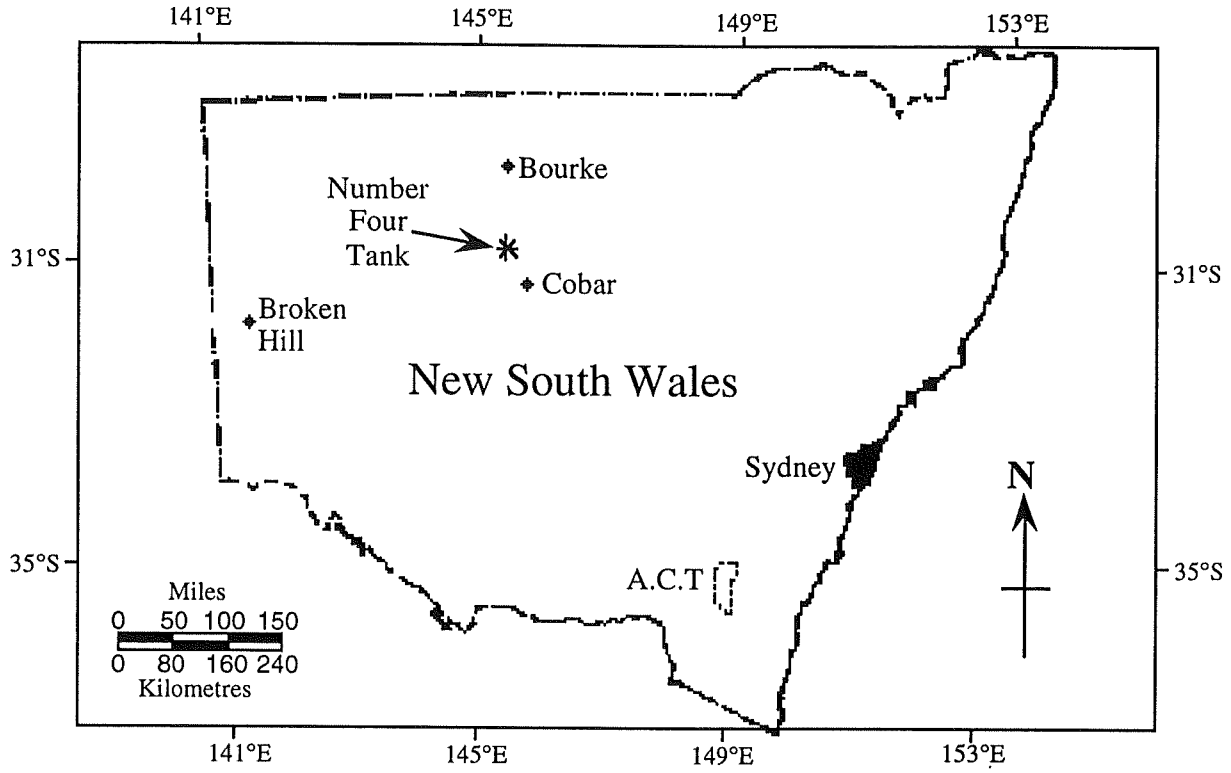

Figure 1: Locality Plan of the Elura Deposit

The Cobar region is thought to be highly prospective for lead, zinc, copper or gold orebodies, but exploration by both geological, geochemical and geophysical methods is hampered by the presence of a deep weathered zone, or overburden, overlying the fresh rock.

The aim of my research is to investigate the geophysical effects of the deeply weathered zone, and to recommend acquisition, processing and interpretation techniques for geophysical exploration of the Cobar Basin.

The method for my research is to perform and interpret various geophysical techniques in an area known to have bedrock topography, and which also contains a line of drill holes down to fresh rock. The collected data will be interpreted using as many techniques as possible, and will then be compared with the drill hole data. The interpretation will focus on determining the conductivity structure of the weathered zone and the depth to fresh rock.

The Cobar region is a relatively flat peneplain environment. Cobar has a semi-arid climate, and has been continuously weathering since the early Miocene, at least 23.5 Ma (Emerson, 1980). Consequently the region exhibits one of the world's best examples of arid weathering profiles.

A schematic drawing of a typical Cobar weathering profile is seen in figure 2 (Smith and Pridmore, 1989). The top of the profile is a thin layer of transported material, usually 2-4 metres thick, but up to 10 metres deep in palaeochannels. The weathered zone underlies the

alluvium down to depths of up to 100 metres. Oxidation has completely weathered the rock, which consists of a porous quartz-kaolin-sericite rock containing very saline ground water.

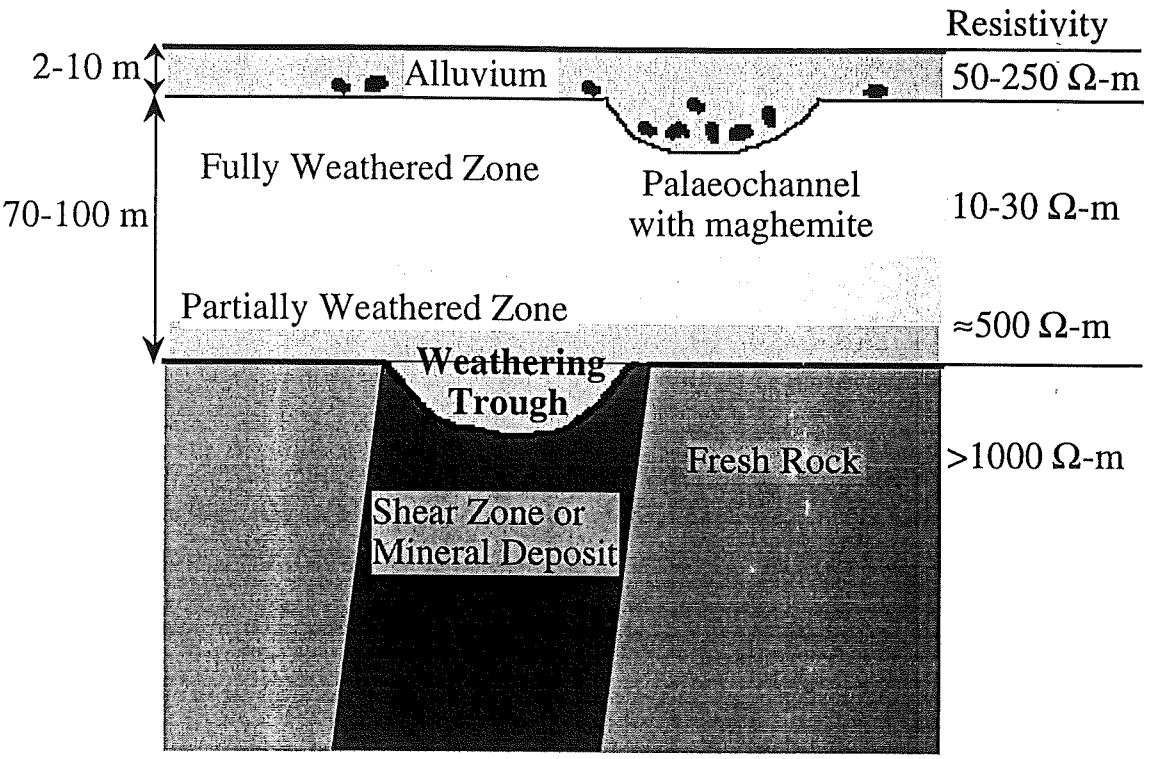

Figure 2: A Typical arid weathering profile with resistivities of the Cobar basin (adapted from Smith and Pridmore, 1989).

The physical properties of the weathered zone cause difficulties for all of the widely used geophysical exploration techniques. The overburden has highly variable depth and density, with low densities generally between 1.8 to 2.3 g/cc. This can cause deeper gravity anomalies to be masked or reduced, and makes gravity corrections difficult (Smith and Pridmore, 1989).

Maghemite, a magnetic lag which forms in the near surface pisolith zone, is abundant in the Cobar region. Ground magnetic surveys in the area are hindered by noise spikes of several thousand nanoteslas caused by the maghemite. The maghemite becomes concentrated in drainage channels which yield high frequency responses on aeromagnetic images, making underlying features harder to interpret. Maghemite is also super-paramagnetic (SPM) which may result in a t^{-1} decay on co-incident loop electromagnetic (EM) surveys (Lee, 1984).

The weathered zone is electrically conductive due to the saline ground water within its pore spaces. Typical resistivities within the Cobar basin are listed alongside figure 2. The completely weathered zone has a resistivity of 10-30 Ohm-m, which grades up to 500 Ohm-m for partially weathered rock and up to around 1500 Ohm-m for fresh (unweathered) Devonian CSA siltstone (Emerson, 1980). The gradational zone from fully weathered to fresh rock is typically 12 to 36 metres thick.

Typical frequency domain electrical and electromagnetic techniques become swamped by the response of the overburden, and so cannot be used in deeply weathered environments (Nabighian, 1991; Lowrie and West, 1965). Time Domain techniques have been fairly

successful in conductive terrains, but require large, powerful transmitters and are also hampered by the overburden response (McNeill, 1995; Emerson, 1980).

For electrical methods, current will preferentially flow within the conductive weathered zone and shy away from the resistive fresh rock. Because very little current flows through the fresh rock, the depth of penetration into the fresh rock is reduced (Smith and Pridmore, 1989).

The weathered zone acts as a quasi low pass filter for transient electromagnetic (TEM) techniques. Not only does the overburden have its own response, but it will also broaden, delay and attenuate the primary magnetic field leaving the transmitter, and then filter the secondary magnetic field from a deep conductive body (McNeill, 1995). A conductive overburden can also allow current channelling within targets which are in galvanic contact with the overburden, and also within any conductivity variations in the weathered zone (McNeill, 1985). Galvanic responses can contribute markedly to the geologic noise on TEM surveys.

It is hoped that a further understanding of the geophysical effects of the weathered zone will help in determining processing and acquisition methods to better penetrate the underlying fresh rock in the Cobar basin.

2.0 Regional Geology

Number Four Tank is located in the northern part of the Cobar Basin. All of the mineralisation in the Cobar Basin is hosted by the Cobar Supergroup. The Cobar Supergroup was deposited in the Early Devonian (Emerson, 1980). The Cobar Supergroup consists of shallow marine shelf deposits and deeper turbidity sequences (Schmidt, 1990). Table 1 describes the stratigraphic section for the Cobar basin.

Underlying the weathered zone at Number Four Tank is the CSA siltstone. The CSA siltstone is a member of the Amphitheatre Group, one of four groups in the Cobar Supergroup. The CSA siltstone is a monotonous turbidity sequence of graded siltstones and shales which have been tightly folded. The CSA siltstone consists mainly of quartz and muscovite, with chlorite, albite, carbonate and accessory pyrite (Emerson, 1980).

Rock Unit	Environmernt and Provenance	Age
Mulga Downs Group	Fluviatile; easterly, later westerly provenance	late Early Devonian to Early Carboniferous
	Paraconformity	
Cobar Supergroup		
Winduck Group	Shallow marine shelf deposits	middle Early Devonian
Amphitheatre Group (includes CSA Siltstone)	Turbiditic sequence and minor volcanics; western provenance	Early Devonian
Kopyje Group (Shelf equivilant of Nurri and Amphitheatre Group)	Shallow marine Shelf deposits; some volcanics	
Nurri Group (includes Great Cobar Slate)	Upward fining turbiditic sequence; easterly provenance	
	Unconformity	
Girilambone Group (includes Ballast beds)	Turbiditic; low to medium grade regional metamorphism	Cambro-Ordovician

Table 1: Simplified stratigraphic section of the Cobar basin (adapted from Schmidt, 1990).

There is very little outcrop in the area. The CSA siltstone has been deeply weathered by oxidisation, generally to depths of between 70 and 100 metres. The weathering profile is a typical arid, lateritic profile (figure 2).

The water table stands above the impermeable CSA siltstone at between 80 and 110 metres depth. The ground water is highly saline, having 1.9% dissolved salts, and a resistivity of 0.32 Ohm-m. The weathered rock above the water table has not been desiccated, and contains enough moisture to conduct electricity (Emerson, 1980). Table 2 contains the petrophysical data for the fully weathered, partially weathered and fresh CSA siltstone.

Physical Property	Fully Weathered Rock	Slightly Weathered Rock	Fresh CSA Siltstone
Lithology	quartz kaolin sericite rock	quartz muscovite siltstone	quartz muscovite siltstone
Porosity %, Total (effective)	12 (7)	2 (0.3)	<1
Dry Bulk Density (g/cc)	1.8 - 2.3	2.7	2.75
Water Saturation, S_w%	50+	100	100
Resistivity (Ohm-m)	10-30	500±	1500±
Percent Frequency Effect (IP)	very small	minor	minor
Magnetic Susceptibility, cgs×10^6	20	30	30
Koenigsberger Ratio, Q_n	0.1	0.1	0.1
Velocity, V_P, m/sec	1200 - 1400	5000	5500

Table 2: Typical physical properties of rocks in the Cobar Basin (adapted from Emerson, 1980).

3.0 Number Four Tank Region

A small geochemical copper anomaly is located within the Number Four Tank Region. The geophysical survey was performed to investigate the copper geochemical anomaly, which has been partially constrained by RAB drilling. Geochemical lag and auger sampling has identified an area of anomalous copper in the soil overlying the survey area. This was followed with a line of five RAB drill holes down to fresh rock. The fresh CSA siltstone was encountered at depths of between 70 and 86 metres on four of the drill holes. One drill hole (NFR 469) reached 105 metres depth without encountering fresh rock (figure 3).

The drilling results indicate a weathering trough at least 30 metres deep and 75 metres across and striking roughly north-south. Further geochemical analysis indicated high copper amounts, up to 925 ppm, in the weathered material within the trough.

COMBINED SECTION

Figure 3: Cross section of RAB holes over the Number Four Tank Survey.
Inferred depth to fresh rock is shown by dashed line.

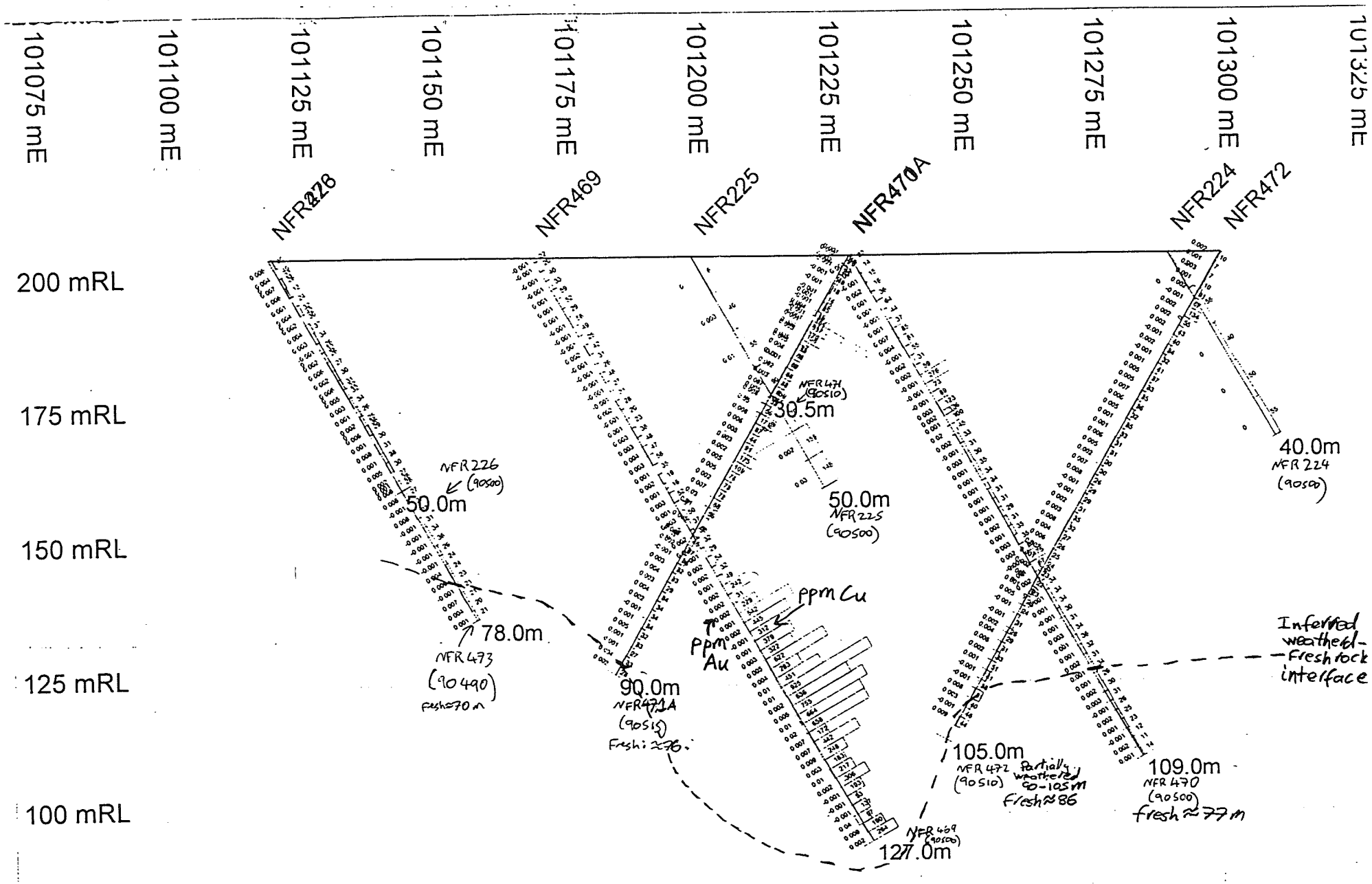

4.0 Acquisition

The geophysical survey (referred to as the 1998 survey) consisted of three one kilometre long east-west lines spaced 250 metres apart (figure 4). Drilling located the trough at 1225E (101225E on the Cobar grid) on the central line (90500N). The acquired data is summarised in table 3. A brief explanation of electrical and electromagnetic methods is given in Appendix 1.

The survey methodology used in the 1998 survey was not ideal for determining a detailed conductivity structure of the weathered zone. The research aims to determine the geophysical effects of the weathered zone for mineral exploration, hence typical mineral exploration survey designs were used. Mineral deposits would be situated within the fresh rock, hence the survey was designed for maximum depth penetration. The conductivity structure and bedrock topography could be better interpreted using smaller loops and dipoles, as well as collecting more early time channels.

Method	Instrument	Tx Size	Rx Size	Station Spacing	Other Information
Electromagnetics	SIROTEM MkIII	10000 m^2	10000 m^2	50m	In-loop geometry, avoids SPM effect. 26 channels. X & Z Component.
Dipole-Dipole IP/resistivity	Scintrex TSQ-4 & IPR-12	100m dipole	100m dipole	100m	On central line only. 1.5Km long line, measured to n=6.
Vertical Electric Soundings	Scintrex TSQ-4 & IPR-12	logarithmically expanding	0.5m or 1.5m	-	Done at 1200E and 1500E on central line.
Gravity	LaCoste & Romburg	-	-	50m and 25m	Elevation surveyed at ± 3.5 mm average error.

Table 3: Summary of acquired data.

4.1 Transient Electromagnetics

(i) Composite time channels gives 26 readings out to 20 milliseconds.
(ii) SATX transmitter system was not used due to synchronisation problems.
(iii) 100 metres square transmitter loop for greater depth of penetration.
(iv) Roving Vector Receiver (RVR) with same effective area as Transmitter loop.
(v) RVR positions 50m north of lines, done to keep Tx loop square.

4.2 Resistivity and Induced Polarisation

(i) 100m dipoles used for better depth penetration.
(ii) Data collected down to n=6 (figure 5), required 1.5 kilometre line.

4.3 Schlumberger Vertical Electric Soundings

(i) Current electrode spacings increase logarithmically in east-west direction.
(ii) Current electrode spacings: 1.5, 2.5, 4.0, 6.5, 10.0, 15, 25, 40, 65, 100, 150, 250 and 400 metres (figure 6). Total of 13 electrode positions, or two and a half decades, per sounding.

Figure 4: Number Four Tank Geophysical Survey

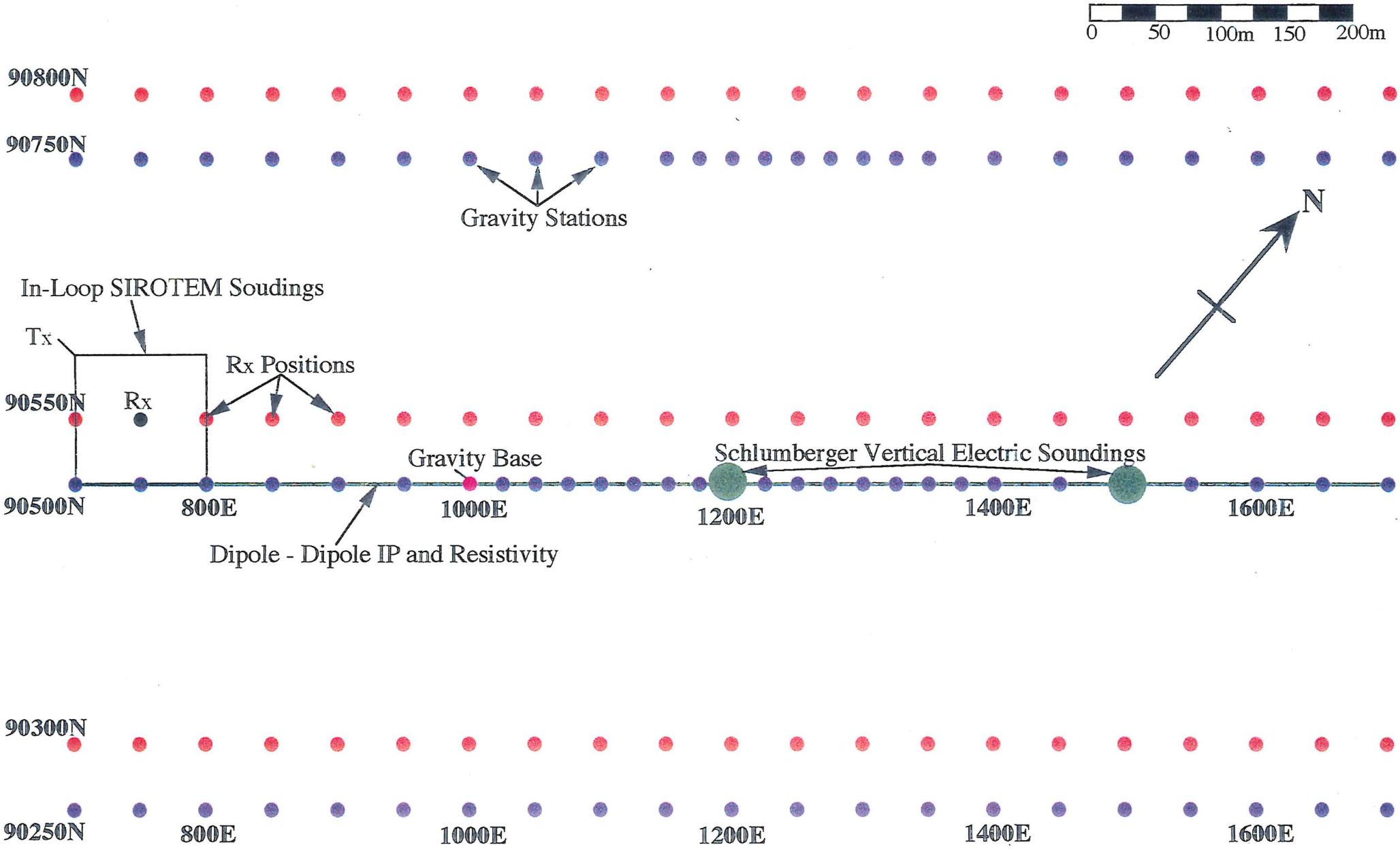

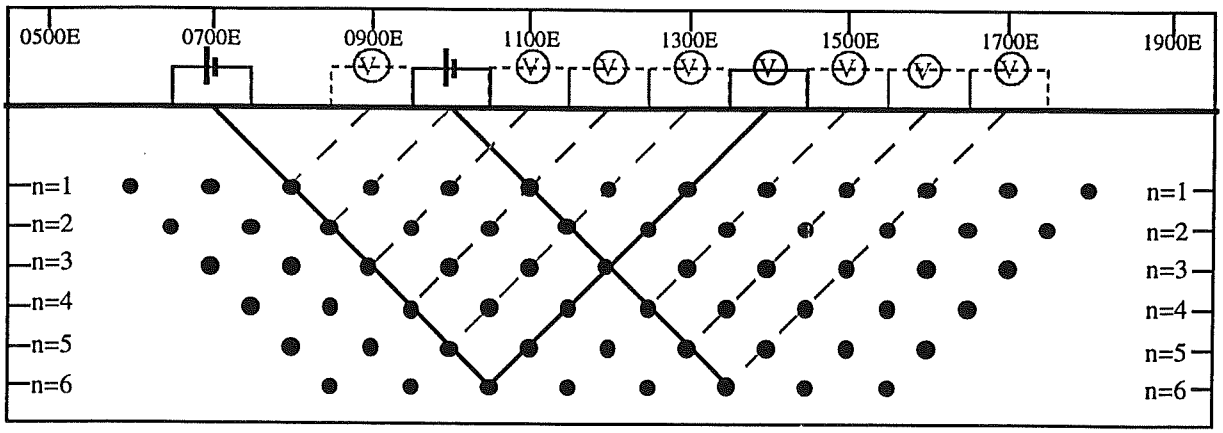

Figure 5: Pseudosection view of dipole-dipole IP and resistivity survey performed on line 90500N.

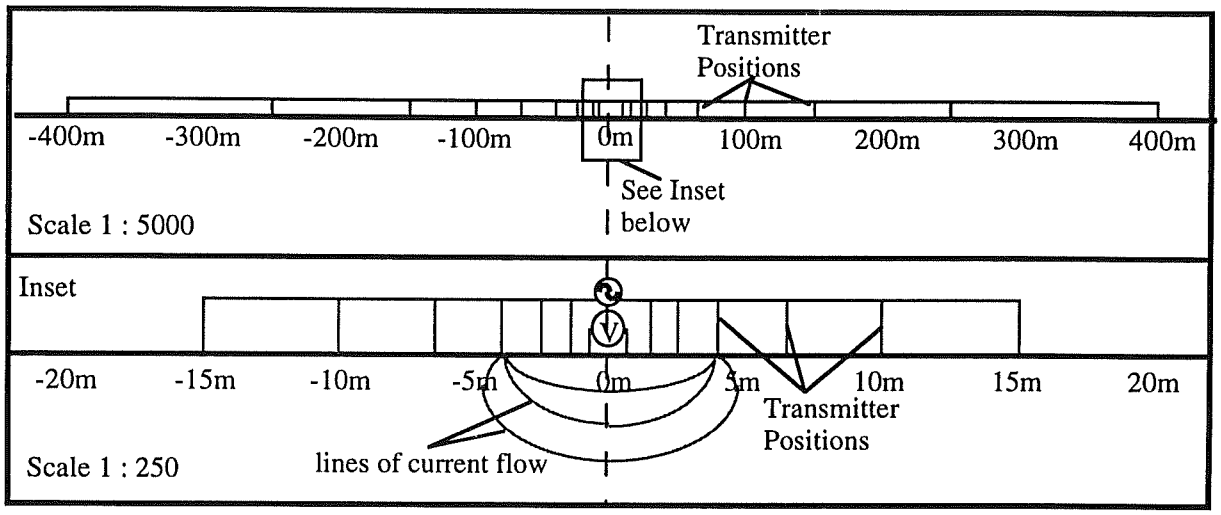

Figure 6: Cross-sectional plan of Schlumberger vertical electric sounding transmitter positions. Inset shows lines of current flow between the 4.0 metre transmitters.

4.4 Gravity

(i) 50m station spacing, reduced to 25m on parts of the central and northern lines to investigate anomalous EM responses.

(ii) Elevations were surveyed by theodolite and staff, 3.5mm average error per station.

4.5 Previously Collected Data

Regional gravity, collected at 100m station spacing and 250m line spacing was supplied over the whole area. This data was used to remove the strong East-West gradient which is of the order of 10 gu per kilometre.

An aeromagnetic survey has also been flown over the region at a line spacing of 150 metres and a flight height of 60 metres.

The RAB hole NFR 470 (figure 3) was recently logged with gamma ray, magnetic susceptibility, apparent conductivity and density logs. The data is collected at 10 centimetre intervals down the hole.

5.0 Forward Modelling

All techniques used at Number Four Tank were designed from research into other surveys in similar environments, and where possible forward modelling was used to test the effectiveness of each method.

5.1 Transient Electromagnetics

Forward modelling of TEM was done using the program ***SAMAYA***, which is a three dimensional finite element modelling program. The ***SAMAYA*** model comprised of an eighty metre thick weathered zone of twenty Ohm-m, overlying a 1500 Ohm-m halfspace. The trough was simulated with a rectangular prism, the top of which was located at the base of the overburden. The dimensions of the trough were 150m wide, 300m long and 40m deep.

The results of ***SAMAYA*** modelling showed that the trough would exhibit a very small vertical component response. The vertical component response is only visible when the channels are examined individually (figure 7). ***SAMAYA*** showed that the X-component should have a larger dynamic range, and a cross-over from positive to negative when moving from west to east (figure 8). Previous surveys in the area have shown that bedrock topography is visible in vertical component TEM surveys (Emerson, 1980), which leads to suspicion about the validity of ***SAMAYA*** modelling.

5.2 Resistivity and Induced Polarisation

Modelling of dipole-dipole resistivity was performed using the 2D modelling program ***RESIX-IP2D***, with the same model used in the TEM modelling. Modelling showed that the trough should be detected using a 100m dipole resistivity survey. Modelling also showed that there would be no IP response, due to the low chargeabilities of all the rock types in the area.

5.3 Gravity

Gravity modelling using the program ***POTENT*** suggests that there would be very little response over a weathering trough, possibly a -0.2 milligal (or -2 gu) anomaly (figure 9). Such a small response would slightly mask any underlying dense bodies, which might be detectable as a slight positive gravity anomaly. Modelling suggests that gravity may be of little use in the survey, but that there is some possibility of detecting bedrock topography.

5.4 Other Techniques

Several other techniques were researched or modelled. Magnetics is not expected to be very useful, as the only rocks in the area having high magnetic susceptibilities are maghemite and pyrrhotite rich ore. Hence the trough is unlikely to be detected. Fixed loop EM, downhole EM, magnetometric resistivity, CSAMT and seismic surveys were also considered.

A fixed loop survey was modelled using ***SAMAYA***, and showed no galvanic or inductive response over the trough. Downhole EM was impractical to perform, and would be unlikely to yield any response. Refraction and reflection seismic were tested over the Elura lead-zinc-silver deposit (located 12 kilometres SSE of Number Four Tank), and proved difficult to accurately

Figure 7: Z-Component SAMAYA model over trough. Comparison of Channels 4 and 20. Trough is 150m wide.

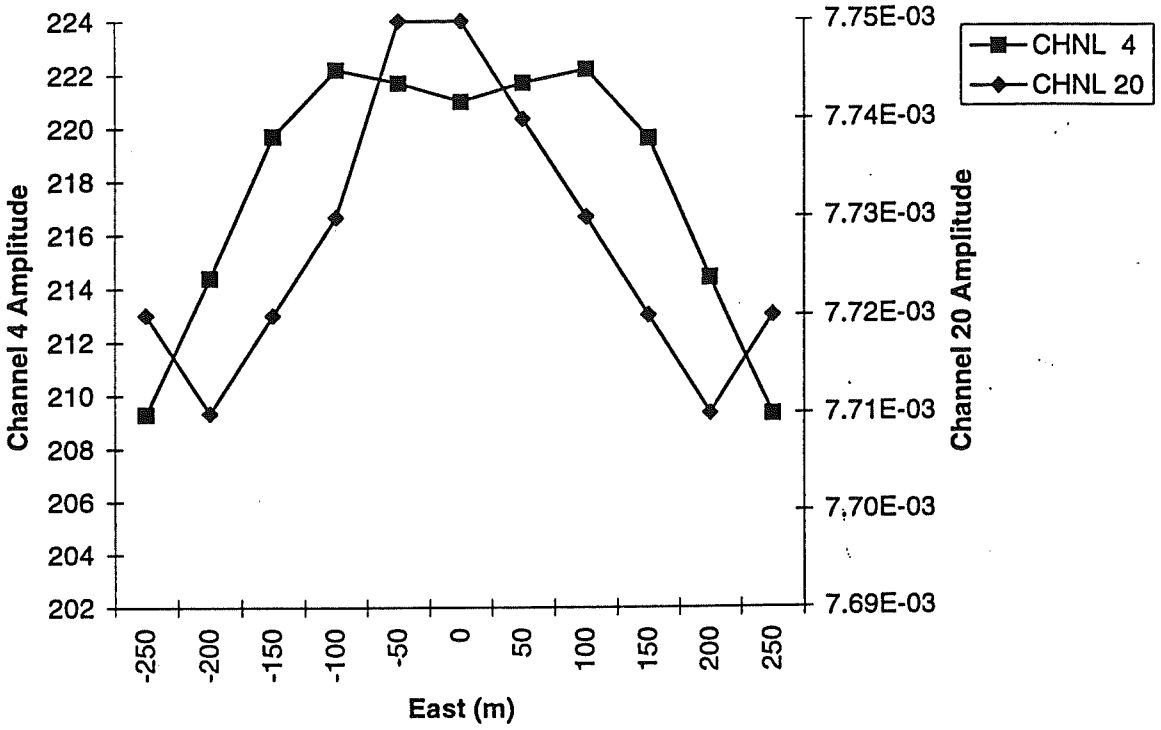

Figure 8: X Component SAMAYA model over Weathering Trough. Channels 8 to 13. Trough is 150m wide

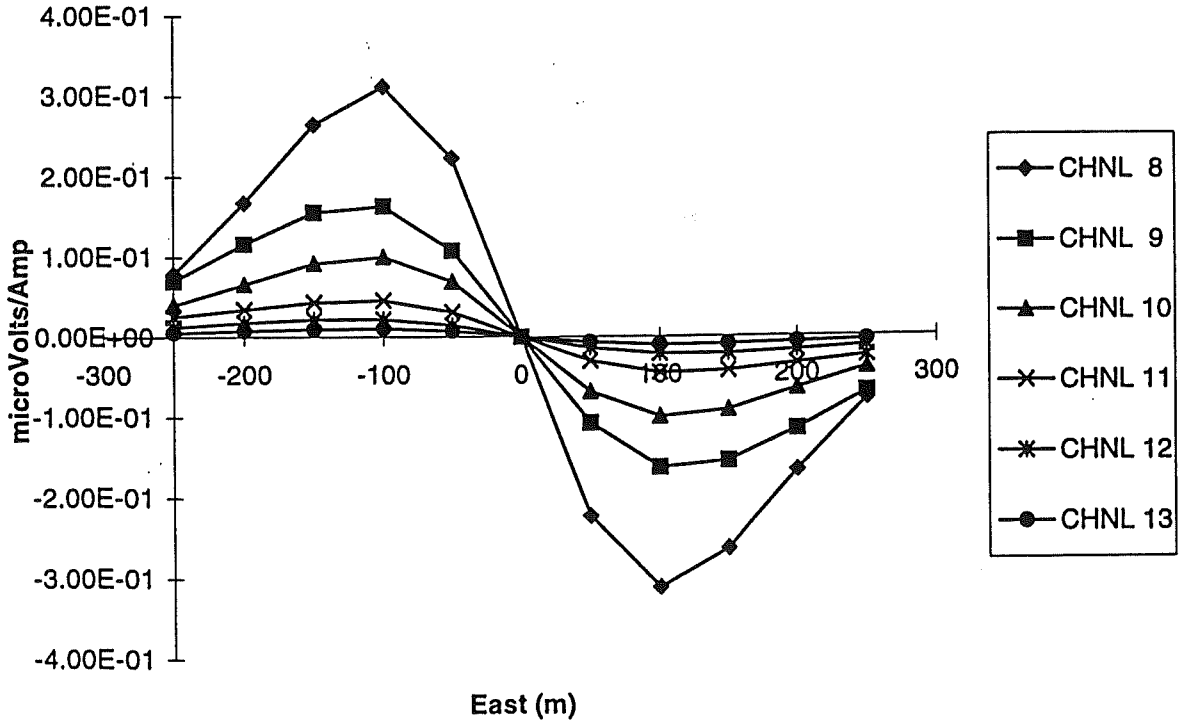

Figure 9: Forward gravity model over 100m wide trough. Yields a -0.2 milligal anomaly.

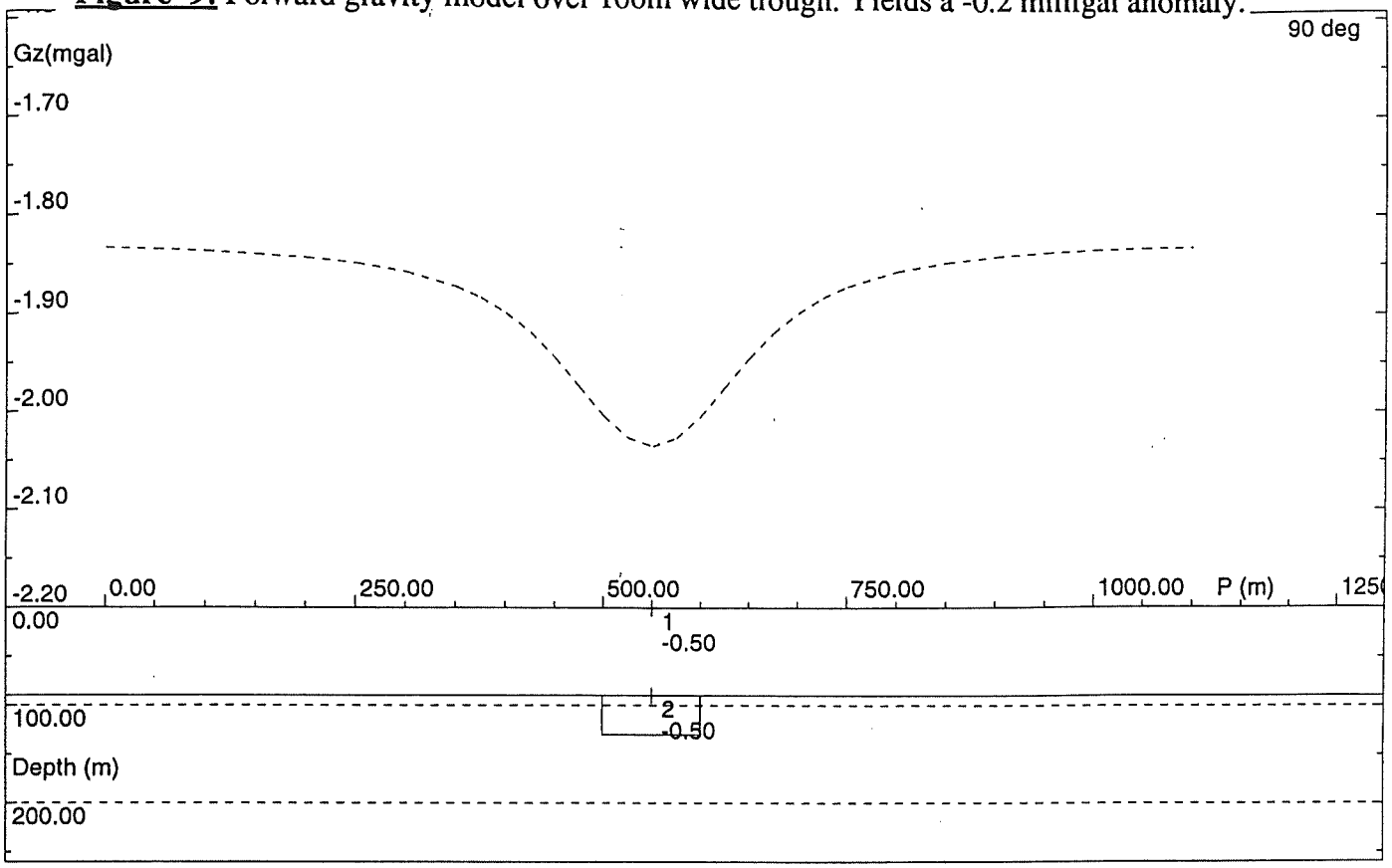

Observations: East , North, Residual
Profile #1; Trough Forward Model
Model:
Calculation mode: Z gravity vector component

Observed: ———— Calculated: - - - - - - - - - -
Residual: . . . . . Individual body: . . . . . .

POTENT v3.09 Profile drawn at 19:37 04/11/1998 for University of Adelaide - Educational use

Trough Forward Model

No.	Type	X	Y	Depth	Density	A	B	C
		m	m	m	gm/cc	m	m	m
1	W. Zone	500	0	0.00	-0.50	3000	3000	90
2	trough	500	0	90.00	-0.50	100	400	40

interpret due to the variable nature of the weathered zone (Emerson, 1980). A refraction or reflection seismic survey would also be costly and impractical, requiring large geophone spacings to penetrate to the fresh rock boundary.

Magnetometric resistivity (MMR) and controlled source audiomagnetotellurics (CSAMT) show promise for exploration in conductive terrains (Hughes, pers. comm.). MMR utilises the increased galvanic current channelling through the weathered zone and into conductive ore bodies, and is excellent for detecting poor conductors. CSAMT is a frequency domain technique which uses a grounded dipole source located a large distance from the survey area, so that the source is effectively a plane wave. CSAMT involves simultaneously measuring the electric and magnetic field strengths over a frequency range of 10Hz to 10kHz. The ratio of electric to magnetic field strengths can be used to calculate an apparent resistivity vertical sounding with depths related to the frequencies studied (Telford, Geldart and Sheriff, 1988; Emerson, 1980). Though these techniques are useful exploration tools, expense and time precluded their feasibility in this study.

6.0 Transient Electromagnetics

6.1 Initial Results and Interpretations

The three vertical (Z) component SIROTEM traverses (figures 10, 11 and 12) show an increased mid time channel response, marked by arrows, on the northern (figure 11) and central (figure 10) lines. No anomalous response is seen on the southern line (figure 12). These responses are associated with the weathering trough, and/or possibly an underlying conductor. Appendix 1 provides a brief explanation of transient electromagnetic (TEM) techniques.

The X- or east component was collected on all three lines because forward modelling indicated that this would have a greater dynamic range over lateral inhomogeneities in layered earth environments. In a Z-component survey, any response from a lateral inhomogeneity will be superimposed on the response of the layered earth, rendering small inhomogeneities less visible. In X-component surveys there will be no layered earth response, and hence the response of any inhomogeneities will be more distinguishable. The X-component is not usually collected because the Z-component has a signal to noise ratio at least five times greater (Smith and Keating, 1996).

Forward modelling indicated that the X-component data should show a positive to negative cross-over when moving from west to east over the trough (figure 8). The three traverses of the X-component SIROTEM (figures 13, 14 and 15) show mid time channel cross-overs on the northern (90750N) and central (90500N) lines. The X-component traverses are very noisy, but cross-overs are visible at 101140E in channels 14 to 18 (figures 13 and 14). The location of the X-component anomaly corresponds with the anomaly in the Z-component data which confirms the presence of a lateral inhomogeneity.

6.2 Decay Curve Analysis

Decay curve analysis was carried out on every sounding to determine which channels were useable and to investigate the basic conductivity structure. It was found that only channels 9 (0.725 ms) to 19 (5.025 ms) were reliable. Earlier channels were still affected by the ramp-off, and later channels were noisy and also showed IP effect.

All curves could be fitted accurately with a power law decay of approximately t^{-4}. This indicates a conductive layer over a resistive halfspace, as expected from the known weathering profile (McNeill, 1995; Kaufmann and Keller, 1983). The alluvium is not detected because it is too thin and resistive to be resolved with a large transmitter loop.

A conductive layer over a resistive basement can be represented by a horizontal thin sheet, the vertical component SIROTEM response of which is given by Equation (1) (adapted from Kaufmann and Keller, 1983).

$$\frac{\mu\text{Volts}}{\text{Amp}} = \frac{(3*10^{-6})M^2\mu^4S^3}{16\pi I^2 t^4} \qquad (1)$$

M=Mutual inductance of Transmitter Loop, I=Transmitter Current,

S=Sheet Conductance=Sheet thickness/resistivity, t=time

Figure 10: Line 90550N In-Loop SIROTEM traverse, Anomaly visible from 1000E to 1350E.

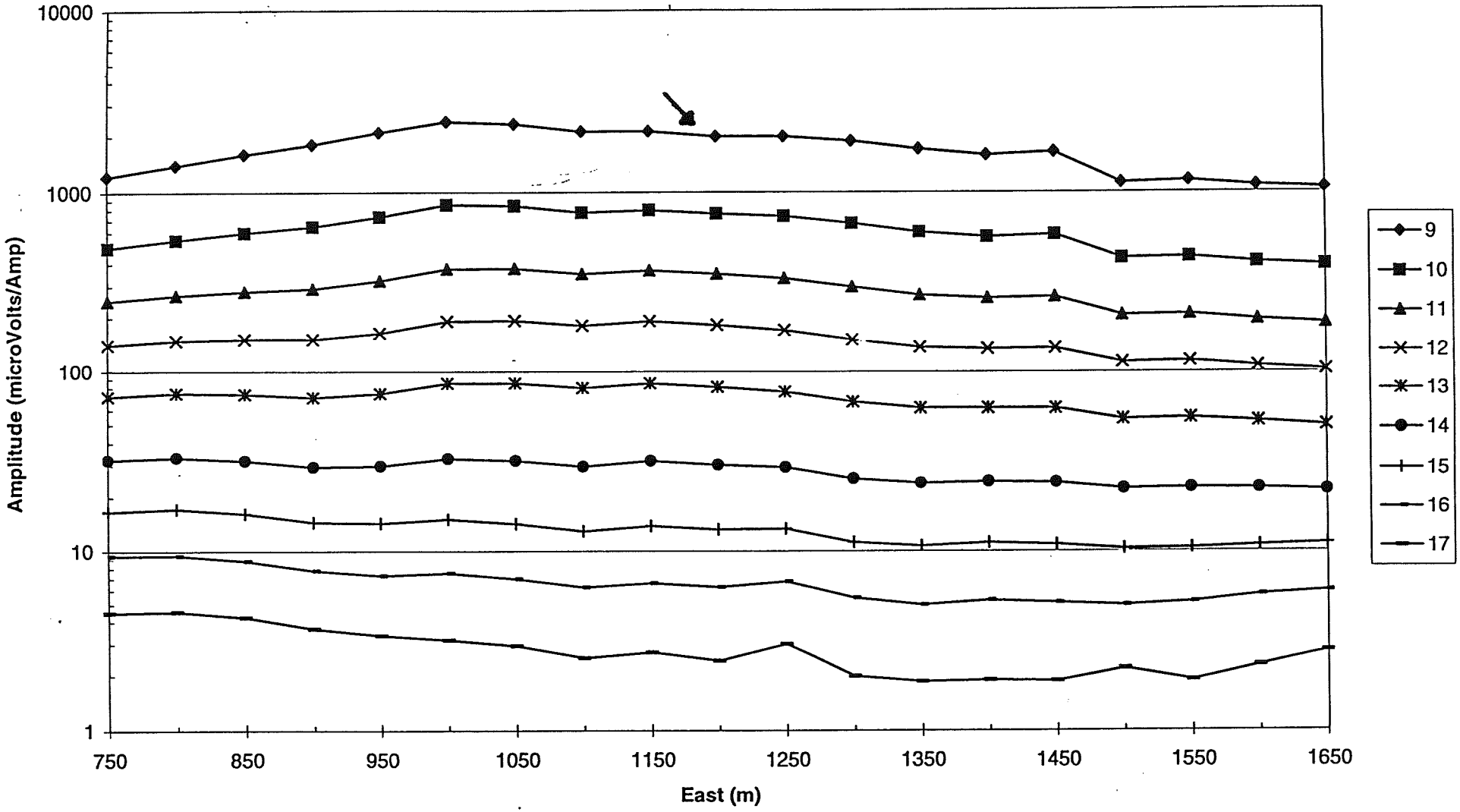

Figure 14: Line 90800N X-component SIROTEM traverse channels 15-18. Note cross-over at 1140E

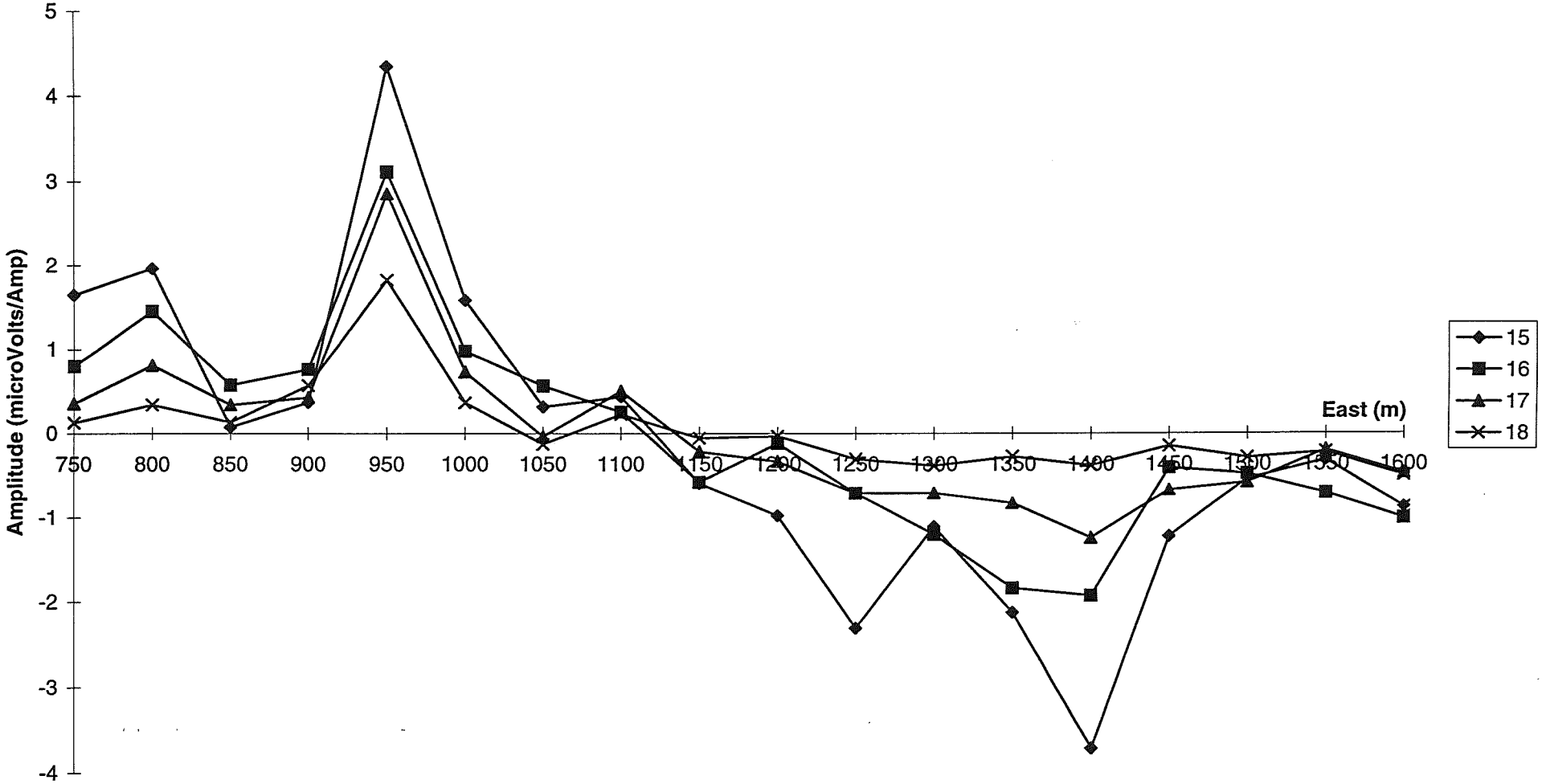

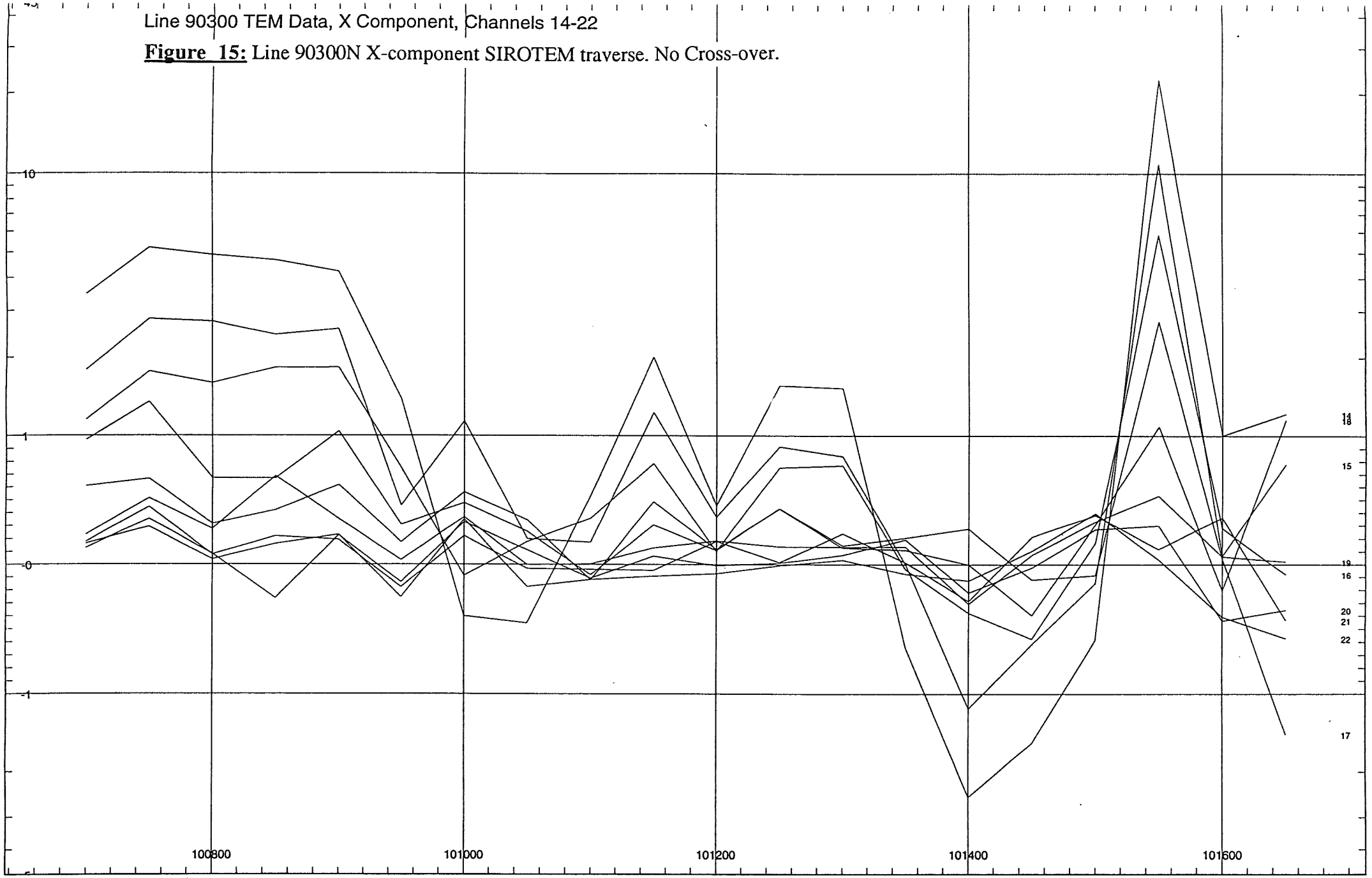

Figure 15: Line 90300N X-component SIROTEM traverse. No Cross-over.

Equation (1) indicates that the response of the weathered zone is proportional to the cube of the layer conductance. Hence even small variations in weathered zone thickness and conductivity should yield visible responses.

6.3 Stripping

The decay curves of the anomalous responses seen on the northern and central lines exhibit a slight curvature away from the straight line power law decay (figure 16). This is caused by another conductor's response, possibly the trough, being superimposed on the weathered zone response. To investigate this a power law decay was stripped away from each sounding (Asten, 1992) on the northern and central lines.

Stripping involves calculating the background power law decay, by fitting a power law to the first and last few channels. The background decay is then subtracted from all the channels, leaving a residual which can then be plotted as a traverse for each line.

Stripping does not yield a perfect inductive response of an underlying conductor. Stripping only removes the inductive response of a horizontal thin sheet. The remaining residual is the inductive response from an underlying conductor plus any galvanic response from the target and overburden (geologic noise), in addition to any errors arising from the stripping (Asten, 1992).

At certain time channels the inductive response of a bounded conductor will be most prominent, and should exhibit an exponential decay given by Equation (2) (adapted from Kaufmann and Keller, 1983).

$$\frac{\mu Volts}{Amp} = k \times e^{-t/\tau} \qquad (2)$$

k=Intercept, t=time (ms), τ=Time Constant (ms).

Stripping uncovered a clear anomaly on the northern line (90800N) from 1050E to 1250E, in channels 9 to 16 (figure 17 (a) and (b)). These stations correspond with the anomaly seen on the initial traverse.

Decay curve analysis of the stripped response shows an exponential decay on the anomalous soundings in channels 11 (1.114 ms) to 16 (2.814 ms). The exponential curves have time constants of approximately τ=0.45 ms (figure 18), indicating a moderately conductive body. A good conductor would show a time constant of between 1 and 3 ms. The channel 11 to 16 detection window correlates with the theoretical detection times. The theoretical detection window of a target under conductive overburden is between $2^1/_2\tau$ and 6τ (McNeill, 1995), which would be from 1.125 ms to 2.7 ms for a target with a 0.45 ms time constant.

The anomaly on the SIROTEM traverse over the central line (90550N) is broader and of lesser amplitude than that seen on the northern line. Consequently the stripped response is also broader and smaller (figure 19). The central line anomaly is visible from 1000E to 1300E.

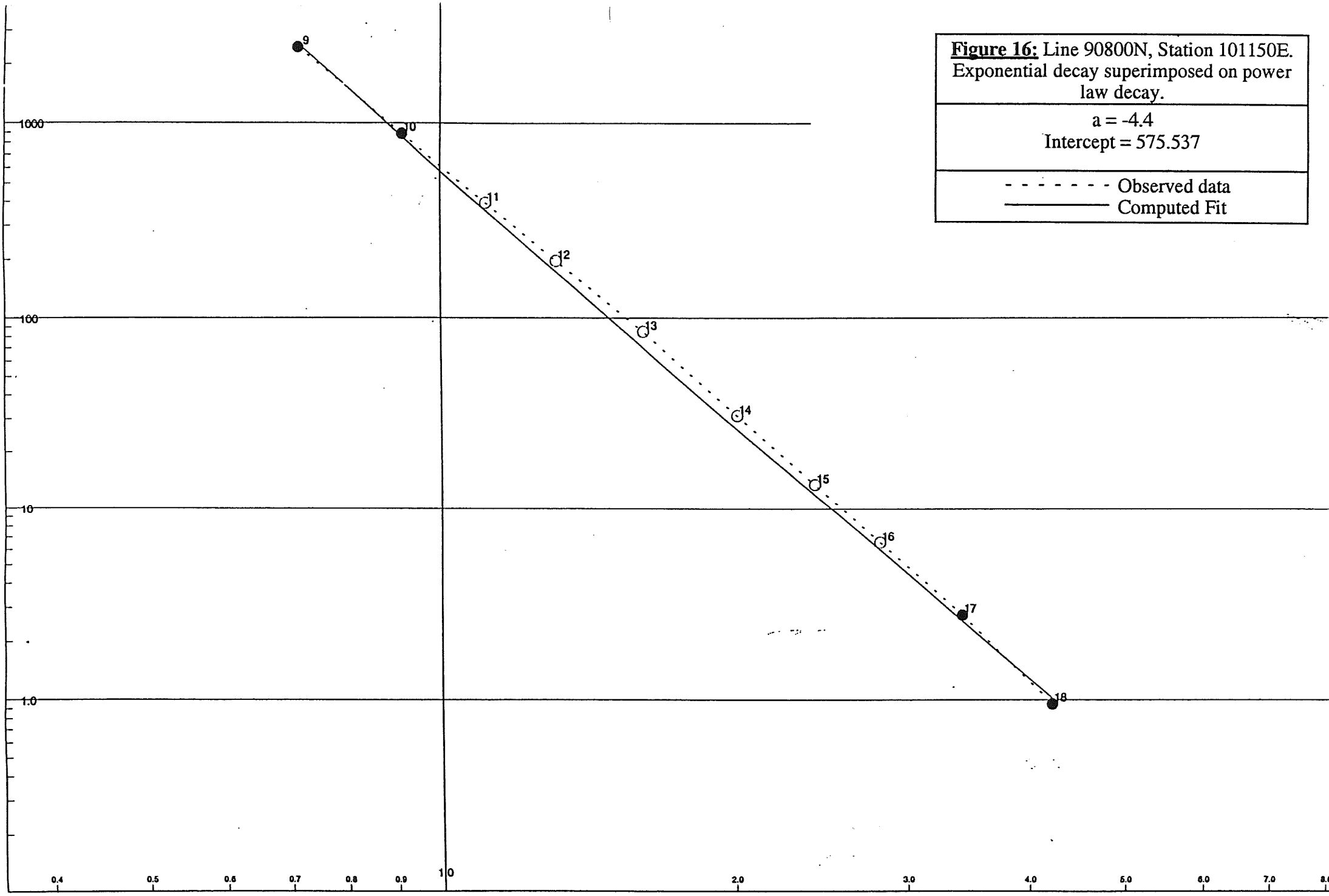

Figure 16: Line 90800N, Station 101150E. Exponential decay superimposed on power law decay.

a = -4.4
Intercept = 575.537

- - - - - - - - Observed data
———— Computed Fit

Figure 17 (a): Line 90800N with Power Law Decay Stripped from Channels 9-13. Anomaly seen from 1050E to 1250E.

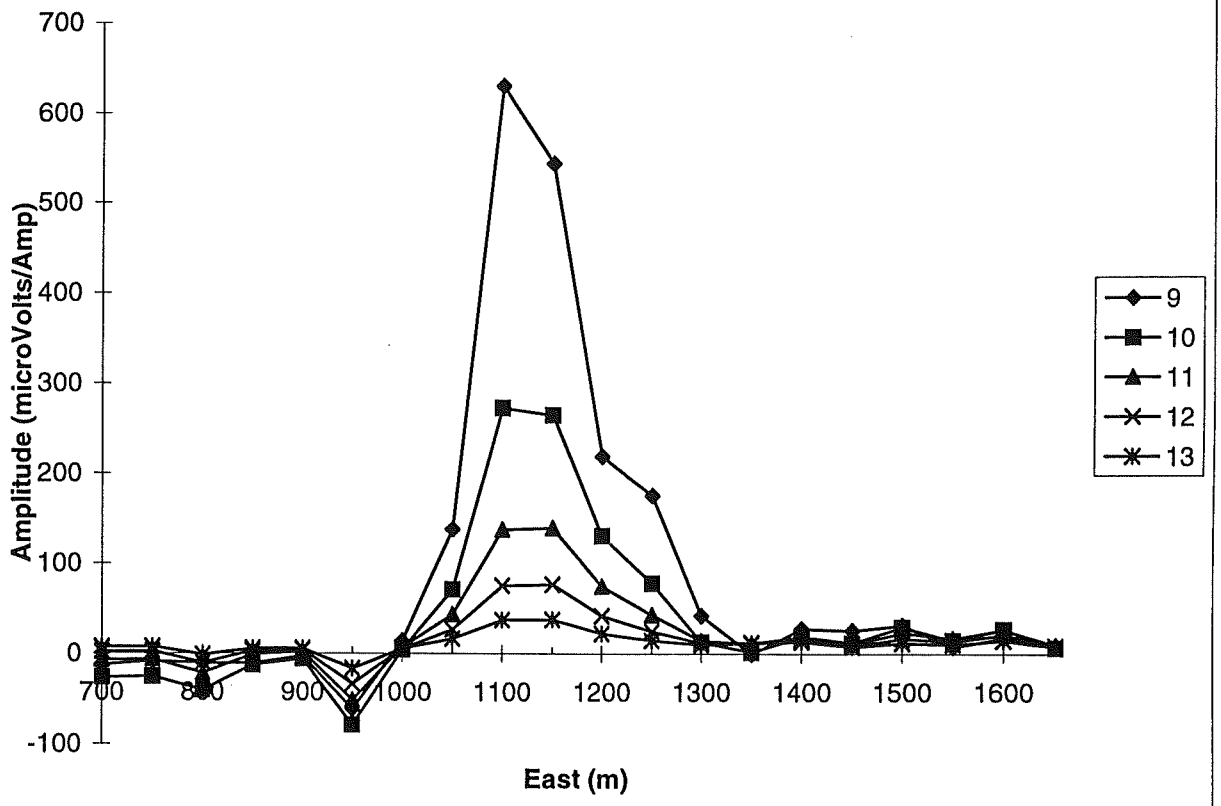

Figure 17 (b): Line 90800N with Power Law Decay Stripped from Channels 14-19. Anomaly seen from 1050E to 1250E.

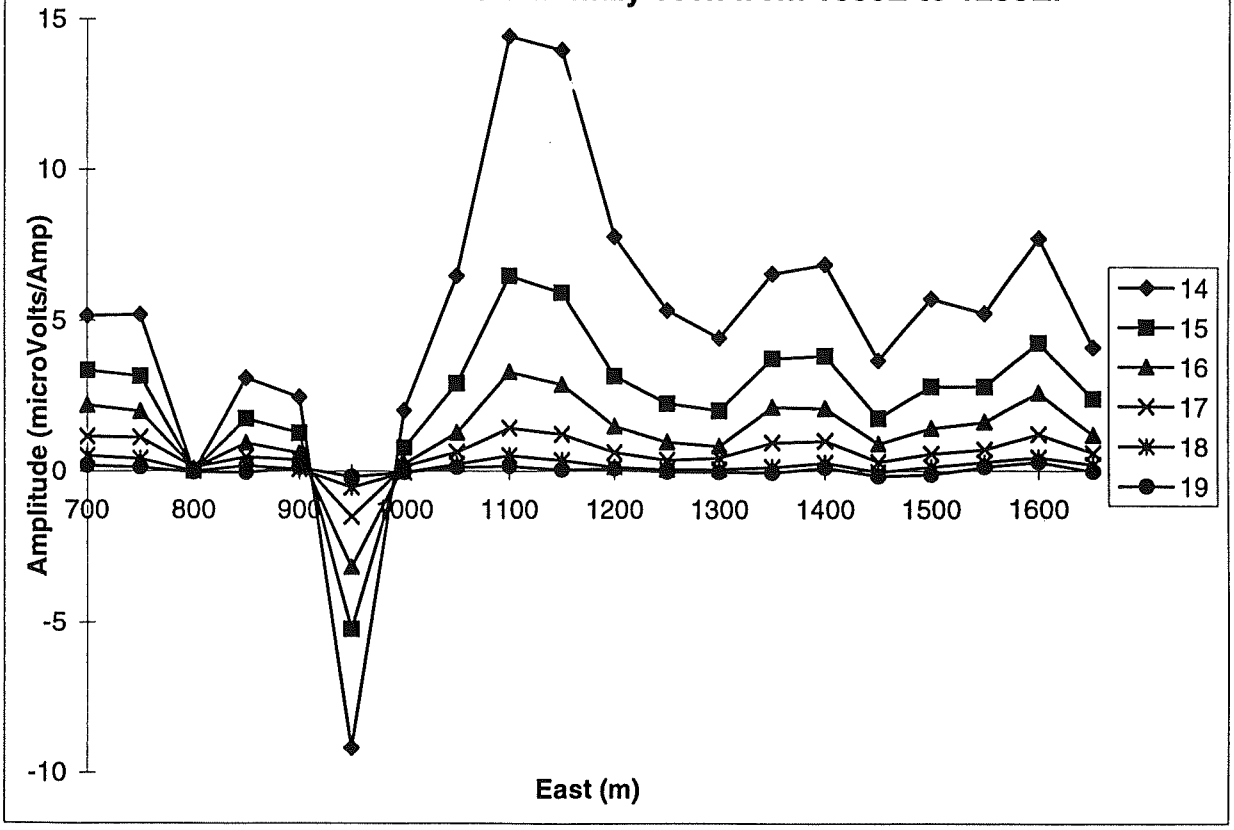

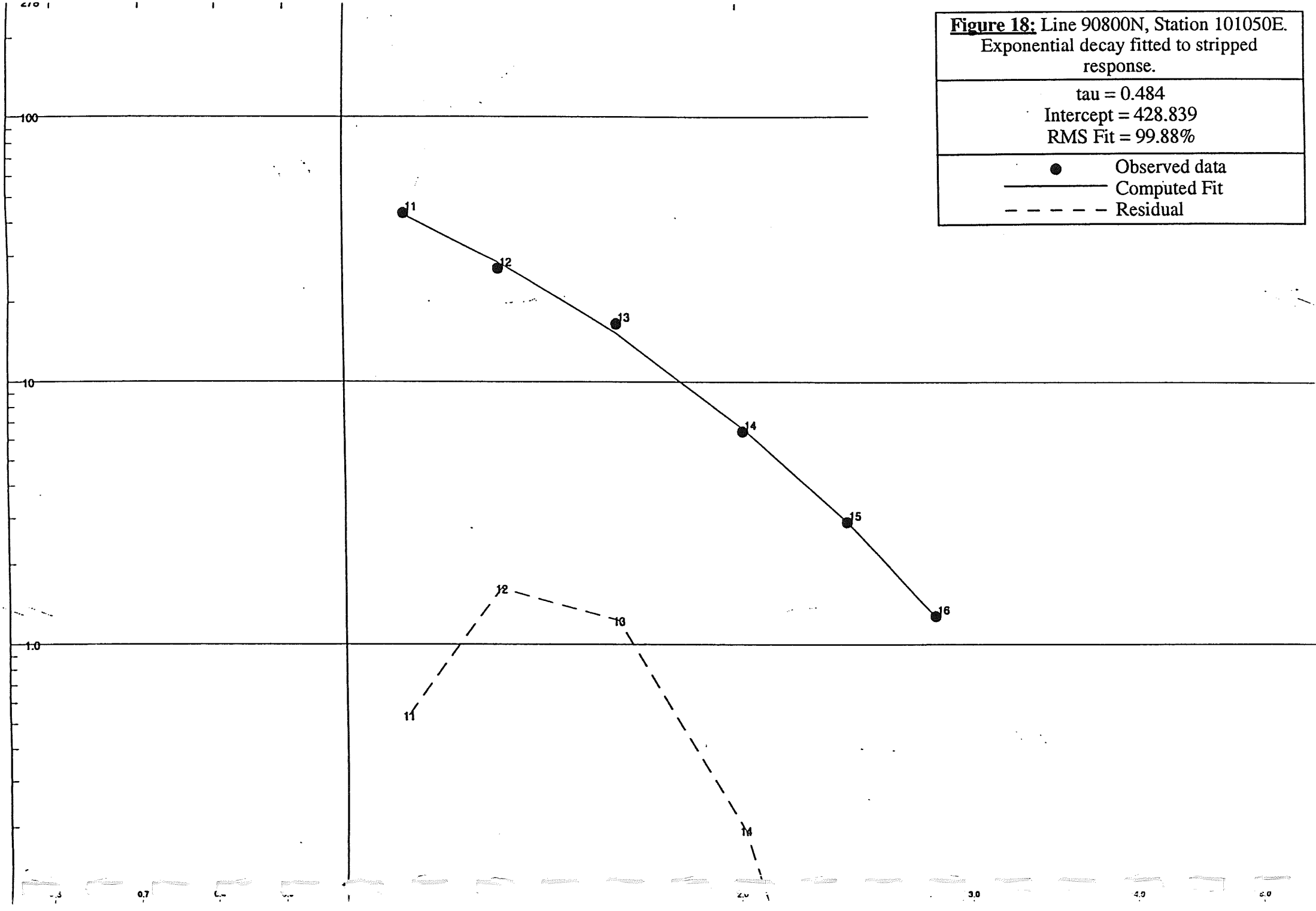

Figure 18: Line 90800N, Station 101050E. Exponential decay fitted to stripped response.

tau = 0.484
Intercept = 428.839
RMS Fit = 99.88%

Observed data
Computed Fit
Residual

Figure 19: Line 90550N with Power Law Decay Stripped from Channels 11-16. Anomaly seen from 1000E to 1300E.

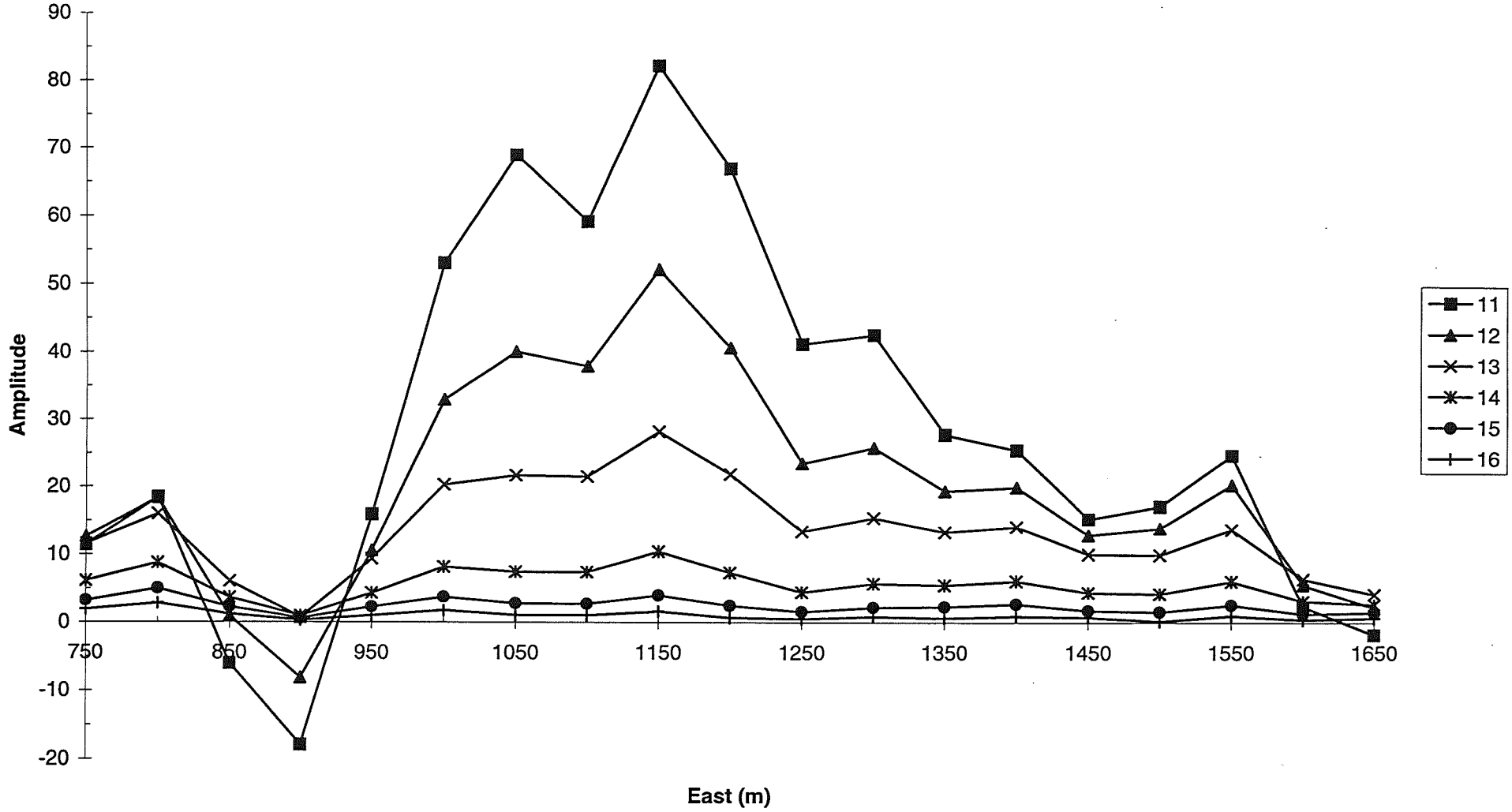

Decay curve analysis on the central line anomaly also showed an exponential decay, with an average time constant of 0.44 ms seen on channels 10 to 16. These channels also correlate well with the theoretical detection window.

The decay curve analysis indicates that there is a conductor underlying the northern and central lines. If this conductor is the weathering trough, or possibly a basement feature, then it strikes approximately 320° and must terminate before reaching the southern line. Initial interpretation suggests that the conductor is shallower on the northern line because of the greater amplitude and shorter wavelength of the anomaly.

6.4 Modelling the Stripped Response

The stripped data was further investigated by modelling the anomaly on the northern and central lines. This was done using the ***PLASI*** algorithm on ***EMVISION***, which calculates the inductive response of one or more plates. The models found were created only to fit the stations which exhibit an anomalous response.

Two models were found for the northern line. The first model (figure 20) used an almost horizontal plate (3° dip) with a length of 160m, strike length of 200m and conductivity thickness product (conductance) of 17.0 Siemens. This would best represent the response of a rectangular prism shaped body, with a depth to top of approximately 95m. The width of the conductor would be approximated by the length of the plate. A problem with this model is that a wide plate (160m) must be used, while the trough is known to be, at most, 100m wide.

The second model for line 90800N consisted of two steeply dipping plates (figure 21), the dimensions of which are in table 4. The geological feasibility of this model is unknown; perhaps the plates could represent the boundaries of a steeply dipping conductive zone (Hughes pers. comm.). The plates are 100m apart, which is approximately the known width of the trough. The problem with this model is that the plates are quite shallow, only 50m deep. The two completely different models equally fit the stripped data, which emphasises the ambiguity of electromagnetic modelling.

Plate	Strike length	Depth Extent	σd (Siemens)	Dip	X Posⁿ.	Z Posⁿ.
Western	200m	78.3m	25.0	150.6°	1168E	-46.8m
Eastern	200m	45.9m	50.0	135°	1256E	-53.5m

Table 4: Plate dimensions of the two plate model for line 90800N.

A horizontal thin sheet model was found for the stripped response of the central line (figure 22). The sheet used was very wide, 540m, and had a strike length of 650m. The plate dips at 2.8° and had a very low conductance of 6 Siemens. This model does not represent any geological feature likely to be present in the survey region.

The modelling was restricted to plate modelling. Sphere and loop models do not fit the observed data. Even though EM modelling is restricted, it is still a useful technique because approximate values for width, depth or shape of an anomalous response can be obtained.

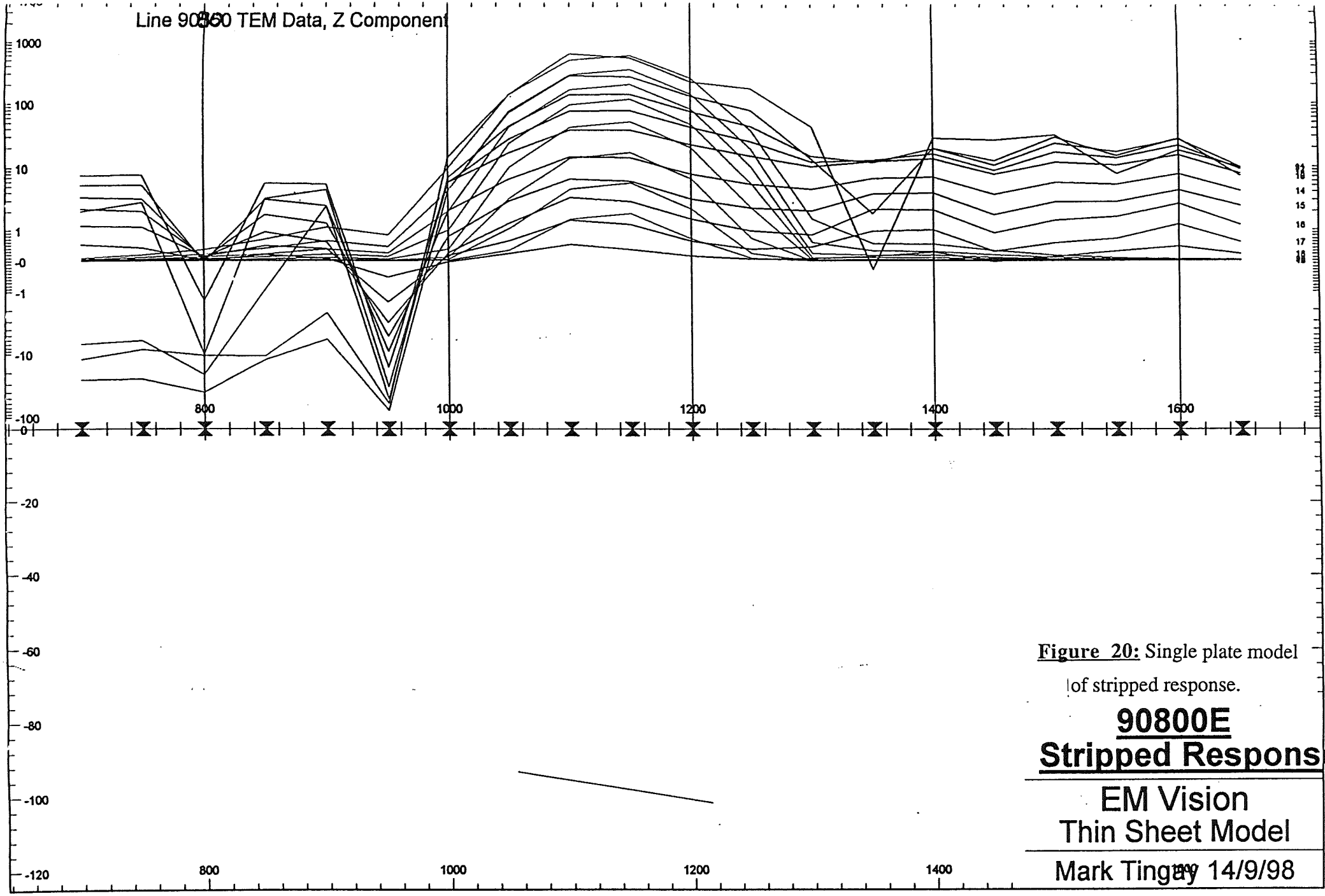

Figure 20: Single plate model of stripped response.

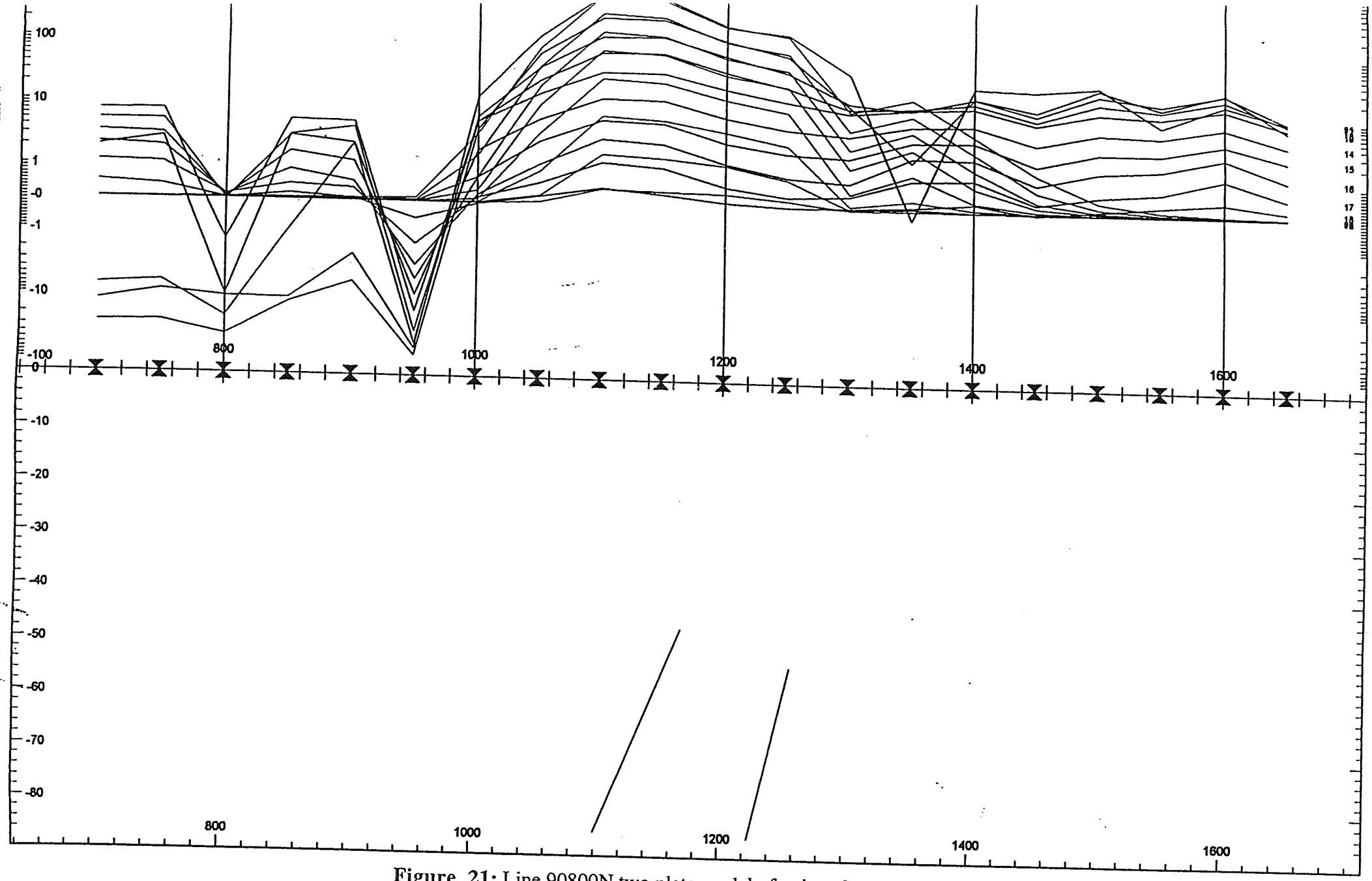

Figure 21: Line 90800N two plate model of stripped response.

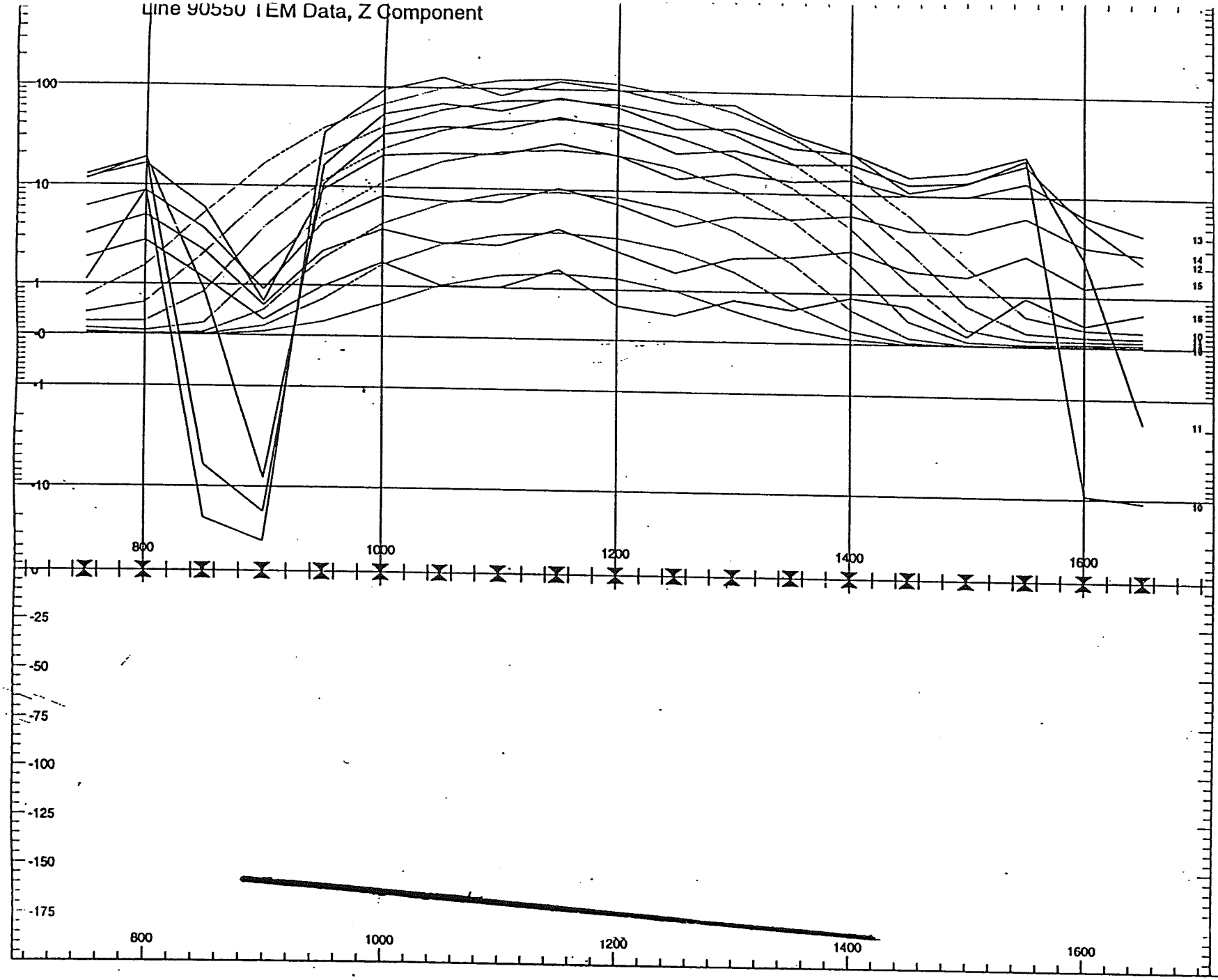

Figure 22
Line 90550N
Stripped response
Single plate model

6.5 Three Dimensional Modelling

The three dimensional forward modelling program *SAMAYA* was used to attempt modelling the original SIROTEM traverses. Firstly a body 150m wide, 340m deep and with a resistivity of 20 Ohm-m was placed at the base of an 80m thick, 25 Ohm-m weathered zone. Despite the size of this body, no obvious response was seen. The fact that modelling failed to yield a good response suggests problems with the *SAMAYA* program. Three dimensional electromagnetic modelling is extremely complicated, and is not considered fully reliable.

Despite these problems, several models were run using a body of different sizes and resistivities, and also with two bodies; a small body representing a trough and a deeper, larger body representing an underlying conductor. The resistivities of both of these bodies were varied in an attempt to model the observed response. None of the models were successful. Models either had a response which was too small (ie too resistive), or were too conductive and gave a late time negative trough due to null coupling (when the loop is directly over a bounded conductor).

An important feature of the observed data is that the anomalous responses are large, yet are constrained to only a narrow time range, and only a few stations. The anomaly can only be detected in channels 8 (0.575 ms) to 14 (2.025 ms), with later time channels exhibiting no obvious response. This also suggests that a finite target must be yielding the anomalous response, because an infinitely sized target (eg a conductive layer, or cylinder of infinite depth extent) would exhibit an anomalous response across all time channels. This was highlighted when the data was inverted using the one dimensional inversion algorithm ***GRENDL***.

6.6 *GRENDL* Layered Earth Inversion

One dimensional, or layered earth inversions are the current leading edge in electromagnetic software. The SIROTEM soundings were inverted using the ***GRENDL*** algorithm on ***EMVISION***. ***GRENDL*** creates a "pseudo-bedrock topography" by performing a layered earth inversion on each sounding, but plotting the results in a cross-sectional format. The model presented by the ***EMVISION*** output is made up of 20 layered earth models, and not the single "blocky topography" shown. If the "blocky topography" could be forward modelled, the response would not be the same as the "20 layered earths" response.

There are lateral inhomogeneities in the conductivity structure of the weathered zone at Number Four Tank (ie the trough and conductor). Hence interpretations from a layered earth inversion must be considered cautiously. It would be reasonable to expect the inversion to work well on the ends of the line, because the response from the conductor is minimal, and the structure would be closest to a layered earth. Figures 23, 24 and 25 show the results of the two layer ***GRENDL*** inversions over the three SIROTEM traverses.

The southern line (90300N, figure 25) shows no response from the conductor. The inverted model is seen to have a weathered zone varying between 16 and 28 Ohm-m, (averaging 23 Ohm-m). The thickness of the weathered zone is generally around 70 to 75m, but

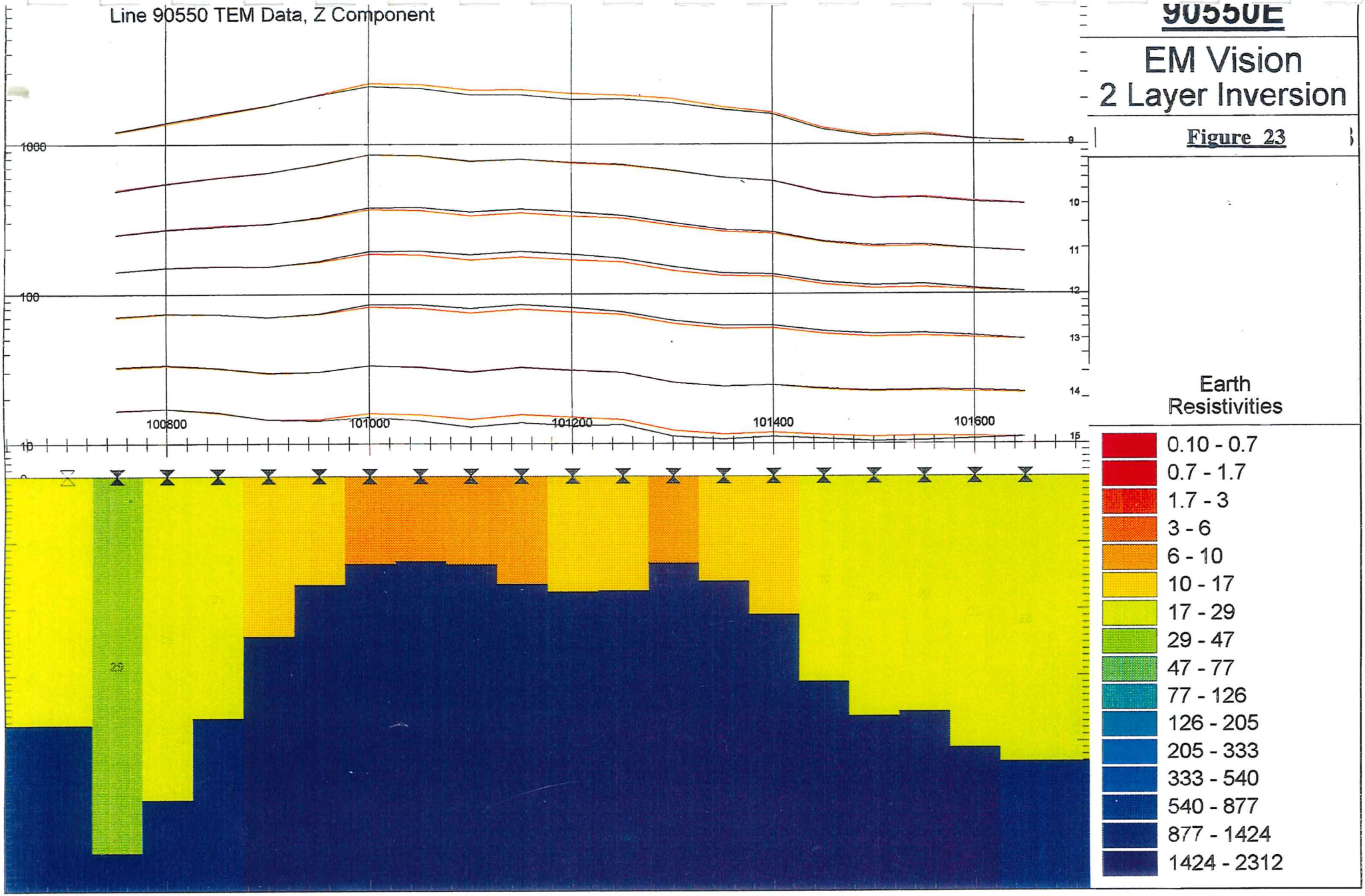
Line 90550 TEM Data, Z Component
1000
100
10
100800
101000
101200
101400
101600
9
10
11
12
13
14
15
90550E
EM Vision
2 Layer Inversion
Figure 23
Earth
Resistivities
0.10 - 0.7
0.7 - 1.7
1.7 - 3
3 - 6
6 - 10
10 - 17
17 - 29
29 - 47
47 - 77
77 - 126
126 - 205
205 - 333
333 - 540
540 - 877
877 - 1424
1424 - 2312

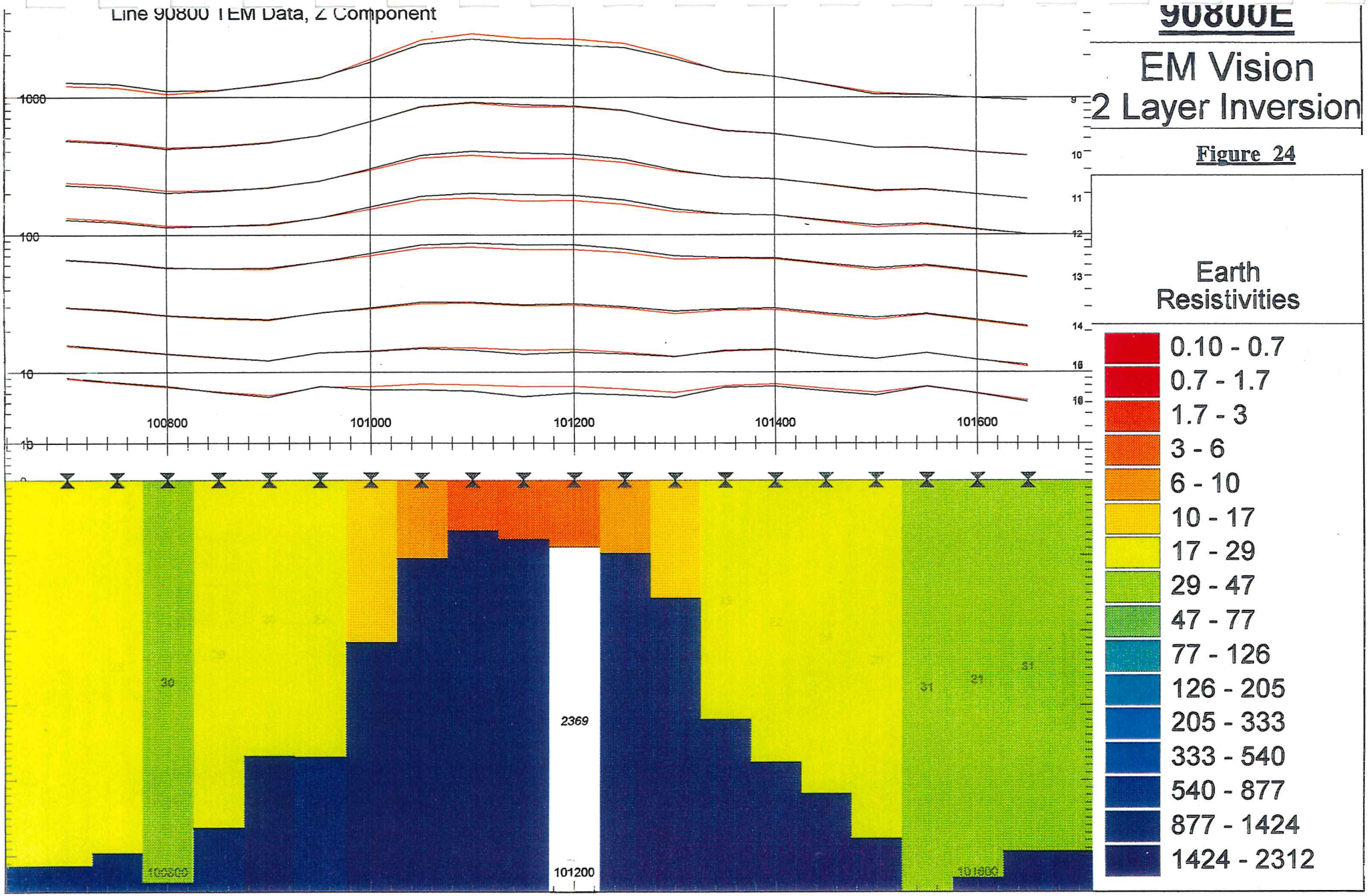
Line 90800 TEM Data, Z Component
1000
100
10
1
100800
101000
101200
101400
101600
9
10
11
12
13
14
15
16
2369
101200
90800E
EM Vision
2 Layer Inversion
Figure 24
Earth
Resistivities
0.10 - 0.7
0.7 - 1.7
1.7 - 3
3 - 6
6 - 10
10 - 17
17 - 29
29 - 47
47 - 77
77 - 126
126 - 205
205 - 333
333 - 540
540 - 877
877 - 1424
1424 - 2312

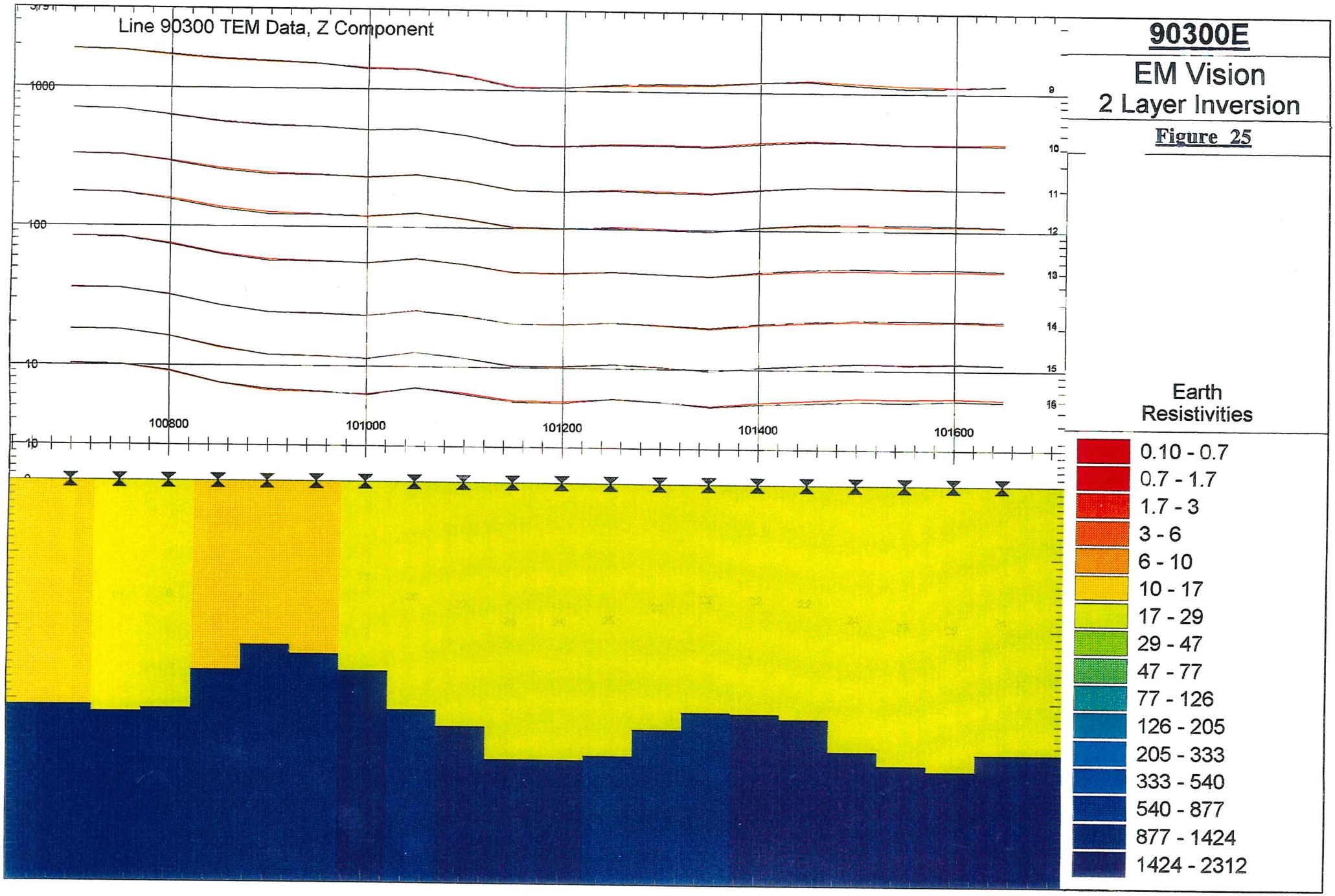
Line 90300 TEM Data, Z Component
1000
100
10
1
100800
101000
101200
101400
101600
9
10
11
12
13
14
15
16
90300E
EM Vision
2 Layer Inversion
Figure 25
Earth Resistivities
0.10 - 0.7
0.7 - 1.7
1.7 - 3
3 - 6
6 - 10
10 - 17
17 - 29
29 - 47
47 - 77
77 - 126
126 - 205
205 - 333
333 - 540
540 - 877
877 - 1424
1424 - 2312

there are three apparent topographic highs at 100700E, 100900E and 101400E. As will be shown later, these apparent highs may in fact be bedrock topographic lows.

The central (figure 23) and northern (figure 24) lines show a drastic thinning of the weathered zone. Simultaneously, the modelled weathered zone also becomes more conductive, and the bedrock becomes more resistive. The results of the inversion are in complete contrast to the trough structure which was hoped would be the output of the inversion. The results for the inverted model are explicable when one considers how the inversion algorithm works. We can also use the statistics which ***GRENDL*** calculates with the output to determine the acceptability of the inverted model.

As mentioned before, ***GRENDL*** performs a layered earth inversion, therefore the program is attempting to fit a one dimensional model to a three dimensional earth. Decay curve analysis found that the anomalous decays were slightly curved, while a decay curve measured from a thick conductive layer overlying resistive basement would generally exhibit a straight line power law decay.

The more conductive the overburden, the slower the passage of the EM fields through it; and the slower the decay (Nabighian, 1979). If a very conductive, but very thin, overburden is modelled; then the early times will decay slowly while the EM fields (ie the "smoke ring") move through it. However, because the surface layer is only 10-15 metres thick, the "smoke ring" will have passed through the conductive layer, and into the resistive basement by the mid time channels. The EM fields move rapidly through the resistive fresh rock, so the decay will become very fast in the mid to late time channels. Hence a model with a thin conductive weathered zone would show a curved decay similar to the observed decays.

Stripping and decay curve analysis found an exponential decay superimposed on the overburden power law decay, indicating a finite conductor. However ***GRENDL*** can only fit a layered earth, and hence determines the layered earth which best models the decay curve. The layered earth model which will best fit the curved decays would have a very thin and conductive overburden on top of a very resistive basement, which is not synonymous with the survey area. The inversion does, however, appear to yield a reasonable fit to the observed data, so the calculated inversion statistics must be used to determine if the inverted model is acceptable.

GRENDL calculates a wide range of statistics on each inversion. Table 5 summarises the most useful statistics and values for a good inversion. Each of these statistics is described in more detail in Appendix 2.

The basement resistivity is not usually well bounded because electromagnetics detects conductors, and so very little diagnostic information can be gathered on a resistive body.

Statistic	Good Inversion	Poor Inversion
Standard Error	< 2%	> 5%
Average Predicted Residual Error (APRE)	< 2%	> 5%
Mean Percent Symmetric Error	< 1%	> 2%
68% Confidence Interval Bounds for overburden resistivity	< ±5% of Estimated Value	< ±10% of Estimated Value
68% Confidence Interval Bounds for overburden thickness	< ±10% of Estimated Value	< ±20% of Estimated Value

Table 5: Summary of ***GRENDL*** statistics.

The inversion statistics for stations 100850E and 101200E on the central line are shown in figures 26 and 27. Figure 26 is an example of a good inversion, while figure 27 shows an unreliable inversion. The relevant statistics have been highlighted. Note the very low errors and excellent bounds on the overburden resistivity (±3%) and thickness (±6%) for the 100850E inversion. These statistics show a very tight, well constrained inversion. The results of the 100850E inversion, a 21 Ohm-m and 73m thick weathered zone, correspond with the RAB drilling and the VES results.

The statistics of the 101200E inversion show very large errors, and poorly bounded weathered zone resistivity (±40%) and thickness (±50%). Given the limitations of the use of ***GRENDL***, viz attempting to fit a layered earth model to a heterogeneous earth, the statistics demonstrate that the inversion cannot be relied upon.

The lower resistivity bound for the basement in the poor inversions is very conductive (only 4.4 Ohm-m for the 101200E inversion), but the basement is of little significance in these inversions. This suggests that a basement of 20 Ohm-m, for example, is feasible in the model. Hence, although thinning is suggested by the inversion, these results do not preclude a thickening of the weathered zone.

To test whether a thickened weathered zone could be modelled, a three layered inversion was trialed. The second layer in the inversion represented the more resistive partially weathered zone. The inversion statistics showed that even a 50 Ohm-m, 30 metre thick partially weathered zone would have little effect on the model. Hence only the conductive top layer is important in the inversion.

The two layer inversion was also performed with the weathered zone resistivity fixed at 20 Ohm-m. This was done to "force" a thickening of the weathered zone. The inversions correlated poorly with the observed data, and hence were not further investigated.

Another aim of the earlier three dimensional forward modelling was to test the ***GRENDL*** inversion. Every ***SAMAYA*** model was put into ***EMVISION*** and then inverted using ***GRENDL***. The ***SAMAYA*** models did not show as large an anomaly as the observed data, but some did show a smaller mid time amplitude increase. Layered earth inversions on these models also

Figure 26: 100850E good ***GRENDL*** inversion statistics.

Begin Report for Line 90550 - Station 100850

```
 ********************************
 * FINAL MODEL AFTER INVERSION *
 ********************************

  GRENDL communication file

     I      RESISTIVITY       THICKNESS         DEPTH

     1        20.73             72.96
                                                72.96
     2        1405.

 STANDARD ERROR =  1.16 PERCENT

 NOISE TO SIGNAL RATIO =    .11 PERCENT

 ****************************************************
 * ERROR STRUCTURE OF THE FITTED MODEL FOR TEM DATA *
 ****************************************************
```

CHNL	DELAY TIME (MS)	APPARENT RESISTIVITY OBSERVED	APPARENT RESISTIVITY CALCULATED	OBSERVED VOLTAGE (MU V)	CALCULATED VOLTAGE (MU V)	WEIGHTED PERCENT SYMMETRIC ERROR
5	.021	899.5	20.1	1605.	0.1995E+06	-.0
6	.121	136.9	18.5	1605.	0.2675E+05	-.0
7	.221	65.9	20.5	1605.	8512.	-.0
8	.321	40.5	22.4	1605.	3783.	-.0
9	.471	23.9	24.3	1605.	1572.	2.0
10	.671	28.3	28.1	598.6	603.9	-.9
11	.871	32.2	31.8	280.6	285.3	-1.6
12	1.071	35.7	35.4	151.4	153.4	-1.2
13	1.371	39.8	39.8	73.49	73.47	0.0
14	1.771	46.6	46.9	32.01	31.73	.9
15	2.171	53.4	53.7	16.17	16.02	.9

```
 MEAN PERCENT SYMMETRIC ERROR =   .99
 MAXIMUM PERCENT SYMMETRIC ERROR =  2.02
 MAXIMUM SYMMETRIC ERROR OCCURED AT OBSERVATION   5

 ****************************************************
 * LAYER THICKNESS PARAMETER SENSITIVITY ANALYSIS *
 ****************************************************

 THE NUMBER OF EFFECTIVE PARAMETERS IS     2.000

 ************************************
 * ERROR BOUNDS FOR LAYER THICKNESS *
 ************************************

   LAYER RESISTIVITIES  -  68 PERCENT CONFIDENCE INTERVAL (UNDAMPED)

 LAYER     RES(I)        BOUND(1)      BOUND(2)     IMPORTANCE

   1        20.73         20.10         21.38         1.00

   2        1407.         476.9         4151.          .06

   LAYER THICKNESSES  -  68 PERCENT CONFIDENCE INTERVAL (UNDAMPED)

 LAYER     THK(I)        BOUND(1)      BOUND(2)     IMPORTANCE

   1        72.97         68.92         77.26         1.00

 ************************************************************
 * AVERAGE PREDICTED RESIDUAL ERROR (APRE) =  2.13 PERCENT *
 ************************************************************
```

Figure 27: 101200E poor ***GRENDL*** inversion statistics.

Begin Report for Line 90550 - Station 101200

****
* FINAL MODEL AFTER INVERSION *
****

GRENDL communication file

I	RESISTIVITY	THICKNESS	DEPTH
1	10.99	34.75	34.75
2	1877.		

STANDARD ERROR = **7.25 PERCENT**

NOISE TO SIGNAL RATIO = .70 PERCENT

****
* ERROR STRUCTURE OF THE FITTED MODEL FOR TEM DATA *
****

CHNL	DELAY TIME (MS)	APPARENT RESISTIVITY OBSERVED	APPARENT RESISTIVITY CALCULATED	OBSERVED VOLTAGE (MU V)	CALCULATED VOLTAGE (MU V)	WEIGHTED PERCENT SYMMETRIC ERROR
5	.019	855.7	9.5	1992.	0.3033E+06	-.0
6	.119	119.9	10.8	1992.	0.5250E+05	-.0
7	.219	57.3	13.9	1992.	0.1463E+05	-.0
8	.319	35.1	16.5	1992.	5842.	-.0
9	.469	20.7	19.4	1992.	2186.	-9.3
10	.669	24.1	24.3	761.3	752.1	1.2
11	.869	27.6	28.9	352.7	329.3	6.9
12	1.069	31.5	33.4	182.6	167.4	8.7
13	1.369	37.3	39.0	81.08	75.86	6.7
14	1.769	48.2	47.8	30.43	30.88	-1.5
15	2.169	61.4	56.3	13.15	14.94	-12.8

MEAN PERCENT SYMMETRIC ERROR = **6.18**
MAXIMUM PERCENT SYMMETRIC ERROR = 12.81
MAXIMUM SYMMETRIC ERROR OCCURED AT OBSERVATION 11

****
* LAYER THICKNESS PARAMETER SENSITIVITY ANALYSIS *
****

THE NUMBER OF EFFECTIVE PARAMETERS IS 1.997

****
* ERROR BOUNDS FOR LAYER THICKNESS *
****

LAYER RESISTIVITIES - 68 PERCENT CONFIDENCE INTERVAL (UNDAMPED)

LAYER	RES(I)	BOUND(1)	BOUND(2)	IMPORTANCE
1	**10.99**	**7.832**	**15.43**	1.00
2	**1877.**	**4.464**	**0.7893E+06**	.08

LAYER THICKNESSES - 68 PERCENT CONFIDENCE INTERVAL (UNDAMPED)

LAYER	THK(I)	BOUND(1)	BOUND(2)	IMPORTANCE
1	**34.75**	**22.62**	**53.38**	1.00

****
* AVERAGE PREDICTED RESIDUAL ERROR (APRE) = **13.43 PERCENT** *
****

showed the weathered zone to become thinner and more conductive for the anomalous responses, but on a much reduced scale than seen in the observed data.

The layered earth inversion can be used as a processing step to highlight bedrock topography or small conductors, under conductive overburdens. Small conductors and bedrock topographic features may be quickly located by inverting the data and looking for poorly inverted stations with thinner, more conductive weathered zones. Using this technique, it is possible to detect bedrock topography located at 100900E and 101400E on the southern line (figure 25). One of these anomalies is possibly the weathering trough without the underlying conductor. Neither of these features can be detected from the raw traverses.

6.7 *GRENOCC* Smooth Layered Earth Inversion

GRENOCC is a smooth layered earth inversion program based on the ***GRENDL*** and ***OCCUM*** inversion algorithms. ***GRENOCC*** performs a one dimensional inversion using between 30 and 50 thin layers, and then smooths the layer conductivities without decreasing the model fit. ***GRENOCC*** allows small conductivity variations to be more accurately modelled, and emphasises gradational conductivity changes, such as the transition from fully weathered to fresh rock. ***GRENOCC*** is a one dimensional inversion and hence can not accurately invert data taken over lateral heterogeneities.

All three lines were inverted using ***GRENOCC*** and were then grided and contoured (figures 28, 29 and 30). The northern and central lines show the weathered zone to become thinner and more conductive for the anomalous soundings. The southern line shows a fairly flat fresh rock topography, approximated by the yellow region. The results of the ***GRENOCC*** inversions are very similar to the results of the ***GRENDL*** inversions.

The main difference between the results of the ***GRENDL*** and the ***GRENOCC*** inversions is the apparent depression around 101200E on the central line (figure 28). This depression is directly over the known location of the weathering trough. The apparent depression arises from the response of the weathering trough interacting with the response of the deep conductor.

The response of the weathering trough alone would be a small early-mid time positive peak on a moving loop TEM survey. The TEM responses measured around 101200E are a combination of the weathered zone power law response and the exponential responses of the trough and deep conductor. The response of the trough will be present at slightly earlier times than that of the deep conductor. The earlier time response is highlighted in the stripped decay curves which exhibit an exponential decay for stations over the trough in channels 10 to 16, while this decay is only seen from channels 11 to 16 at all other anomalous stations.

The inversion yields a depression over the trough because the anomaly is seen over a greater time range. ***GRENDL*** modelled a thin conductive weathered zone for the anomalous stations because they exhibit a curved decay. The thin weathered zone model will have a curved decay because the electromagnetic fields decay slowly while they pass through the thin conductive layer (up to channel 13), and then decay rapidly as the fields passed into the very resistive basement (figure 31). Because the anomaly starts at earlier times over the trough, the

Figure 28: *GRENOCC* smooth layered earth inversion result.

Note apparent depression at 101200E.

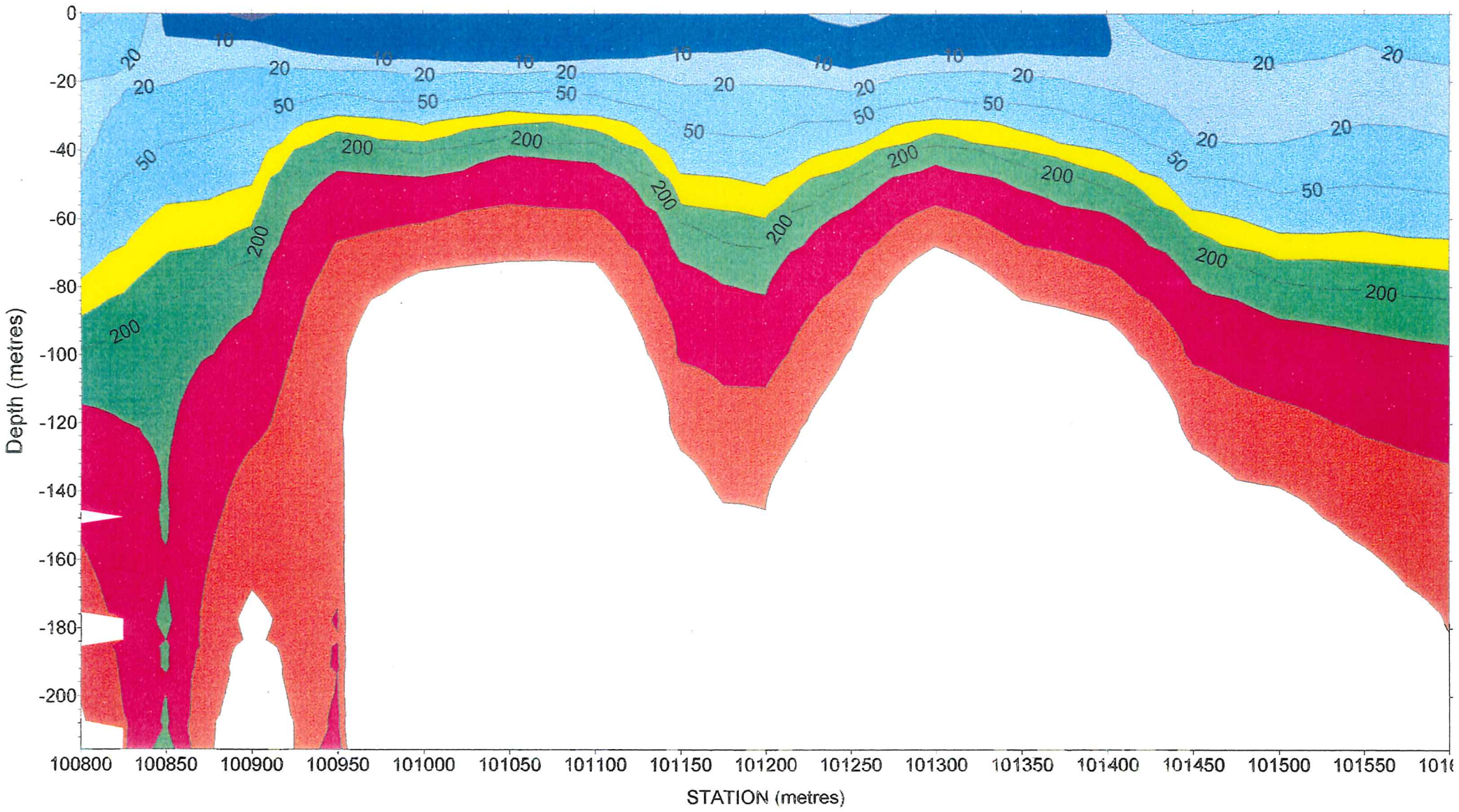

Figure 29: *GRENOCC* smooth layered earth inversion result.

Cobar Line 90800N

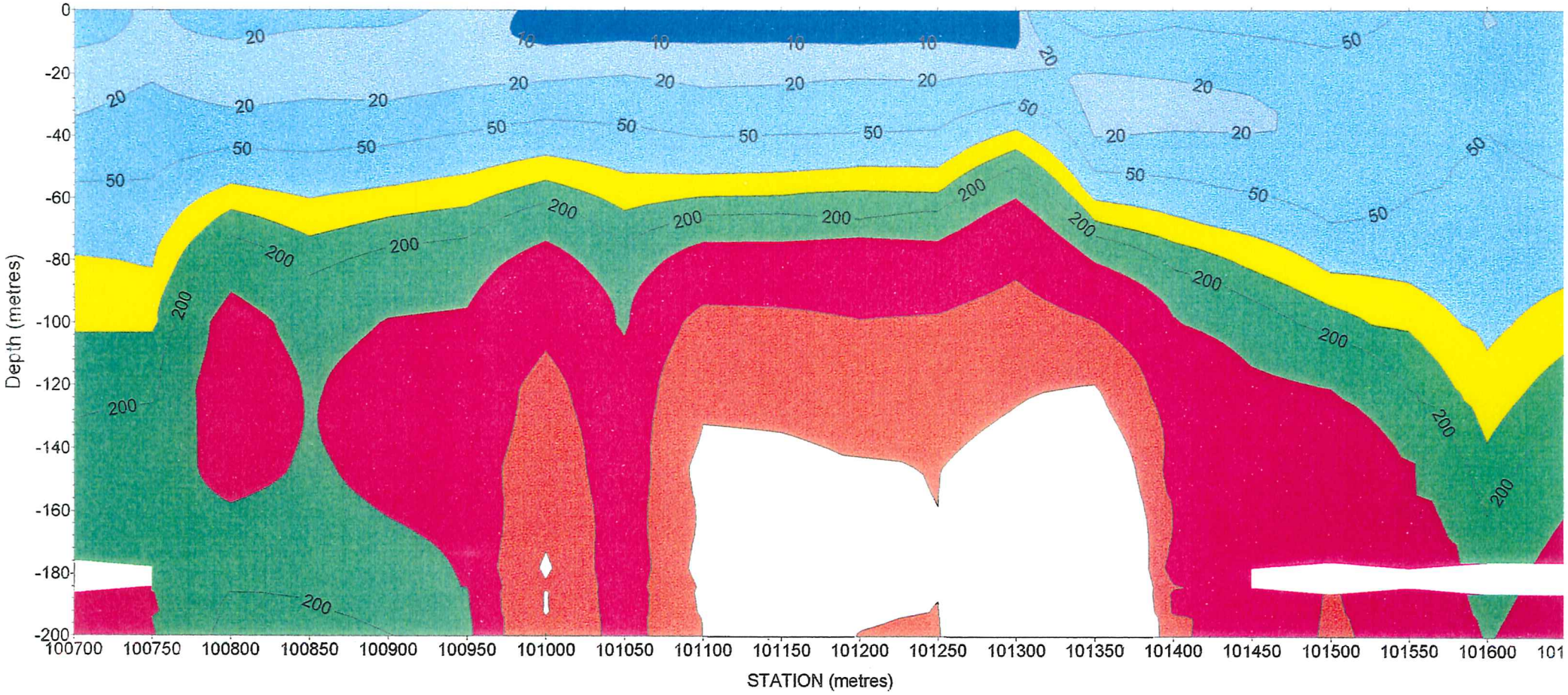

Figure 30: *GRENOCC* smooth layered earth inversion result.

Cobar Line 90300N

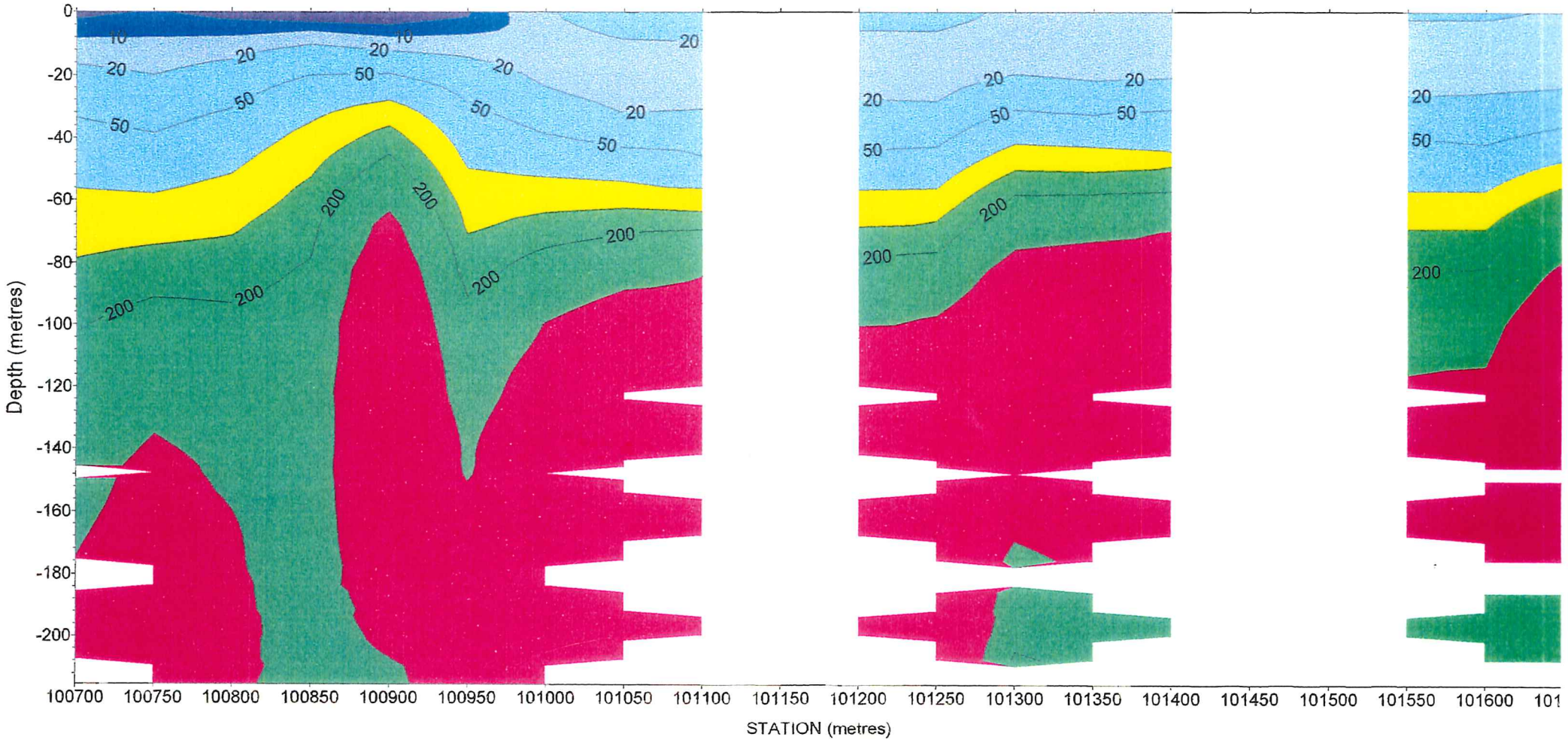

decay is slower over a greater period of time, which indicates a slightly thicker conductive zone (figure 31). Hence ***GRENOCC*** models a small depression over the weathering trough.

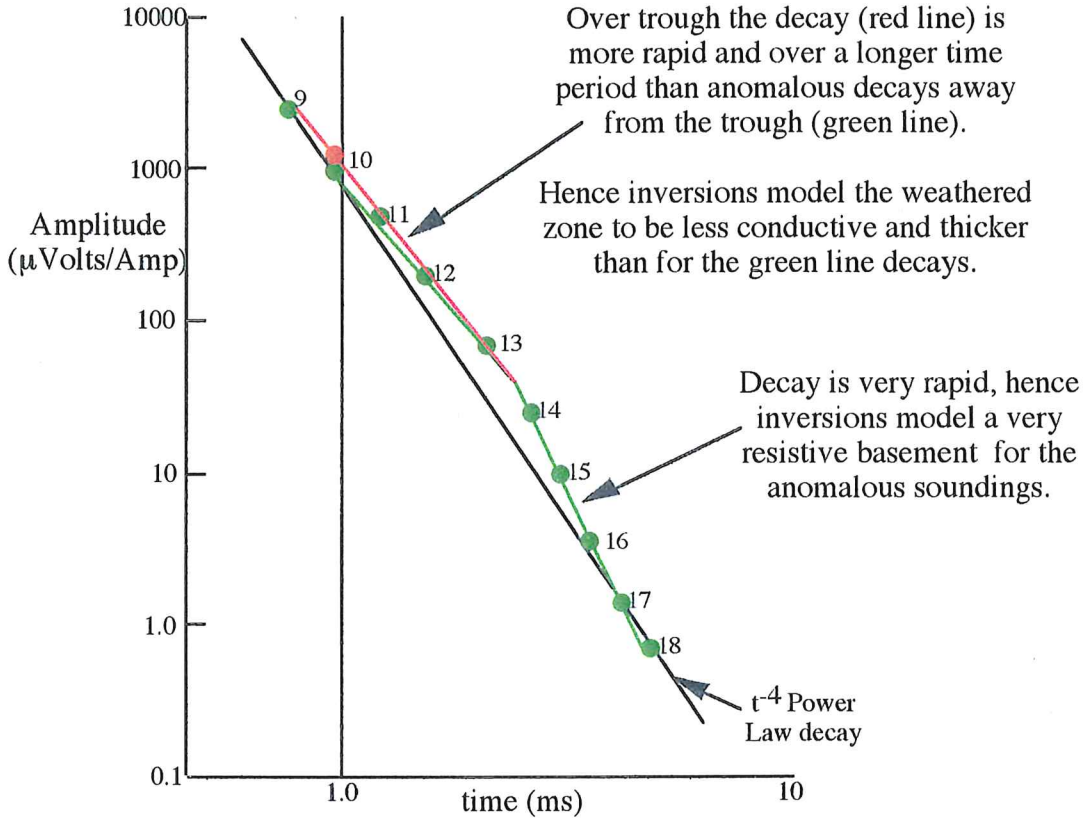

Figure 31: Schematic explanation of the observed weathered zone depression visible on the ***GRENOCC*** inversion of line 90550N (figure 28).

The earlier time response due to the trough causes the apparent depression in the inverted data. However, if the underlying conductor were not present, the inversion result would still show the weathered zone to become slightly thinner and more conductive, because the inversion program attempts to fit a layered earth model to the response of a finite conductor. This can be shown by inverting ***SAMAYA*** models of troughs and conductors.

Inverting the data with ***GRENOCC*** was problematic. Only 10 channels are used in the inversion of over 30 layers. Hence there are far more parameters being inverted than data points, rendering the inversions less reliable. Twelve of the sixty-three soundings could not be inverted with ***GRENOCC***, these were either left blank, or interpolated by griding.

7.0 Schlumberger Vertical Electric Soundings

7.1 Initial interpretation and Curve Matching

The two vertical electric soundings (VES) show three layer H-type curves (figure 32), as would be expected from the weathering profile (figure 2). A brief explanation of vertical electric sounding is given in Appendix 1. The VES at 1500E was first interpreted using curve matching (Telford et al., 1976) with Schlumberger master curves. A reasonable fit was found using 3 layers, the parameters of which are shown in table 6.

Layer	Resistivity (Ω-m)	Thickness (m)
Alluvium	400	3.0
Weathered Zone	25.0	75.0
Fresh Rock	>500	∞

Table 6: Results of curve matching VES at 1500E

The VES at 1200E could not be reliably interpreted by curve matching. When comparing the two soundings, the 1200E VES is more conductive and has a much sharper trough than the 1500E sounding. The very sharp trough makes curve matching of the 1200E VES difficult.

The observed VES curves are incomplete. A complete curve would show the larger transmitter spacings leading upwards at a 45° angle (Telford et al., 1976). An incomplete curve indicates that the weathered zone is still affecting the soundings to some degree, even in the widest transmitter spacings. Larger transmitter separations (eg 650m, 1000m or 1500m) are required to make the conductive overburden a less significant factor in the soundings.

7.2 Layered Earth Inversions

Two layered earth software packages were used to model and invert the VES results. The VES were interpreted by inverting each of the soundings using three, four and five layer models. Several models were made because of the inherent ambiguity of the VES method. For any number of layers greater than or equal to three, there are several models which fit the observed values. The more layers used, the more solutions that can be obtained. Because of the known weathering profile, and to minimise this non-uniqueness problem, a maximum of five layers was used. The top layer represents the resistive alluvium, and the final layer the fresh rock. The weathered zone was represented by one, two or three layers with more resistive layers modelling the partially weathered zone(s).

7.3 Program *VES*

The program ***VES*** is a layered earth forward modelling and inversion program. ***VES*** determines the degree of correlation of the observed and calculated points using the "fit" parameter. The calculation of the fit parameter is unknown, so the standard errors and mean percent symmetric error of all the ***VES*** inversions have been calculated (Appendix 3). The

Figure 32: Comparison of 1200E and 1500E Schlumberger VES

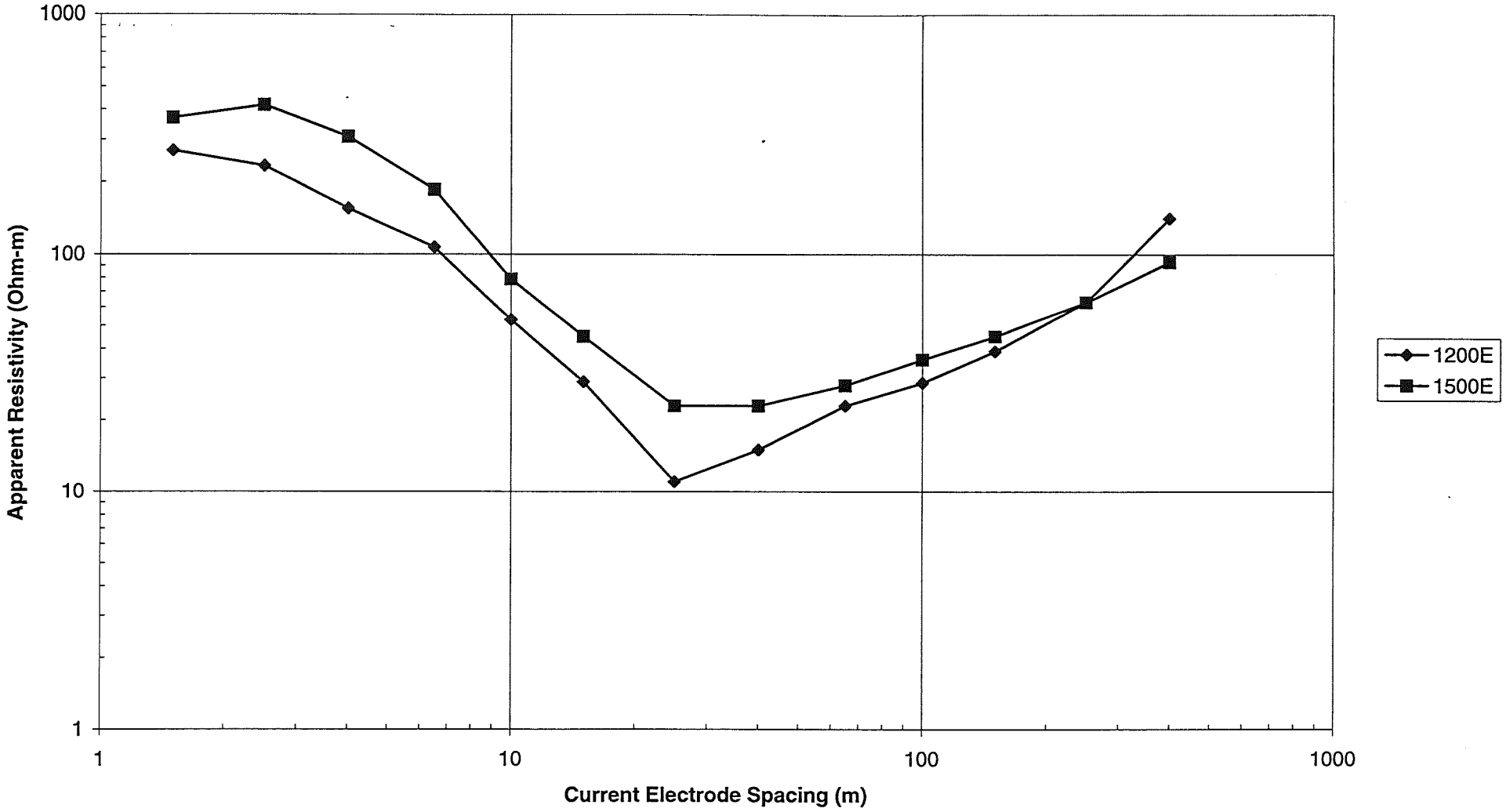

results of the inversions using the program ***VES*** are shown in figure 33. The VES curves calculated using these models are seen in figure 34.

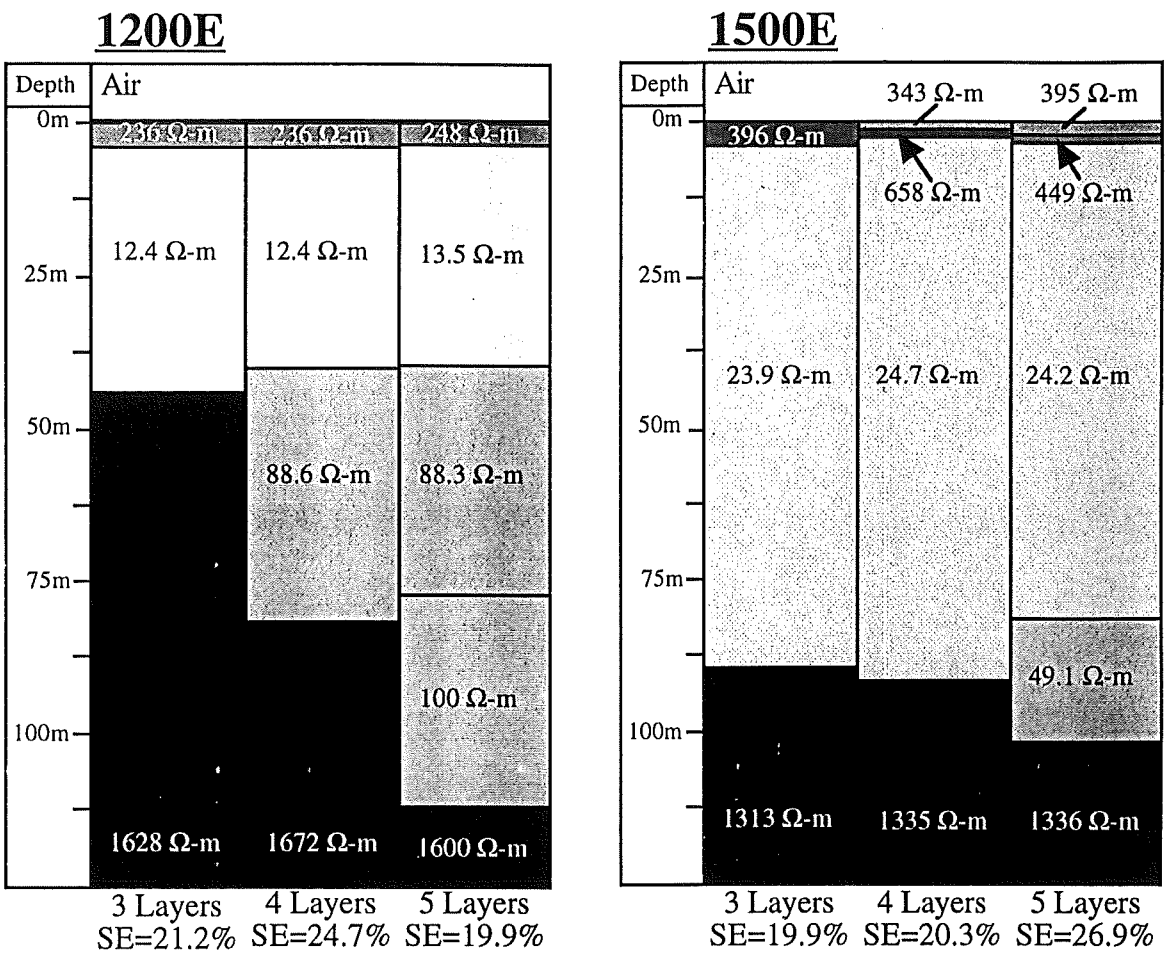

Figure 33: Results for 3, 4 and 5 layer inversions using the program ***VES***.

The 1500E inversion showed better standard errors and mean percent symmetric errors than the 1200E inversion. The 1500E inversion results remain consistent when extra layers are added. The depths to fresh rock and weathered zone resistivities are very similar for all three 1500E inversions. The thin layer(s) of alluvium are about 3.3m thick in all three cases. The second, very resistive layer of alluvium is added because the 2.5m transmitter position measurement has a larger apparent resistivity than the 1.5m measurement (arrow on figure 34). The fresh rock resistivities are all very similar, but these are unlikely to be measured accurately as the field curve is incomplete. The models found for 1500E agree with the curve matching results.

The ***VES*** inversions for 1200E all yielded similar results for the thicknesses and resistivities of the first two layers. The 1200E inversions have resistive layers/basement at shallower depths and larger errors than the 1500E inversions. This is due to the trough on the 1200E curve being much sharper. Because the program is a one dimensional program, the very sharp trough must be fitted by using a thinner and more conductive weathered zone than is seen on the 1500E inversion.

Figure 34: Observed data with 3, 4 and 5 Layer models using program VES.

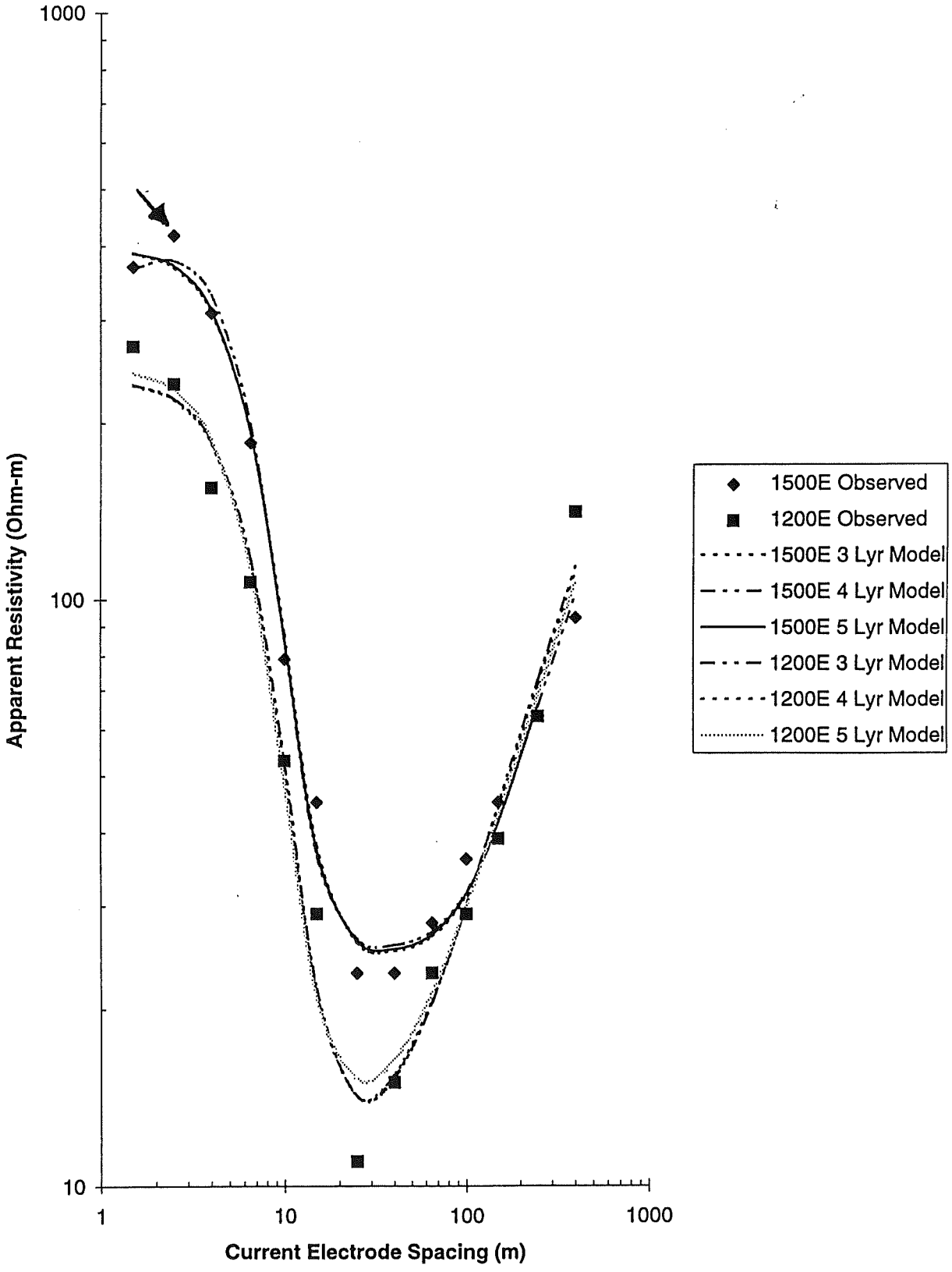

Both the 1500E and 1200E inversions show high standard and mean percent symmetric errors (Appendix 3). The large errors indicate that the ***VES*** inversions are not reliable, even though the inversion results seem reasonable.

The lack of significant improvement in error when extra, deeper layers are added to the inversions indicates that the deep layers are not having much effect on the model. This is better seen using the statistics given by the ***GRENDL*** inversion.

When comparing the calculated curves for the VES inversions, another problem with electrical and electromagnetic inversions becomes apparent. Large changes in the forward model yield only small changes in the calculated curves. In the inverse sense, small changes of the observed data can lead to large changes in the inversion solution. Hence, even though the models for each of the curves can be quite different, the calculated curves are all very similar, and fit the observed data equally well.

7.4 Program *GRENDL*

The ***GRENDL*** algorithm can also perform layered earth VES inversions. The same statistics used for the electromagnetic inversions are used with the VES inversions (Appendix 2). The inversion results are shown in figure 35. The calculated curves for these inversions are shown in figure 36.

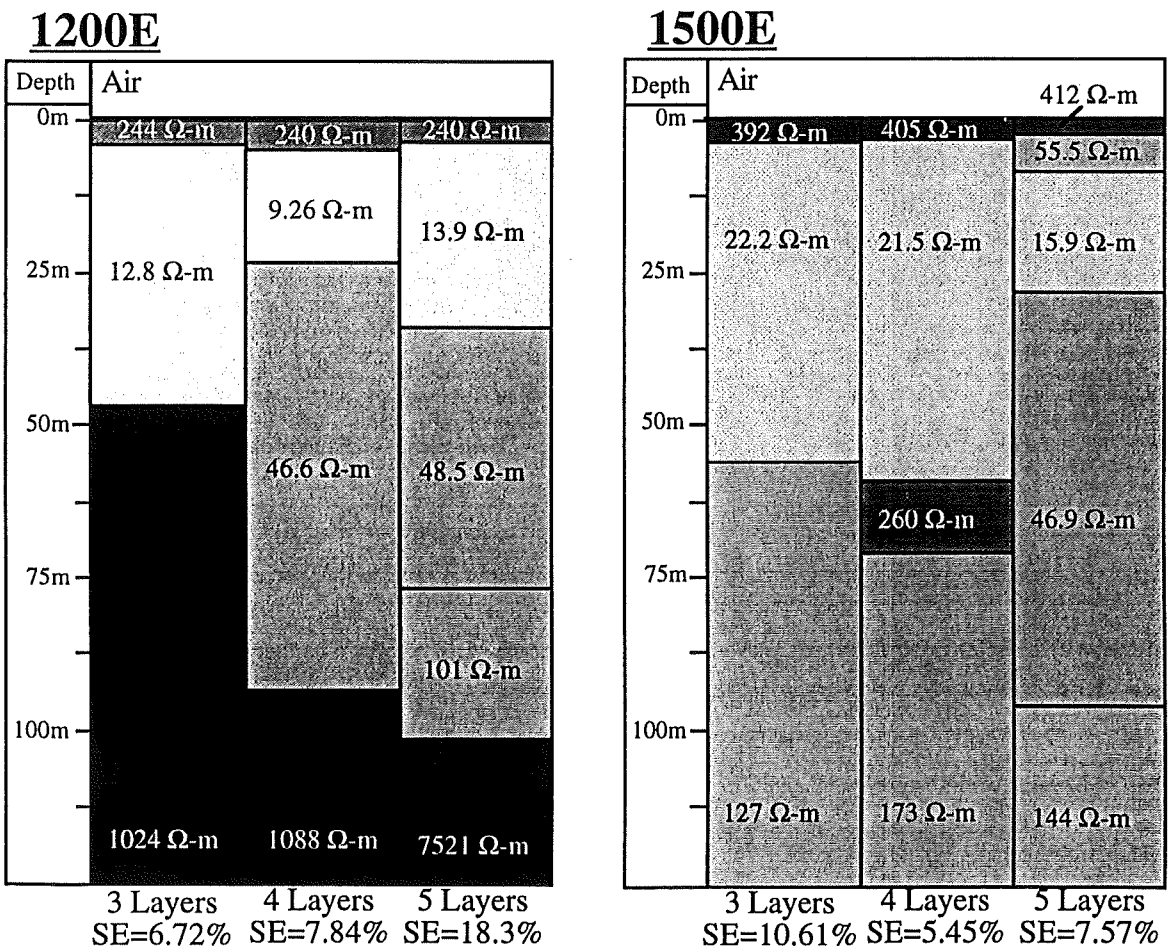

Figure 35: Results for 3, 4 and 5 layer inversions using the program ***GRENDL***.

Figure 36: Observed data with 3, 4 and 5 Layer models using program GRENDL.

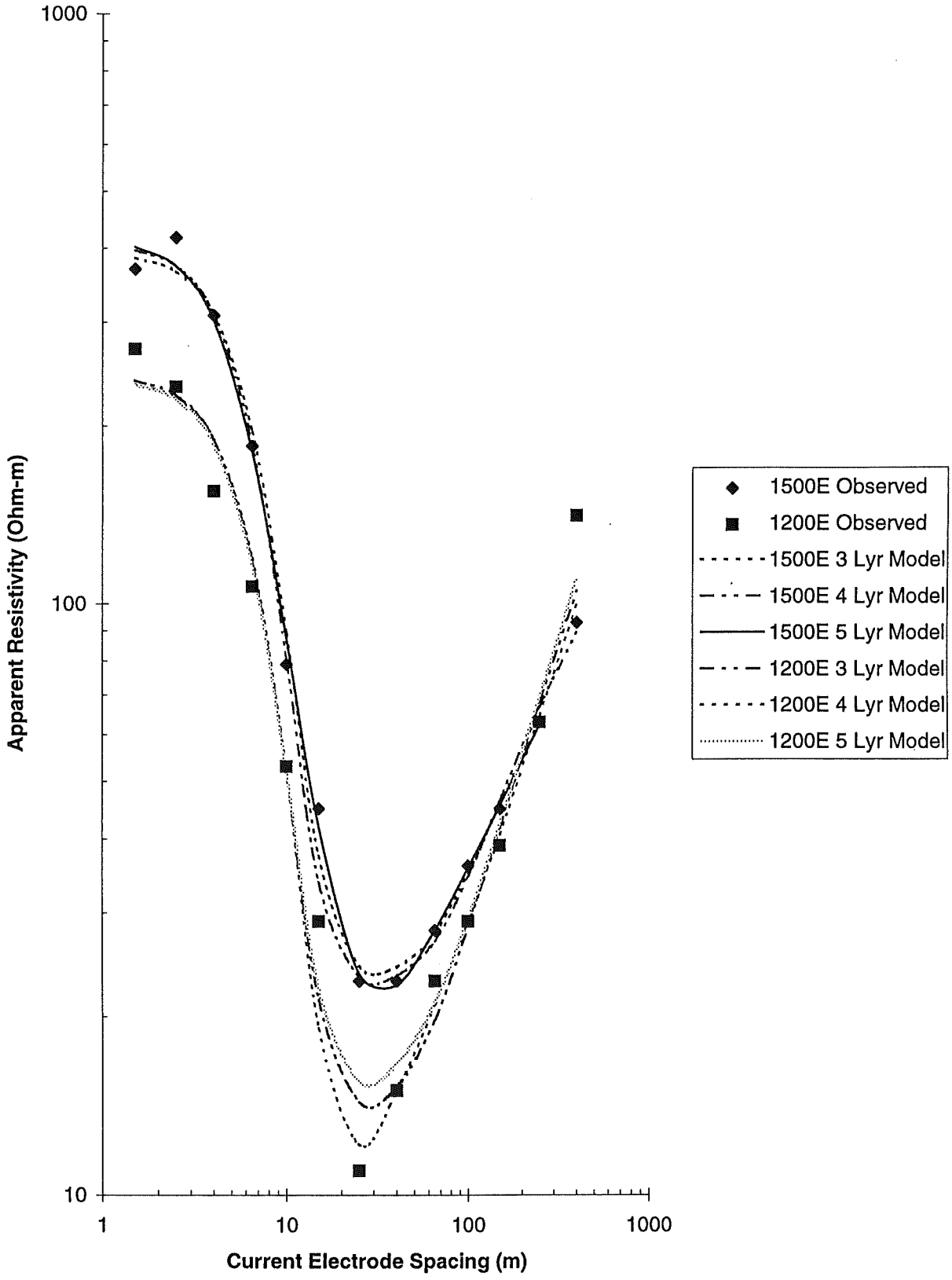

The initial inversions of both the 1500E and 1200E soundings had large errors and were not acceptable. Hence, for all inversions (except 1500E using three layers) weights were applied to some of the observed points. A decreased emphasis (by assigning weights of less than one) was placed on points which showed large weighted percent symmetric errors (ie the worst fitting points).

The results for the 1500E inversions are again better, and more consistent than the 1200E inversions. The four layer inversion was the most accurate of the 1500E inversions, but this is probably due to the use of more weights. The statistics of the four layer inversion (Appendix 4) show that the third and most resistive layer is unbounded for both thickness and resistivity. The top layer (alluvium) is very well interpreted, with results which correspond with the ***VES*** inversion. The conductive weathered zone resistivity is well constrained, and also correlates with the ***VES*** inversions. Neither of the three, four or five layer inversions are statistically reliable, especially the average predicted residual error and layer bounds. The ***GRENDL*** inversions show lower errors than the ***VES*** inversions.

There are several differences between the ***GRENDL*** and ***VES*** inversions for 1500E. ***GRENDL*** interprets the weathered zone to be much thinner; 50-60 metres compared with 80-85 metres using ***VES***, but with similar resistivities. ***GRENDL*** has modelled a relatively conductive basement because the curves are incomplete. The basement resistivity is poorly bounded, the worst example being the 5 layer inversion which gave resistivity bounds from 10 to 2055 Ohm-m. This degree of bounding indicates that the weathered-fresh rock interface is poorly constrained, and cannot be accurately determined by vertical electric sounding.

The ***GRENDL*** inversions of the 1200E VES were heavily weighted on most points (Appendix 4). The three layer ***GRENDL*** model is quite similar to the ***VES*** inversion, and also has the smallest standard error. The alluvium thickness and resistivity, and the weathered zone resistivity are well constrained by the inversion. All other layers are not constrained, and their inverted values cannot be relied upon. The very conductive lower bounds for the bottom layers indicate that the weathered zone is possibly thicker than the inversion suggests.

Both the ***VES*** and ***GRENDL*** inversions over 1200E do not correspond well with the known drilling results. The sounding taken at 1200E was centred directly over the known location of the weathering trough and deep conductor. One dimensional inversions can not accurately interpret data collected over lateral inhomogeneities. Hence a layered earth model cannot give a reasonable interpretation over the weathering trough and conductor. The conductor will channel some of the transmitted current deeper, causing the 1200E sounding to be more conductive and exhibit a sharper trough.

8.0 Joint SIROTEM / Vertical Electric Sounding Inversion

GRENDL provides the option of simultaneously inverting a SIROTEM sounding and VES. Several authors have shown this method to be very accurate (Vozoff and Jupp, 1975; Vozoff and Jupp, 1977; Jupp and Vozoff, 1975; Raiche, 1984; Fitterman, 1988; Raiche et al., 1985). However trials of this method, using the soundings taken at 1500E, showed very poor results, with errors over 100%. Further experiments with weighting the data points managed to reduce this error down to 30%, but the inversion still cannot be relied upon.

It is likely that neither the SIROTEM or the VES are completely sensing the fresh rock. As previously mentioned, electromagnetic methods only give diagnostic information on conductive layers. The VES, even at large transmitter separations, are being significantly influenced by the conductive weathered zone, and hence are incomplete. The weathering trough may also have affected the 1500E VES results, especially on the widest electrode soundings.

The taking of more readings would have greatly enhanced the effectiveness of the joint inversion technique. This could have been achieved by using short SIROTEM time channels, and not the composite channels. The VES could have been improved by taking more readings per decade, and out to greater distances (eg 650m and 1000m). The requirement for greater data density is seen when the 1998 survey is compared with results presented in the Jupp, Vozoff and Raiche articles. Raiche et al. (1995) required 18 current electrode spacings out to 1000m distance to interpret a thin, shallow and very conductive layer (compared with a thicker, less conductive weathered zone).

9.0 Dipole-Dipole Resistivity and Induced Polarisation

9.1 Initial Interpretations

Pseudo-sections of the raw apparent resistivity and chargeability are shown in figure 37. Appendix 1 provides a brief explanation of dipole-dipole resistivity and induced polarisation techniques. The apparent resistivity indicates a generally layered earth response with resistivity increasing with depth. This corresponds with the known conductivity structure. The n=1 dipole spacing would be sensing only the conductive weathered zone. As dipole spacing increases, the bulk resistivity (ie apparent resistivity) will decrease as the resistive fresh rock becomes increasingly more prominent.

A "first glance" interpretation of bedrock topography may be made using the boundary between yellow and green in the resistivity pseudo-section. The bedrock topography appears to show a trough near 101150E (1150E).

The induced polarisation does not show any obvious chargeable bodies. The background chargeability is 1.2 to 1.7 millivolts per volt. There are some deep deviations from this background, with highs of 4.4 mV/V and lows of -2.0 mV/V. These deviations are not large and tend to be localised. There are no "pants leg" anomalies that indicate a chargeable body.

9.2 Zonge Smooth Model Resistivity Inversion

The two dimensional Zonge Engineering smooth model inversion was applied to the resistivity and IP data (figures 38 and 39). The inversion results are separated into three parts. The bottom diagram is the pseudosection of the raw data. The top figure is the inversion results plotted as a cross-section. The middle diagram is a forward model pseudosection using the inverted model. The forward model can be compared with the observed pseudosection to determine the accuracy of the inversion. Both the IP and resistivity forward models show good correlations with the observed data.

The resistivity inversion confirms much of the initial interpretation. The Zonge program is a two dimensional smooth model inversion. A smooth model inversion will not give sharp resistivity contrasts, especially for double dipole data, because bulk resistivity is measured over a large volume for each reading. Hence the resistivity inversion shows a gradational variation from a shallow conductive zone (<25 Ohm-m) to a deep resistive zone (>251 Ohm-m). The generally low resistivity at depth is due to the effect of the conductive overburden. Apparent resistivity is, essentially, the average resistivity over a volume of rock. Hence the conductive surface zone will lower the average resistivity measured by the larger dipole separations.

The actual specifics, namely depth and resistivity/chargeability of any double dipole inversion must be considered suspect. One hundred metre dipoles were used in the survey, so even at the n=1 spacing the transmitter and receiver centres are 200 metres apart (figure 5). Hence even at n=1 spacing, the bulk resistivity is being determined from a large volume of rock. The large dipoles were used to increase the depth of penetration in a region that is known to have a conductive weathered zone. Resolution, both lateral and vertical, was sacrificed for increased depth penetration. Hence the resistivities seen in the inversion, especially at depth (n=3 to 6), must not be used. Instead it is the *change* in resistivity which should be considered.

Figure 37: Dipole-dipole resistivity and induced polarisation pseudosections.

LINE 90500E

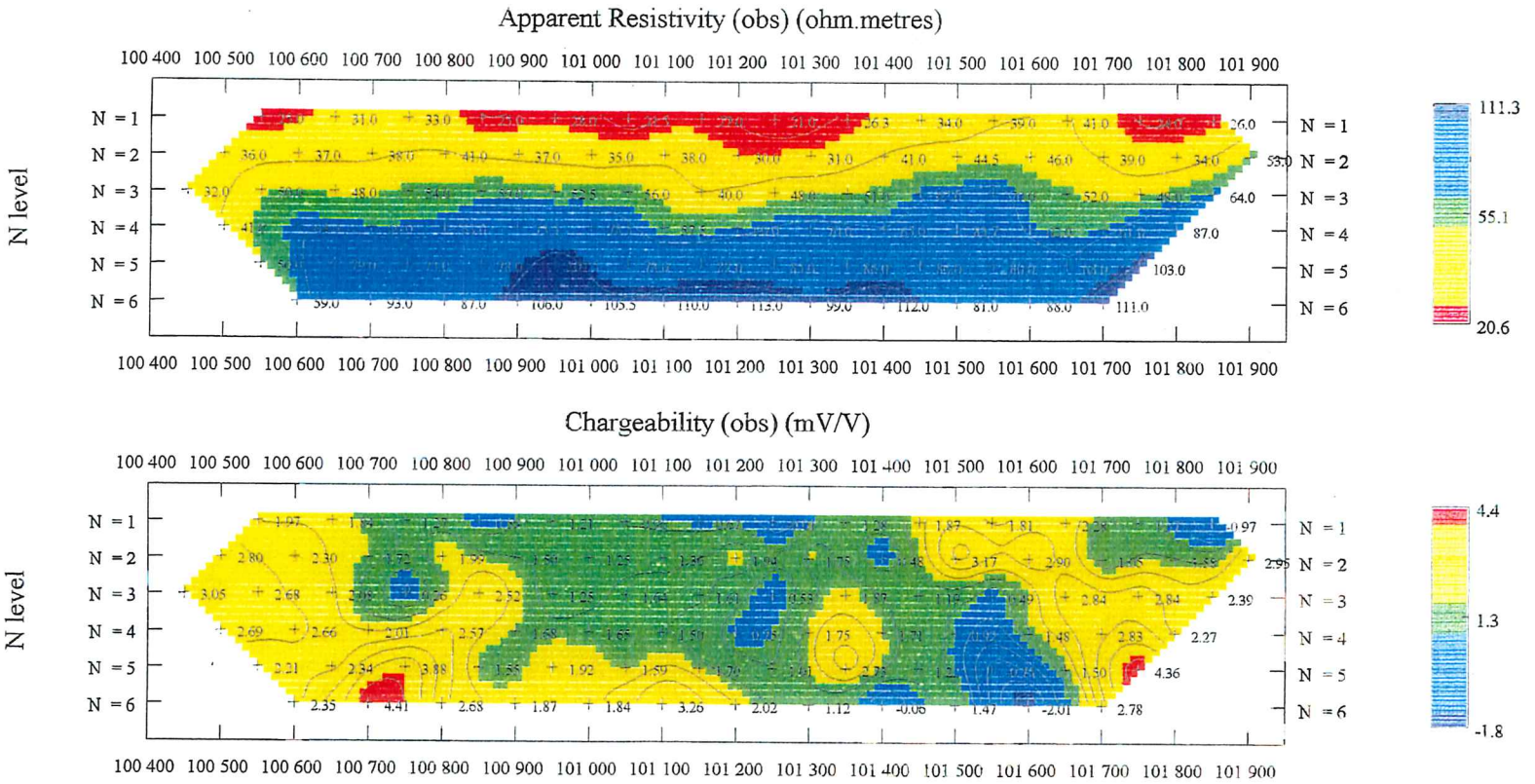

Scale 1: 10 000

0 200 400 600 800

meters

MARK TINGAY	
NUMBER 4 TANK 100M DIPOLE - DIPOLE	
SCINTREX TSQ-4 SCINTREX IPR-12	
Author :	Ref :
Drawn :	
Date : 14-Jul-1998	Report No :
Scale 1: 10 000	Plan No :

Figure 38
Number 4 Tank
Line 90500N

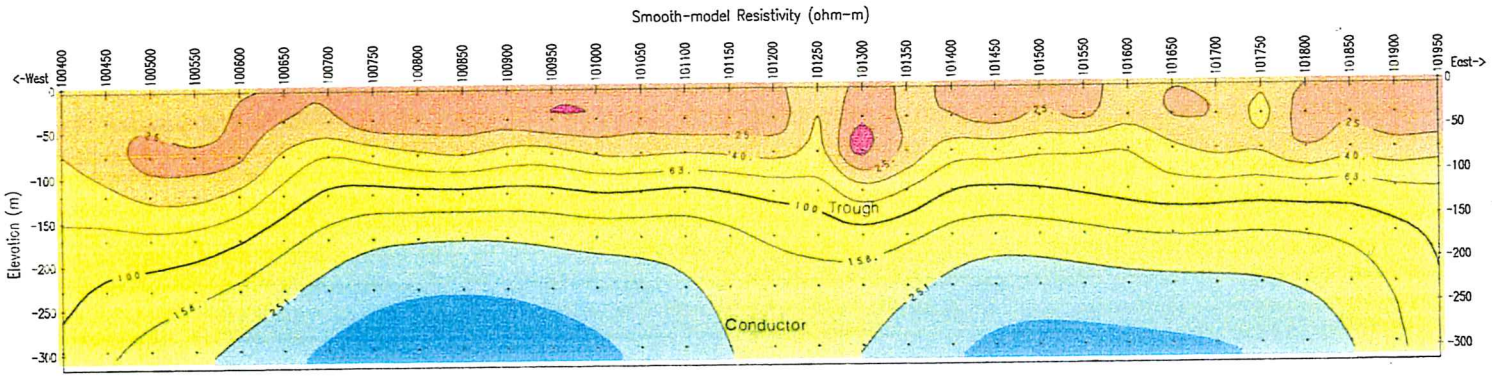

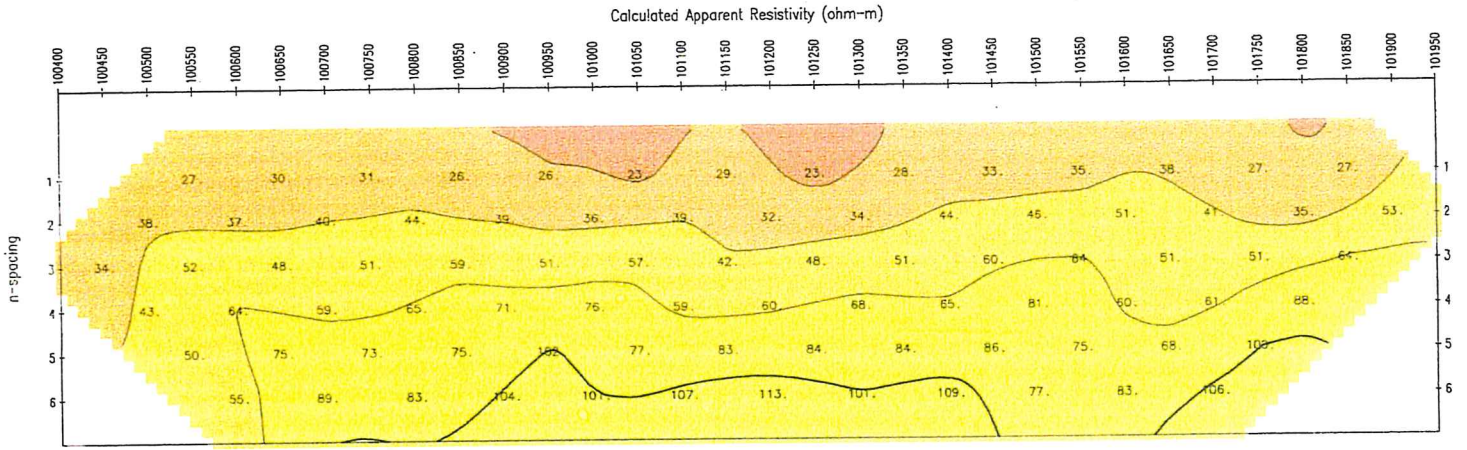

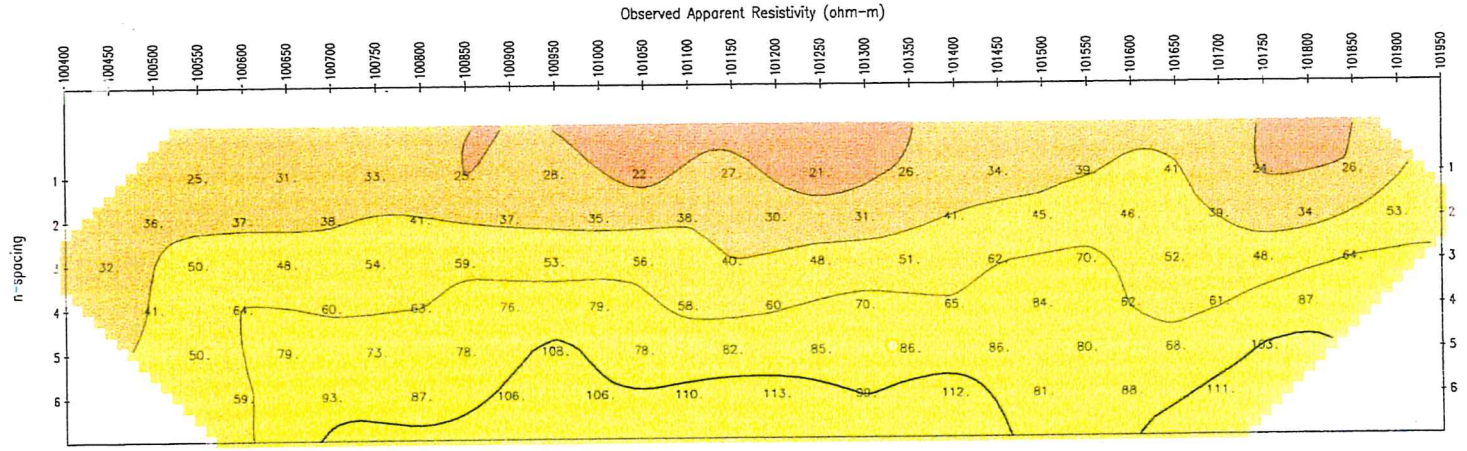

Survey Parameters:
100m dipole-dipole data
0.125 hertz repetition rate
Observed data from 90500.Z

Inversion Control Parameters:
Receiver: Scintrex IPR-12

Inversion control parameters:
ResSmth=1.0,dpW=1,dxW=1,dzW=1

631
251
100
40
16
6
Resistivity ohm-m

50 0 50 100 150 200 250 300 350
(metres)

Zonge

Mark Tingay

Number 4 Tank

Line 90500N

2D Smooth-model Inversion of Dipole-Dipole Resistivity Data

AUTHOR	DRAWN	DATE	SCALE	REPORT
Zonge	Zonge	030698	1:5000	
PEF: Job			B90500.*	JOB 4-378

Figure 39
Number 4 Tank
Line 90500N

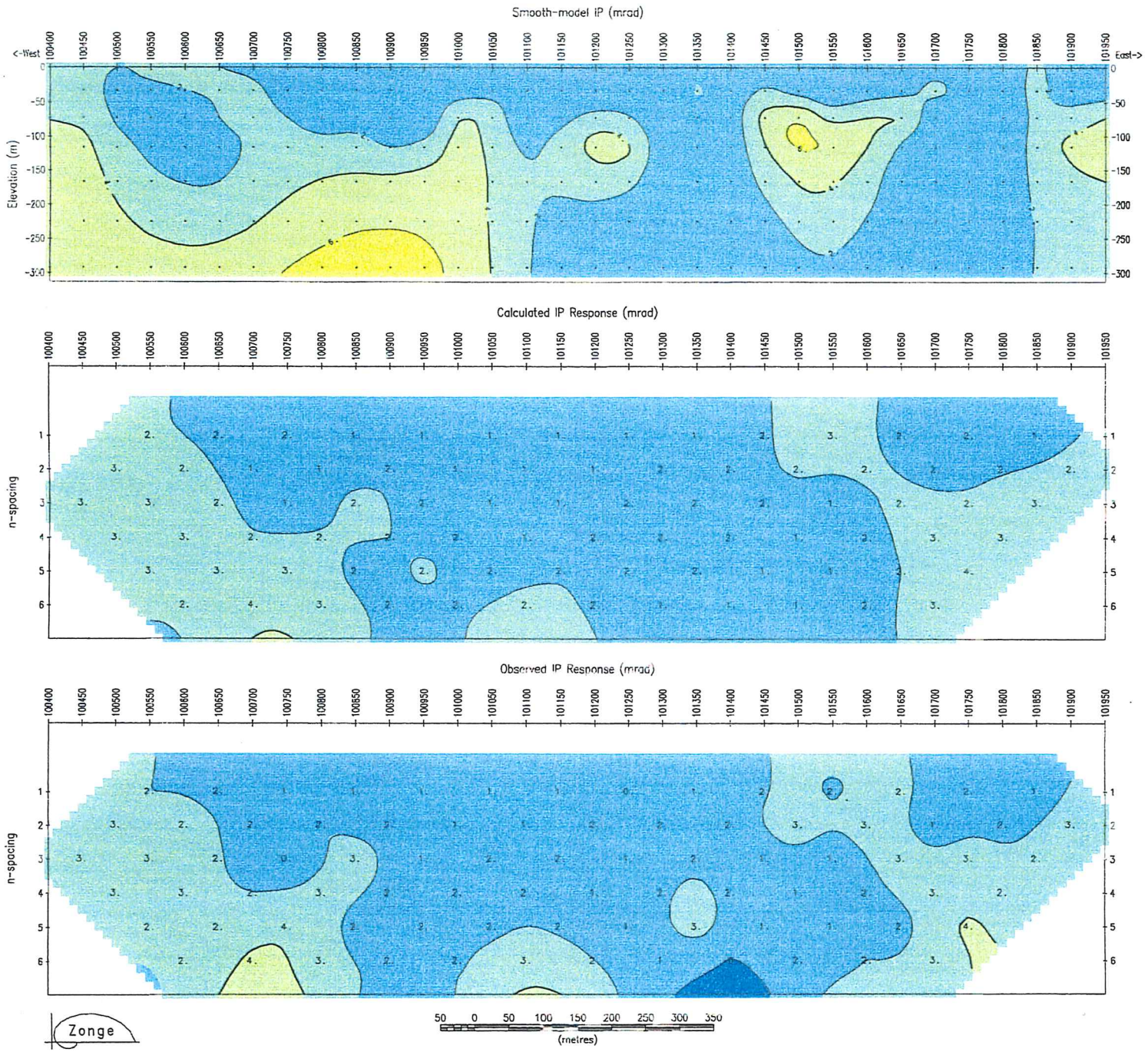

Survey Parameters:
100m dipole-dipole data
0.125 hertz repetition rate
Observed data from 90500.Z

Inversion Control Parameters:
Receiver: Scintrex IPR-12

Inversion control parameters:
IPSmth=0.1,dpW=0.5,dxW=1.,dzW=1.

28 24 20 16 12 8 4 0
IP mrad

Mark Tingay

Number 4 Tank

Line 90500N

2D Smooth-model Inversion of Dipole-Dipole IP Data

AUTHOR	DRAWN	DATE	SCALE	REPORT
Zonge	Zonge	030698	1:5000	
REF: Lab			890602.*	JOB 4-378

The inversions will also give unrealistic depths. The rule of thumb for 100m dipoles would be that n=6 corresponds approximately with 300-350 metres maximum depth of exploration. A thick, conductive surface layer causes the current to be "short circuited", shying away from the resistive fresh rock. Consequently, even at the n=6 level the current would be unlikely to be sensing the fresh rock at any significant depth (Telford et al., 1976; Dobrin and Savit, 1988). Hence the 300 metre depths shown by the inversion are unlikely to be accurate. The change in depth must be used in interpretation, just as for resistivity.

The major feature of this inversion is that it is two dimensional, which provides a measure of the bedrock topography, and also of the conductivity variations within the weathered zone and fresh rock. The weathered-fresh rock interface appears to dip gently to the west.

A bedrock depression is shown near 101300E (1300E) by following the 63, 100 and 158 Ohm-m contours. This depression is most likely the weathering trough defined by the RAB drilling. The inverted location of the trough is 75 metres to the east of its known position (figure 3). This offset is due to the decrease in lateral resolution when using large dipoles. A survey performed with 50 metre dipoles would probably better define the position and size of the trough.

The depths given by the inversion cannot be relied upon, but we can use the relative change in depth to determine bedrock topography. Using inversion results, or preferably drill hole information as a starting depth, the bedrock topography can be approximated by interpolating along the resistivity contours.

An average of the change of the 63, 100 and 158 Ohm-m contours was used to interpolate the bedrock topography. The 1500E VES, the 850E and 1650E SIROTEM sounding, and RAB holes NFR 470 and 473 (figure 3) were used as starting points. The interpolation results (figure 40) show that the two SIROTEM interpolations gave the best results for trough depth. The interpolated trough is wider than expected because of the decreased resolution when using large dipoles. The trough is still displaced 75m to the east. The similarity between the two SIROTEM interpolations is further confirmation of the ***GRENDL*** TEM and Zonge resistivity inversions.

A zone which is more conductive than the surrounding rocks underlies the depression. This deep conductive zone is approximately 100 metres wide, and underlies the known location of the weathering trough. This further confirms the presence of a conductor at depth, as indicated by the SIROTEM. The good results shown by the dipole-dipole resistivity make this a very useful method. The electromagnetic anomaly visible on the northern line (90800E) would be a good location for another line of double dipole resistivity.

9.3 Zonge Smooth Model Induced Polarisation Inversion

The inverted IP results (figure 39) confirm the initial interpretation that there are no chargeable bodies detected by the survey. The induced polarisation was not expected to show any response, as there are very few chargeable rocks in the area. Both the weathered zone and CSA siltstone have a very low chargeability. Only an ore body, or disseminated pyritic layer would be likely to exhibit a good IP response.

Figure 40: Comparison of Depth to Fresh Rock Interpolations with RAB results. RAB results shifted 75m east to compare troughs.

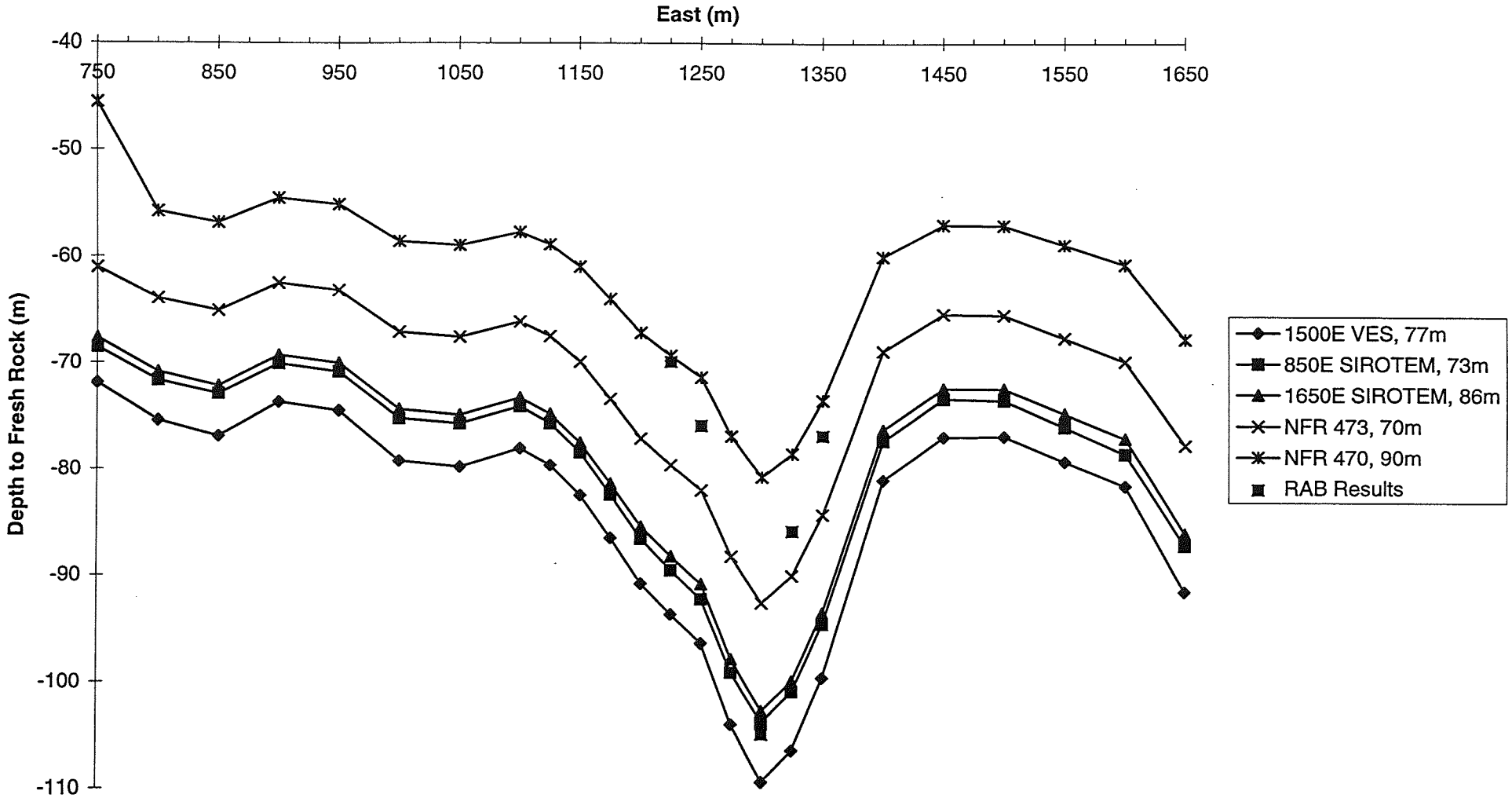

When examining the IP decay curves, seven curves were found to have bad decays. Figure 41 shows eight decay curves, with the 101100E curve being a normal, good decay. Electromagnetic coupling is present in both 101250E curves, the 101350E curve and possibly the two 101850E curves. EM coupling is caused by "mutual inductance between the current and potential wires both directly and through the ground in their vicinity" (Telford et al, 1990). EM coupling is most prominent in weathered terranes and is usually seen as a negative early time response because of the galvanic response of the conductive weathered zone. Time domain, dipole-dipole surveys minimise the effects of EM coupling, hence very few measurements in this survey exhibited EM coupling.

Figure 41: Bad IP decay curves. 101100E is a normal decay curve. 101250E, 101250E and 101350E decay curves exhibit EM coupling.

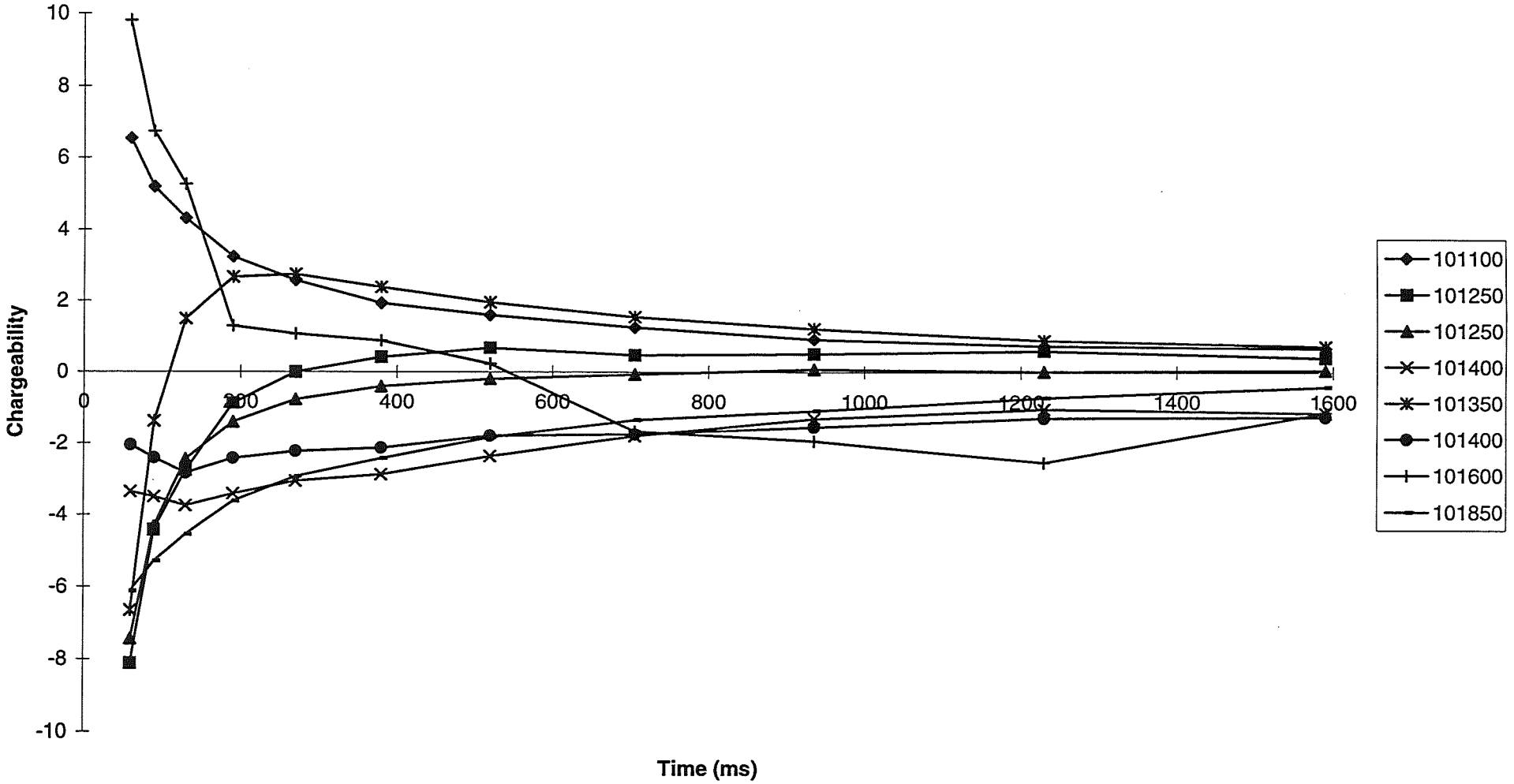

10.0 Gravity

The raw gravity data was firstly drift and instrument corrected. The surveyed elevations were used for the free air and Bouguer correction. A Bouguer density of 2.6 g/cc was used in the Bouguer correction. There is very little terrain in the region and less than 8 metres elevation difference over the survey area, hence no terrain corrections need be applied.

10.1 Regional Removal

The Bouguer corrected gravity highlighted a very strong regional gradient, which is common in the Cobar region. The regional gradient was calculated from the regional survey previously performed over the area. Pasminco has collected regional gravity data at 100m station spacing, and with a line spacing of 250m. The regional data was collected along the same lines as the 1998 survey hence 33 of my 75 stations were repeats of the regional data. The repeated 1998 survey station measurements compare well with the regional survey results.

The regional gravity over the Number Four Tank area was calculated on the program ***GEOSOFT***. The strong regional gradient dips east in the same direction as the survey lines.

10.2 Prospect Scale Residual

The regional gradient was first subtracted from the regional data to create a residual map over the entire prospect (figure 42). The residual gravity shows that there is a 14 gu variation over the entire region, and about 5 gu variation over my survey area (three black lines near AMG co-ordinates 368500, 6564000). The residual gravity indicates that the survey was carried out over a broad gravity high which strikes north-west. The survey area is located at the edge of a narrowing of the north-west trending high, from 3.0 kilometres wide to less than 1.5 kilometres wide. The north-west trending high is also decreased in amplitude, by approximately 3 gu, over the survey area. The half-width of these features indicates that their sources are located within the basement, at depths of at least 150m.

The fold axes plunge north-west in this region of the Cobar basin (Schmidt, 1990) and the parallel north-west trending gravity highs are possibly associated with this folding. The narrowing of the gravity high is possibly related to the north-east trending transfer faults which cross-cut the Cobar Basin (Schmidt, 1990).

10.3 1998 Survey Residual

The regional gradient was then removed from my survey data and the gravity profiles modelled using ***POTENT***. A first gravity model (figures 43-46) was created using the bedrock topography interpreted from SIROTEM and resistivity interpretation. The main features of this model are described in table 7. The gently sloping bedrock topography is seen on the dipole-dipole resistivity inversion (figure 38). The southern line (90250N) required an additional body (body 7) to decrease the depth to bedrock. Two small, thin bodies (3 and 4) were added to the central and northern lines respectively to represent small variations in bedrock topography.

The dimensions of the trough and deep conductor (table 7) are estimated from the resistivity and SIROTEM. The gravity responses for the low density trough and high density

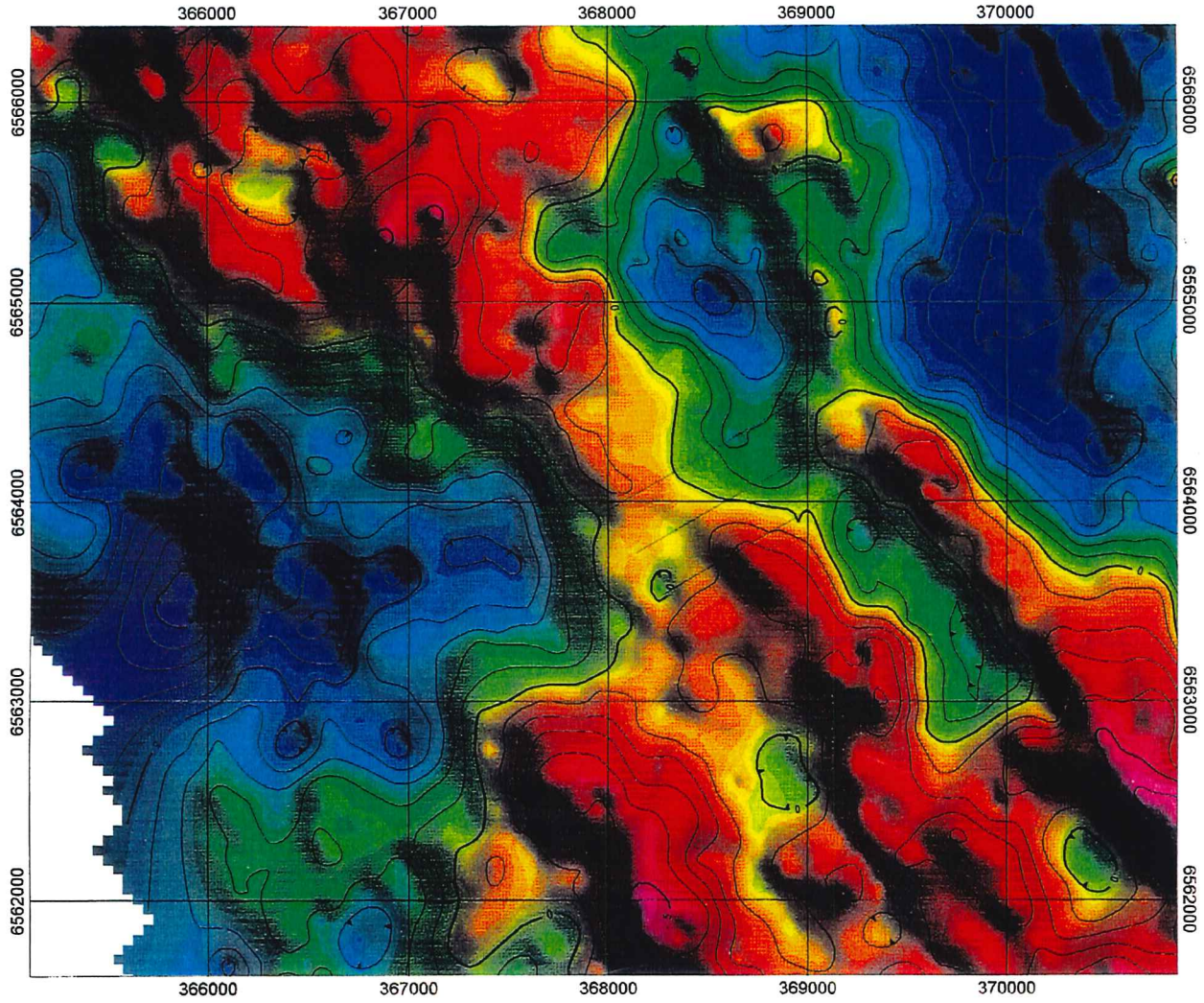

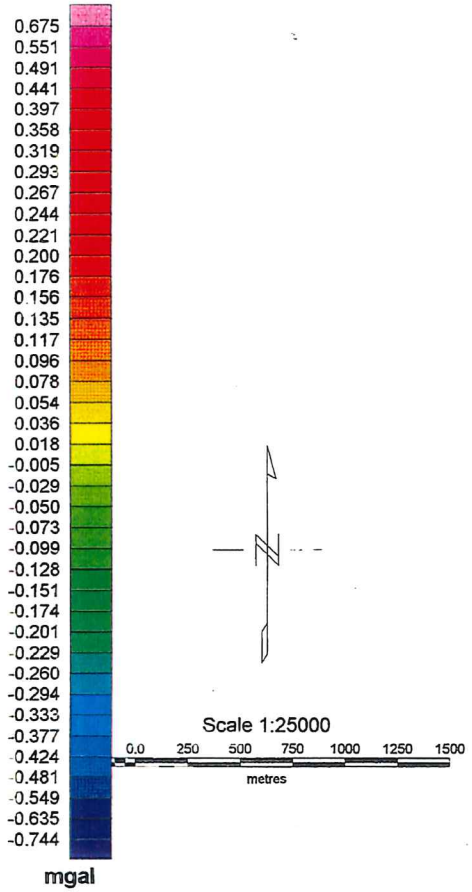

Figure 42

Pasminco Exploration
Number 4 Tank, Cobar, NSW **Residual Gravity**
Data collected at 100m x 250m interval Gridding : Min Q @ 50m Contour Interval : 0.1, 0.5, 2.5 mgal Sunshading : Inclination 60, Declination 45

Figure 43: Plan view of initial gravity model based on SIROTEM and resistivity interpretations.

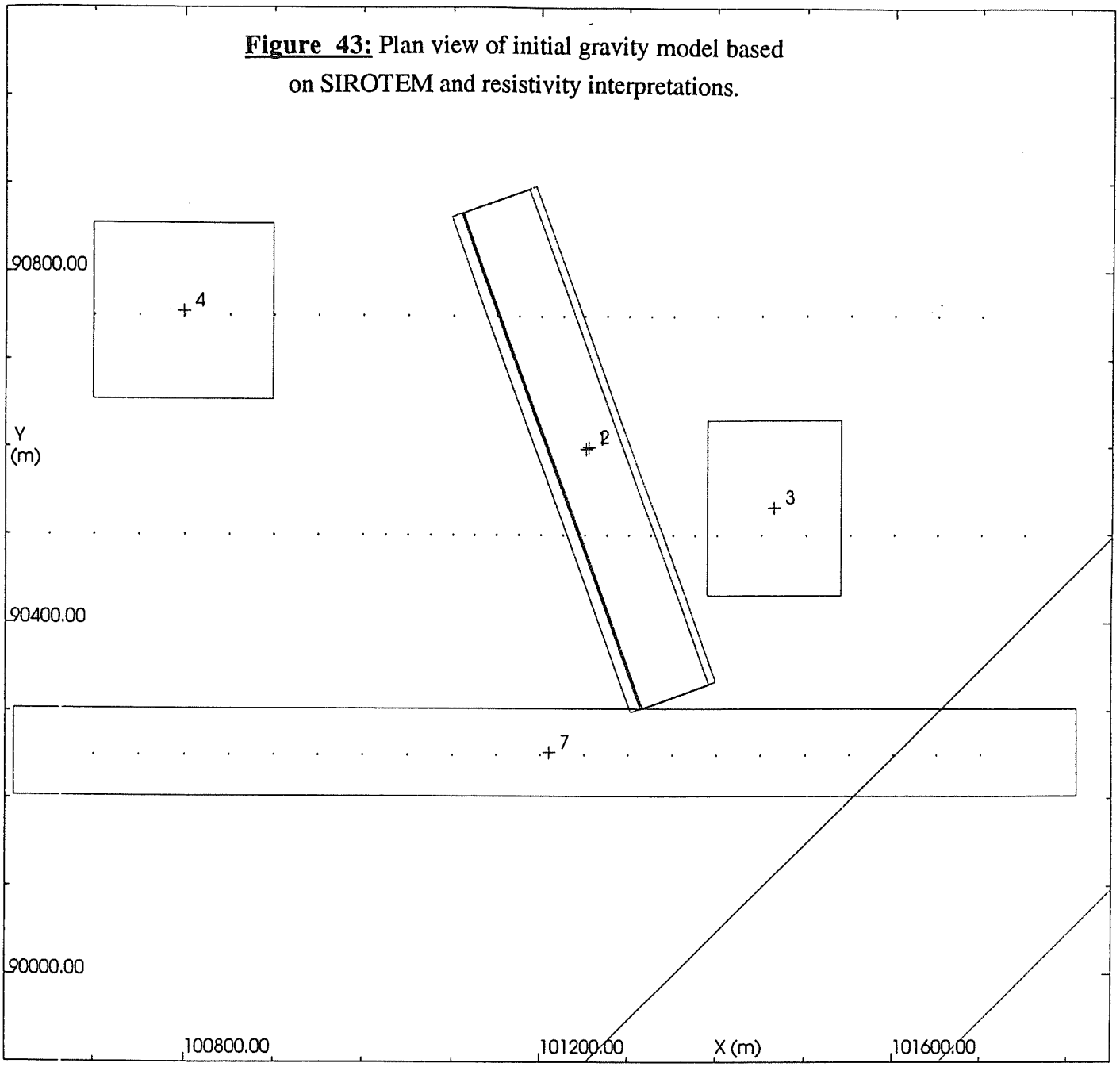

POTENT v3.09 Model Summary Report created at for University of Adelaide - Educational use

Model title:

No.	Type	X m	Y m	Depth m	Strike deg	Dip deg	Plunge deg	Density gm/cc	A	B	C	D
1	Rect	101251.43	90598.52	77.14	340	94	0	-0.60	80.00	600.00	40.00	
2	Rect	101254.29	90600.49	112.86	340	94	0	0.15	90.00	600.00	180.00	
3	Rect	101464.29	90531.36	76.79	0	90	0	-0.90	150.00	200.00	15.00	
4	Rect	100798.56	90754.62	58.57	0	90	0	0.30	200.00	200.00	10.00	
6	Poly	99588.89	90500.00	0.00	45	90	0	-0.90	0.00	Inf	0.00	
7	Rect	101209.99	90253.03	64.29	0	90	0	0.50	1200.00	100.00	30.00	

Figure 44: Line 90500N cross section of initial gravity model based on SIROTEM and resistivity interpretations.

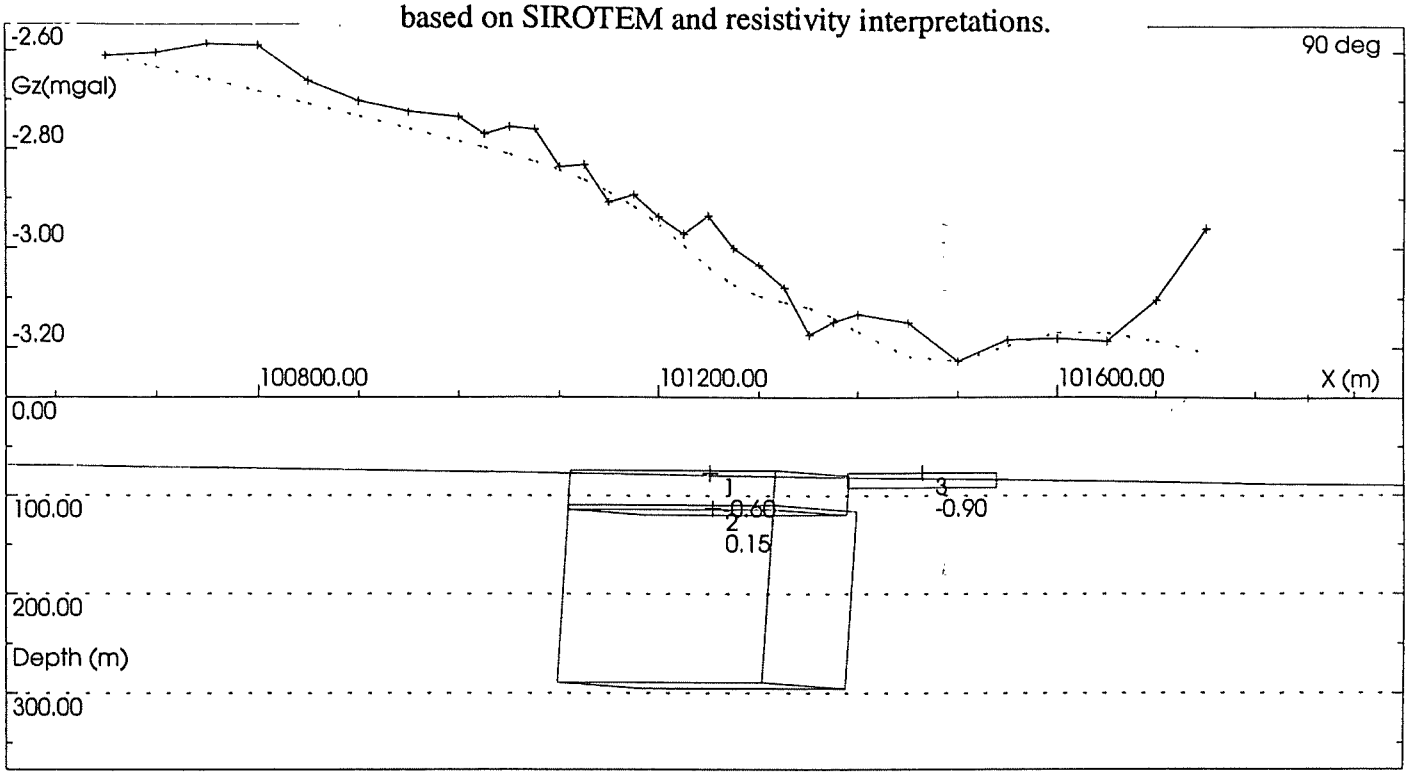

Observations:	East ,North,Residual
Profile #2;	90500N
Model:	
Calculation mode:	Z gravity vector component
Observed:	——————— Calculated: - - - - - - - - -
Residual:	. . . . . Individual body: . . . . .
POTENT v3.09	Profile drawn at 11:08 29/10/1998 for University of Adelaide - Educational use

POTENT v3.09 Model Summary Report created at for University of Adelaide - Educational use

Model title:

No.	Type	X m	Y m	Depth m	Strike deg	Dip deg	Plunge deg	Density gm/cc	A	B	C	D
1	Rect	101251.43	90598.52	77.14	340	94	0	-0.60	80.00	600.00	40.00	
2	Rect	101254.29	90600.49	112.86	340	94	0	0.15	90.00	600.00	180.00	
3	Rect	101464.29	90531.36	76.79	0	90	0	-0.90	150.00	200.00	15.00	
4	Rect	100798.56	90754.62	58.57	0	90	0	0.30	200.00	200.00	10.00	
6	Poly	99588.89	90500.00	0.00	45	90	0	-0.90	0.00	Inf	0.00	
7	Rect	101209.99	90253.03	64.29	0	90	0	0.50	1200.00	100.00	30.00	

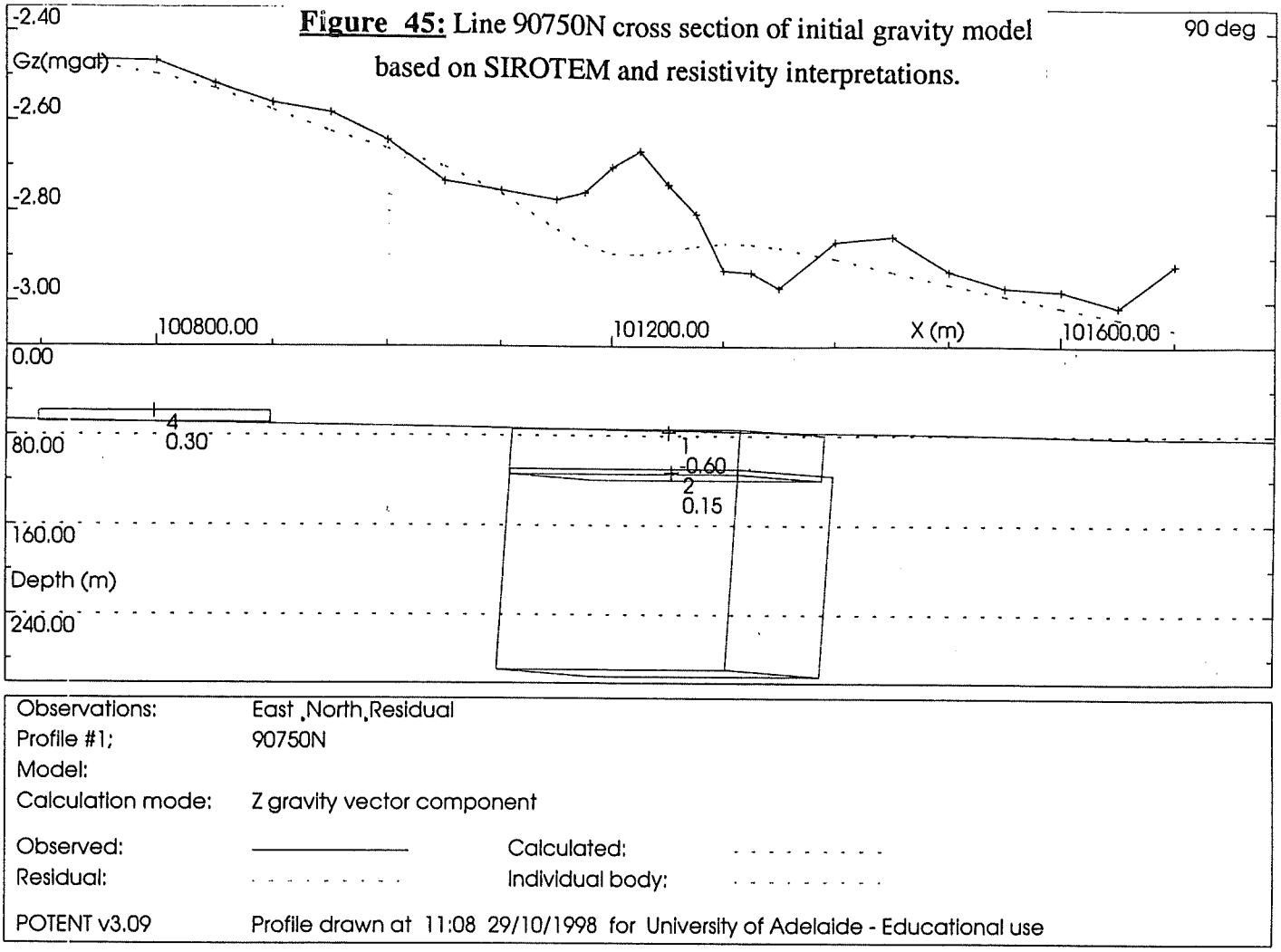

Figure 45: Line 90750N cross section of initial gravity model based on SIROTEM and resistivity interpretations.

POTENT v3.09 Model Summary Report created at for University of Adelaide - Educational use

Model title:

No.	Type	X m	Y m	Depth m	Strike deg	Dip deg	Plunge deg	Density gm/cc	A	B	C	D
1	Rect	101251.43	90598.52	77.14	340	94	0	-0.60	80.00	600.00	40.00	
2	Rect	101254.29	90600.49	112.86	340	94	0	0.15	90.00	600.00	180.00	
3	Rect	101464.29	90531.36	76.79	0	90	0	-0.90	150.00	200.00	15.00	
4	Rect	100798.56	90754.62	58.57	0	90	0	0.30	200.00	200.00	10.00	
5	Poly	99588.89	90500.00	0.00	45	90	0	-0.90	0.00	Inf	0.00	
7	Rect	101209.99	90253.03	64.29	0	90	0	0.50	1200.00	100.00	30.00	

Figure 46: Line 90250N cross section of initial gravity model based on SIROTEM and resistivity interpretations.

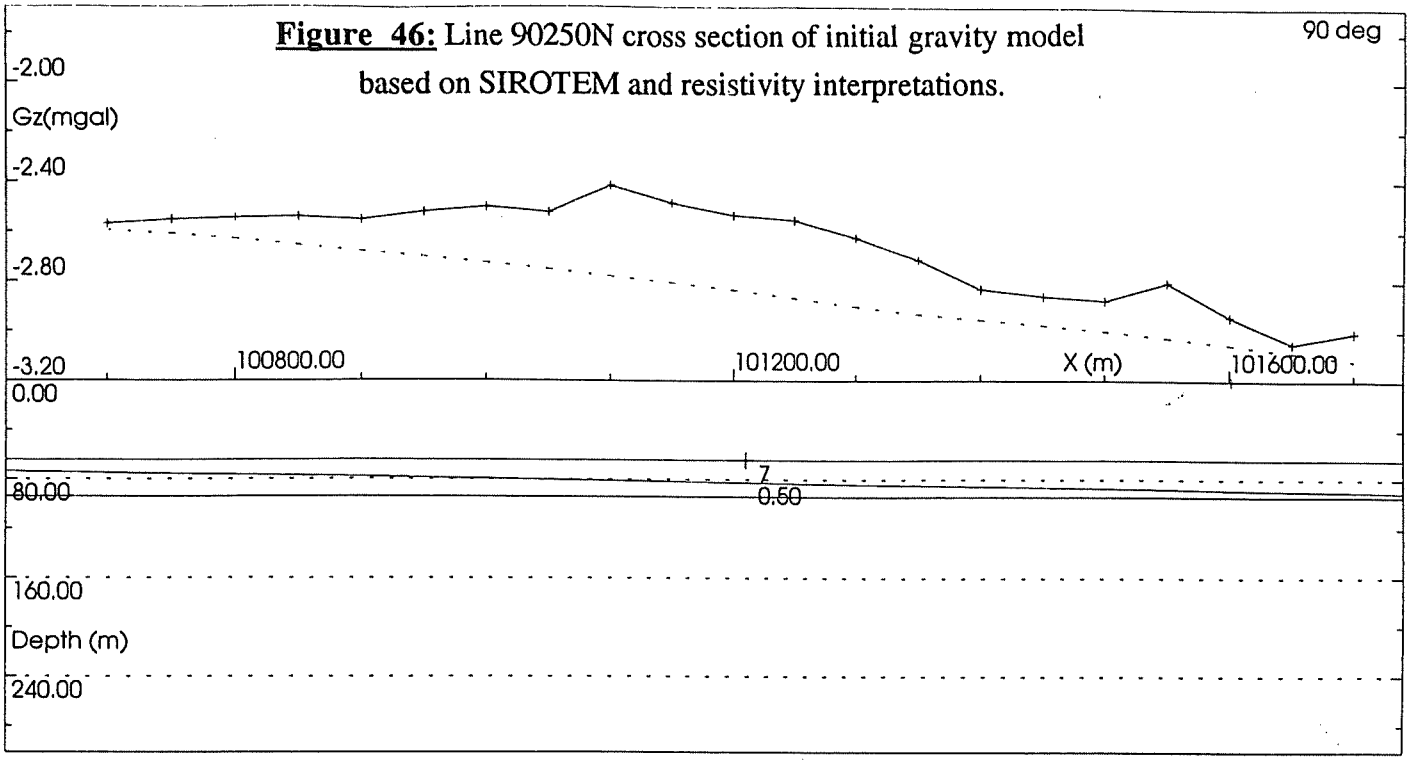

Observations:	East ,North,Residual
Profile #3;	90250N
Model:	
Calculation mode:	Z gravity vector component
Observed:	———— Calculated: . . . . .
Residual:	. . . . . Individual body: . . . . .
POTENT v3.09	Profile drawn at 11:09 29/10/1998 for University of Adelaide - Educational use

POTENT v3.09 Model Summary Report created at for University of Adelaide - Educational use

Model title:

No.	Type	X	Y	Depth	Strike	Dip	Plunge	Density	A	B	C	D
		m	m	m	deg	deg	deg	gm/cc				
1	Rect	101251.4	390598.52	77.14	340	94	0	-0.60	80.00	600.00	40.00	
2	Rect	101254.2	990600.49	112.86	340	94	0	0.15	90.00	600.00	180.00	
3	Rect	101464.2	990531.36	76.79	0	90	0	-0.90	150.00	200.00	15.00	
4	Rect	100798.5	690754.62	58.57	0	90	0	0.30	200.00	200.00	10.00	
5	Poly	99588.89	90500.00	0.00	45	90	0	-0.90	0.00	Inf	0.00	
7	Rect	101209.9	990253.03	64.29	0	90	0	0.50	1200.00	100.00	30.00	

conductor essentially cancel each other out. The model for the northern and central lines (figures 44 and 45) fit the observed data reasonable well. The southern line model (figure 46) is not a good fit, and is dominated by a broad high which is also seen in the prospect scale residual (figure 42). This indicates the presence of density variations that are not detected as conductivity variations by the SIROTEM or resistivity.

Feature	Body	Density	Depth Extent	Width	Comments
Fresh Rock	-	2.7 g/cc	-	-	CSA Siltstone
Weathered Zone	6	1.8 g/cc	70-85m	-	Bedrock topography dips 4° east
Weathering Trough	1	2.1 g/cc	40m	80m	Only on Lines 90500N and 90750N
Deep Conductor	2	2.85 g/cc	180m	90m	Dipping 86° west

Table 7: Summary of gravity model features.

The first model was then refined by adding bodies to the northern and southern lines to create a final gravity model (figures 47-50). Small weathered zone density variations (bodies 5 and 9) are required to fit the short wavelength anomalies on the northern line. The southern line data shows a broad gravity high indicating a deep basement feature. A 3.35g/cc deep body (8) yields a good fit to the gravity data. This body might not be conductive, and is at least 40m below the weathered-fresh rock interface, and hence was not detected by the SIROTEM. The second gravity model fits the observed data well and correlates with the SIROTEM and resistivity interpretations.

Figure 47: Plan view of final gravity model.

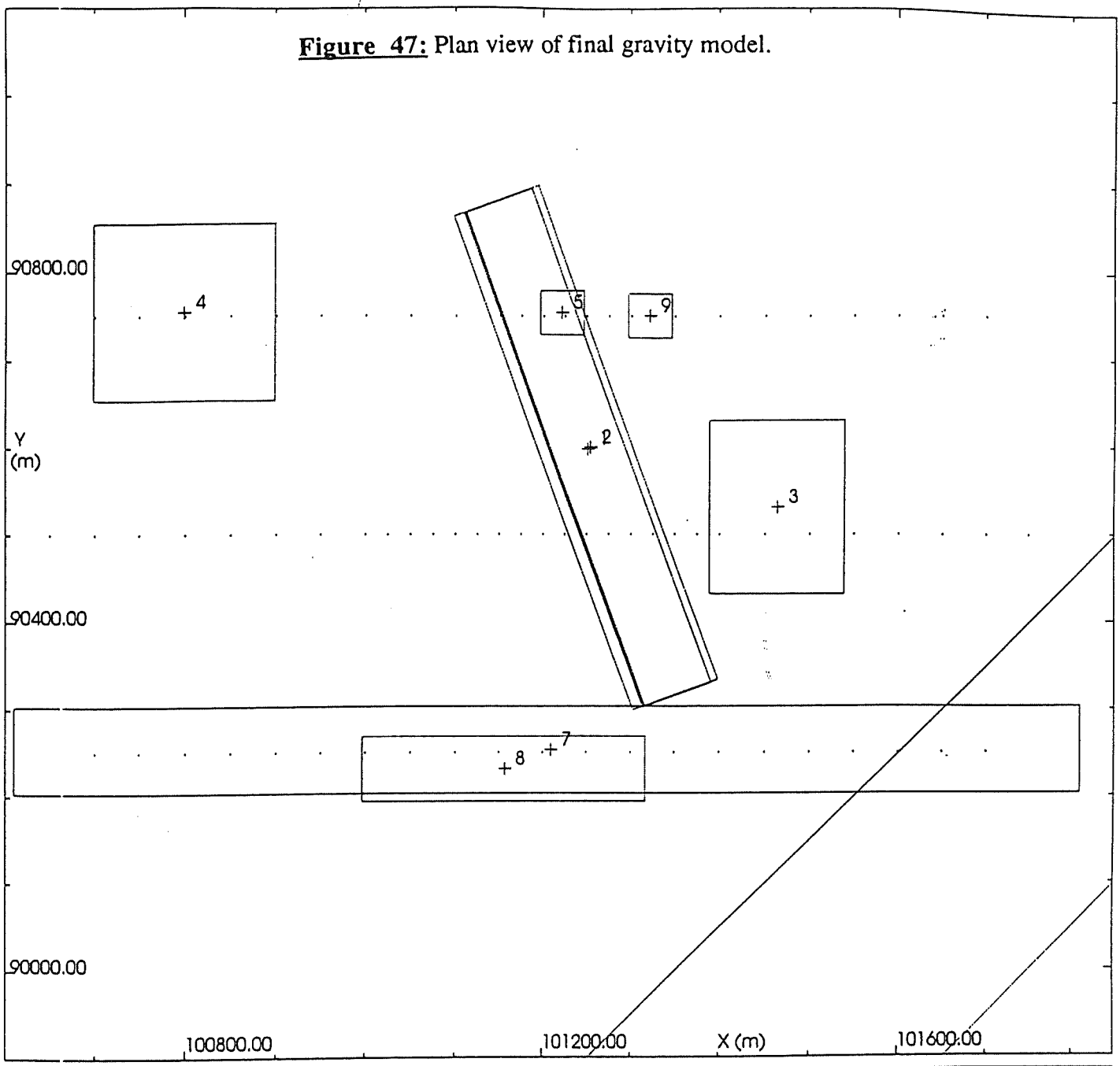

Model title:

No.	Type	X m	Y m	Depth m	Strike deg	Dip deg	Plunge deg	Density gm/cc	A	B	C	D
1	Rect	101251.43	90598.52	77.14	340	94	0	-0.60	80.00	600.00	40.00	
2	Rect	101254.29	90600.49	112.86	340	94	0	0.15	90.00	600.00	180.00	
3	Rect	101464.29	90531.36	76.79	0	90	0	-0.90	150.00	200.00	15.00	
4	Rect	100798.56	90754.62	58.57	0	90	0	0.30	200.00	200.00	10.00	
5	Rect	101221.42	90754.12	14.29	0	90	0	0.60	50.00	50.00	30.00	
6	Poly	99588.89	90500.00	0.00	45	90	0	-0.90	0.00	Inf	0.00	
7	Rect	101209.99	90253.03	64.29	0	90	0	0.50	1200.00	100.00	30.00	
8	Rect	101157.21	90231.09	118.57	0	90	0	0.65	320.00	75.00	150.00	
9	Rect	101321.43	90750.59	27.14	0	90	0	-0.50	50.00	50.00	30.00	

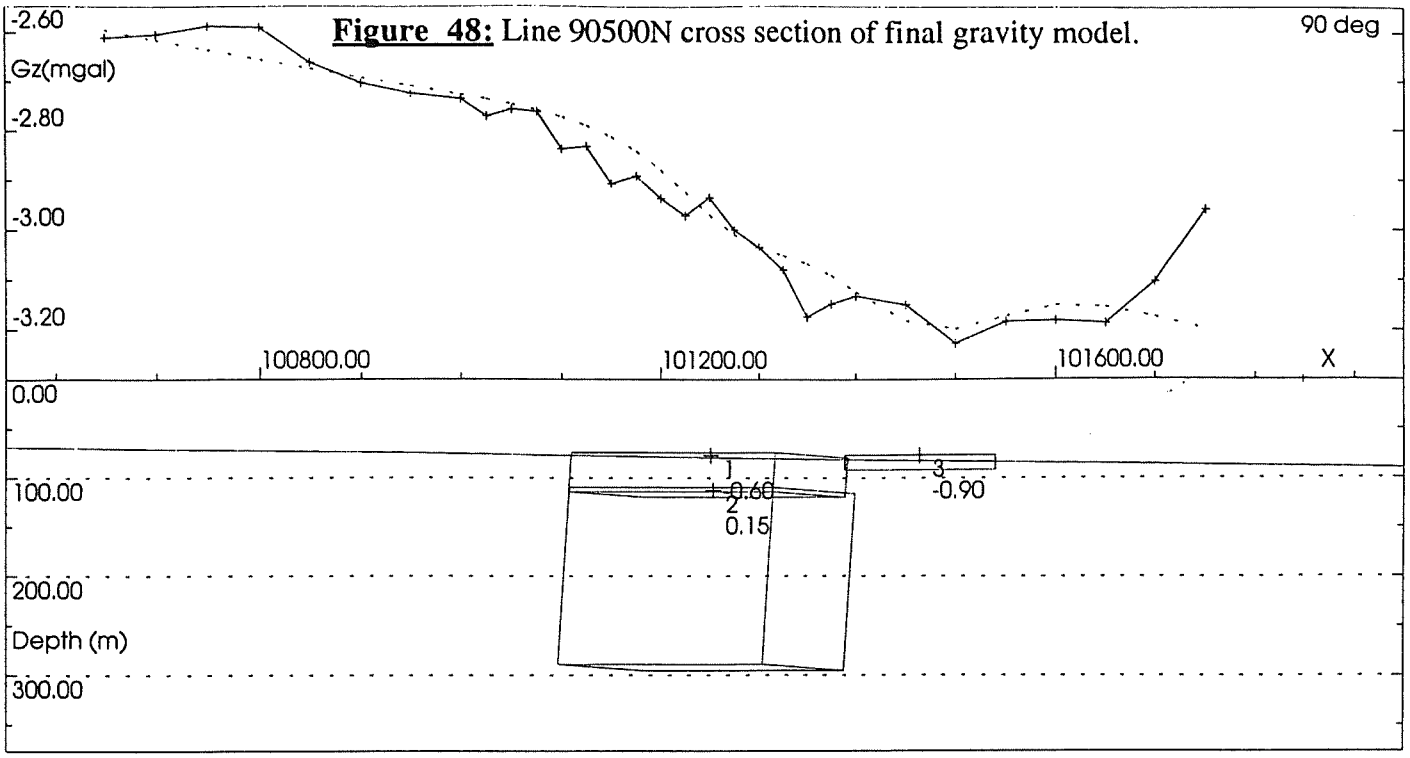

Figure 48: Line 90500N cross section of final gravity model.

Observations:	East ,North,Residual
Profile #1;	90500N
Model:	
Calculation mode:	Z gravity vector component
Observed:	———— Calculated: - - - - - - - - -
Residual:	. . . . . Individual body: . . . . .
POTENT v3.09	Profile drawn at 11:07 29/10/1998 for University of Adelaide - Educational use

POTENT v3.09 Model Summary Report created at for University of Adelaide - Educational use

Model title:

No.	Type	X	Y	Depth	Strike	Dip	Plunge	Density	A	B	C	D
		m	m	m	deg	deg	deg	gm/cc				
1	Rect	101251.4	390598.52	77.14	340	94	0	-0.60	80.00	600.00	40.00	
2	Rect	101254.2	990600.49	112.86	340	94	0	0.15	90.00	600.00	180.00	
3	Rect	101464.2	990531.36	76.79	0	90	0	-0.90	150.00	200.00	15.00	
4	Rect	100798.5	690754.62	58.57	0	90	0	0.30	200.00	200.00	10.00	
5	Rect	101221.4	290754.12	14.29	0	90	0	0.60	50.00	50.00	30.00	
6	Poly	99588.89	90500.00	0.00	45	90	0	-0.90	0.00	Inf	0.00	
7	Rect	101209.9	990253.03	64.29	0	90	0	0.50	1200.00	100.00	30.00	
8	Rect	101157.2	190231.09	118.57	0	90	0	0.65	320.00	75.00	150.00	
9	Rect	101321.4	390750.59	27.14	0	90	0	-0.50	50.00	50.00	30.00	

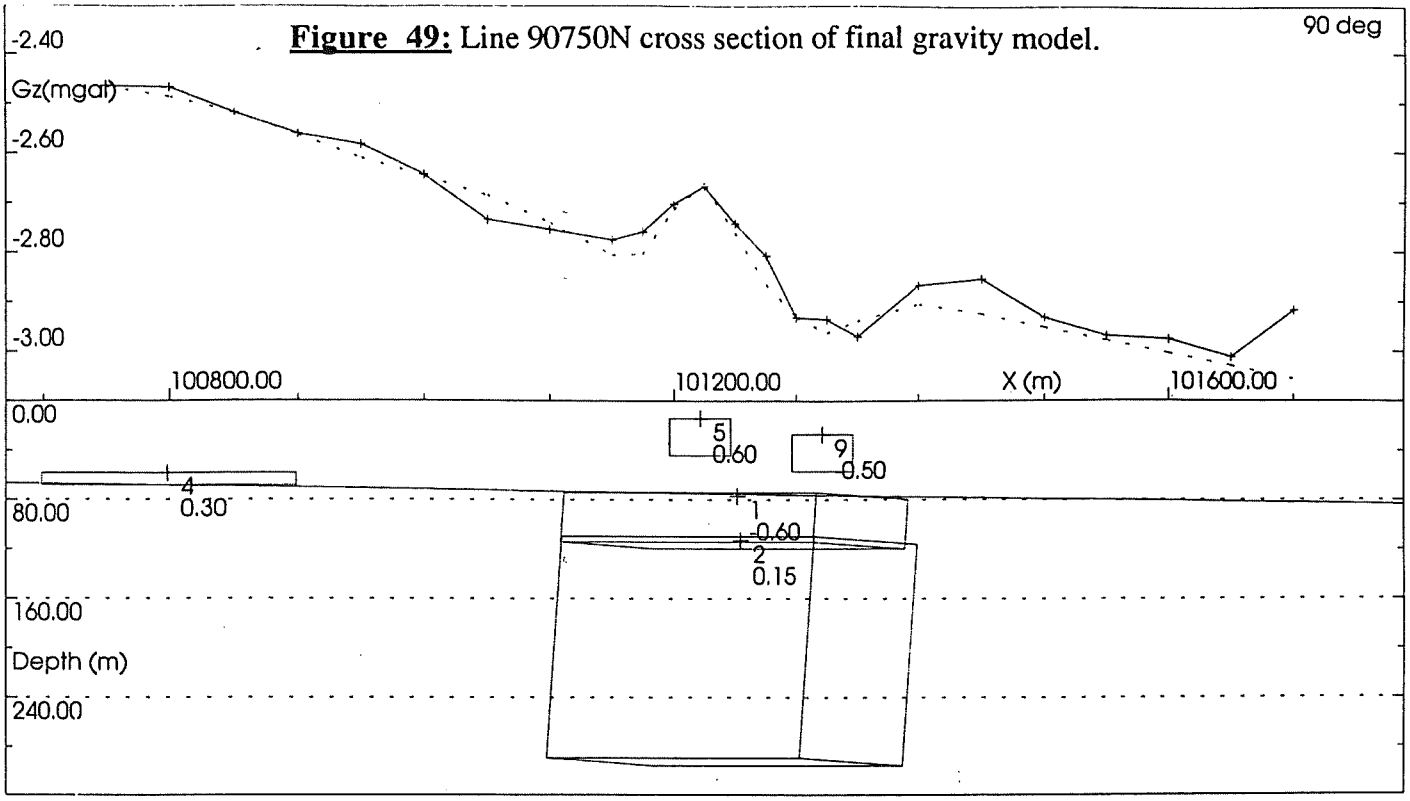

Figure 49: Line 90750N cross section of final gravity model.

Observations:	East ,North,Residual		
Profile #2;	90750N		
Model:			
Calculation mode:	Z gravity vector component		
Observed:	———————	Calculated:	- - - - - - - - -
Residual:	. . . . .	Individual body:	. . . . .
POTENT v3.09	Profile drawn at 11:06 29/10/1998 for University of Adelaide - Educational use		

POTENT v3.09 Model Summary Report created at for University of Adelaide - Educational use

Model title:

No.	Type	X m	Y m	Depth m	Strike deg	Dip deg	Plunge deg	Density gm/cc	A	B	C	D
1	Rect	101251.4	390598.52	77.14	340	94	0	-0.60	80.00	600.00	40.00	
2	Rect	101254.2	990600.49	112.86	340	94	0	0.15	90.00	600.00	180.00	
3	Rect	101464.2	990531.36	76.79	0	90	0	-0.90	150.00	200.00	15.00	
4	Rect	100798.5	690754.62	58.57	0	90	0	0.30	200.00	200.00	10.00	
5	Rect	101221.4	290754.12	14.29	0	90	0	0.60	50.00	50.00	30.00	
6	Poly	99588.8	990500.00	0.00	45	90	0	-0.90	0.00	Inf	0.00	
7	Rect	101209.9	990253.03	64.29	0	90	0	0.50	1200.00	100.00	30.00	
8	Rect	101157.2	190231.09	118.57	0	90	0	0.65	320.00	75.00	150.00	
9	Rect	101321.4	390750.59	27.14	0	90	0	-0.50	50.00	50.00	30.00	

Figure 50: Line 90800N cross section of final gravity model.

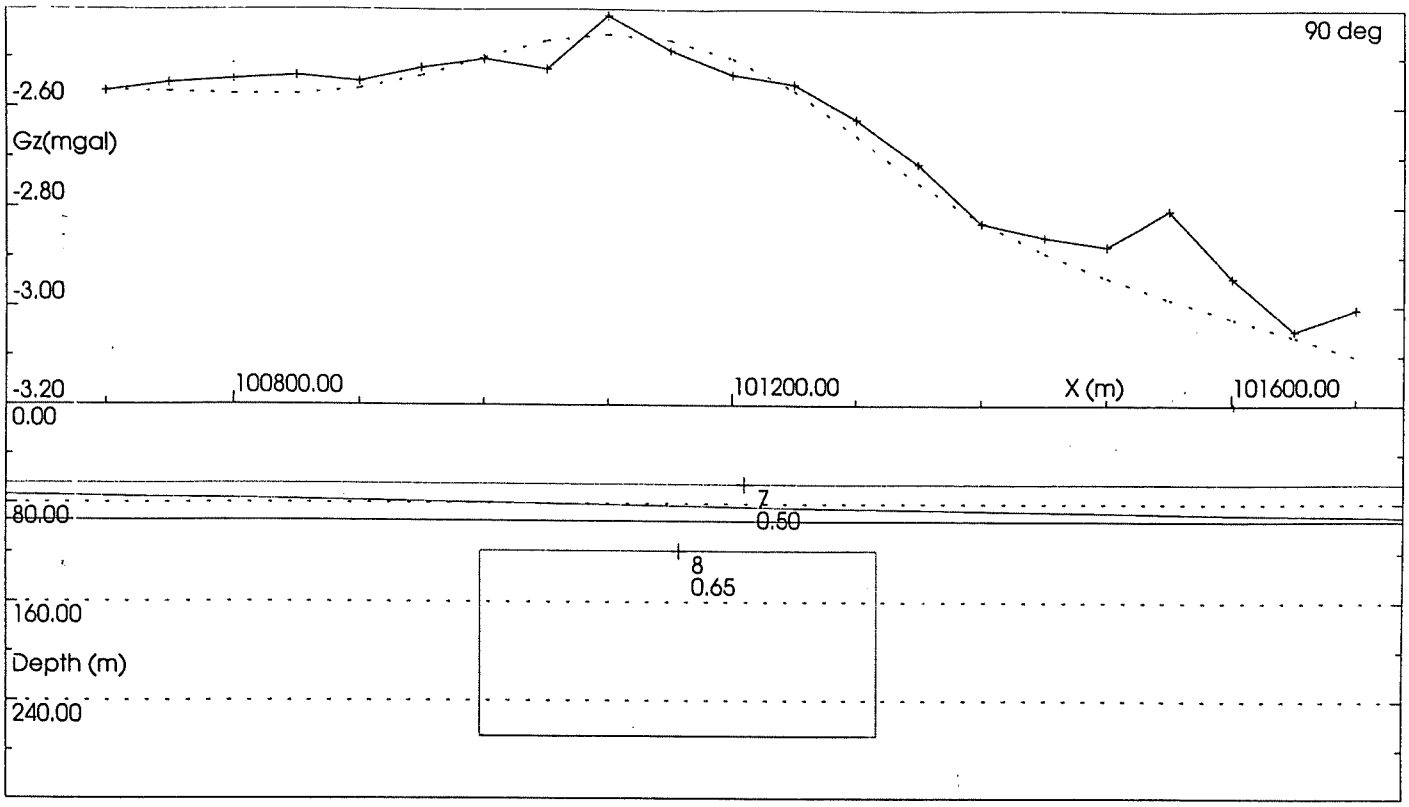

POTENT v3.09 Model Summary Report created at for University of Adelaide - Educational use

Model title:

No.	Type	X m	Y m	Depth m	Strike deg	Dip deg	Plunge deg	Density gm/cc	A	B	C	D
1	Rect	101251.43	90598.52	77.14	340	94	0	-0.60	80.00	600.00	40.00	
2	Rect	101254.29	90600.49	112.86	340	94	0	0.15	90.00	600.00	180.00	
3	Rect	101464.29	90531.36	76.79	0	90	0	-0.90	150.00	200.00	15.00	
4	Rect	100798.56	90754.62	58.57	0	90	0	0.30	200.00	200.00	10.00	
5	Rect	101221.42	90754.12	14.29	0	90	0	0.60	50.00	50.00	30.00	
6	Poly	99588.89	90500.00	0.00	45	90	0	-0.90	0.00	Inf	0.00	
7	Rect	101209.99	90253.03	64.29	0	90	0	0.50	1200.00	100.00	30.00	
8	Rect	101157.21	90231.09	118.57	0	90	0	0.65	320.00	75.00	150.00	
9	Rect	101321.43	90750.59	27.14	0	90	0	-0.50	50.00	50.00	30.00	

11.0 Downhole Petrophysical Logging

Several downhole logs were previously run through the RAB hole NFR 470 (figure 3). The logs collected were apparent conductivity, magnetic susceptibility, gamma ray and two density logs.

The gamma ray log (figure 51) yielded high API (American Petroleum Institute) values for the weathered zone, between 200 and 240 API. The fresh rock is shown by a decrease in the natural gamma radiation down to approximately 135 API.

The apparent conductivity log (figure 52) shows the highly variable conductivity structure of the weathered zone. The apparent conductivity varies from 100 milliSiemens per metre to 15 mS/m, and fluctuates rapidly. The apparent resistivity was averaged into two metre blocks (figure 53) to better correlate resistivity with the RAB drill hole results. The averaged apparent resistivity can be used to approximate a layered earth conductivity structure down the hole (figure 53, shown in red). Layers in the weathered zone have resistivities as low as 15 Ohm-m, and as high as 50 Ohm-m. The contacts between the layers can be gradational or sharp. There is very little correlation between the logged resistivity and the downhole geology.

The density logs agree well with each other, giving fairly uniform densities of between 1.75 and 2.0 g/cc (figure 54). The magnetic susceptibility log shows very low susceptibilities down the entire hole (figure 55), although these do increase slightly with depth.

Figure 51: NFR 470 Gamma Radiation Log

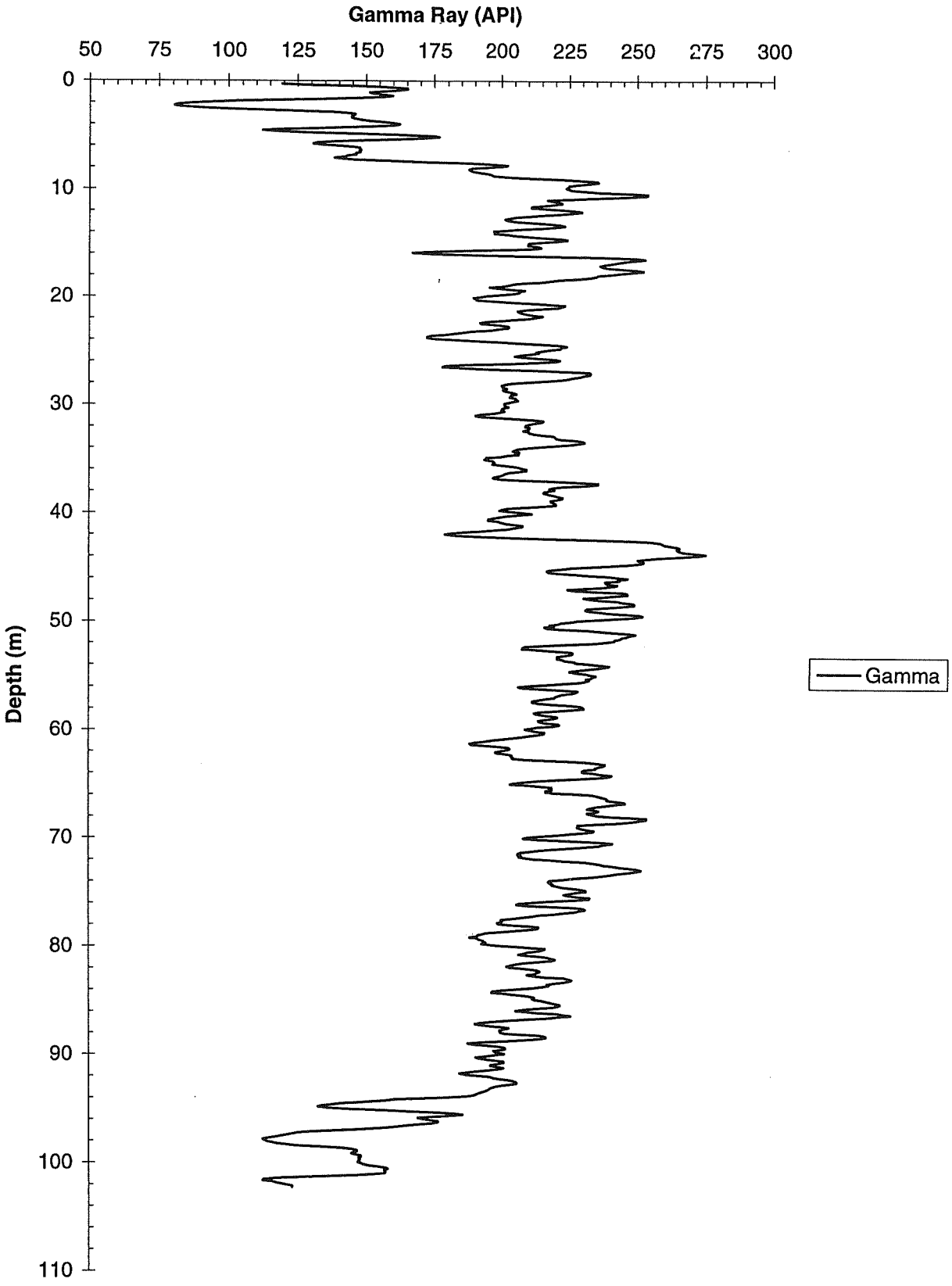

Figure 52: NFR 470 Apparent Conductivity Log

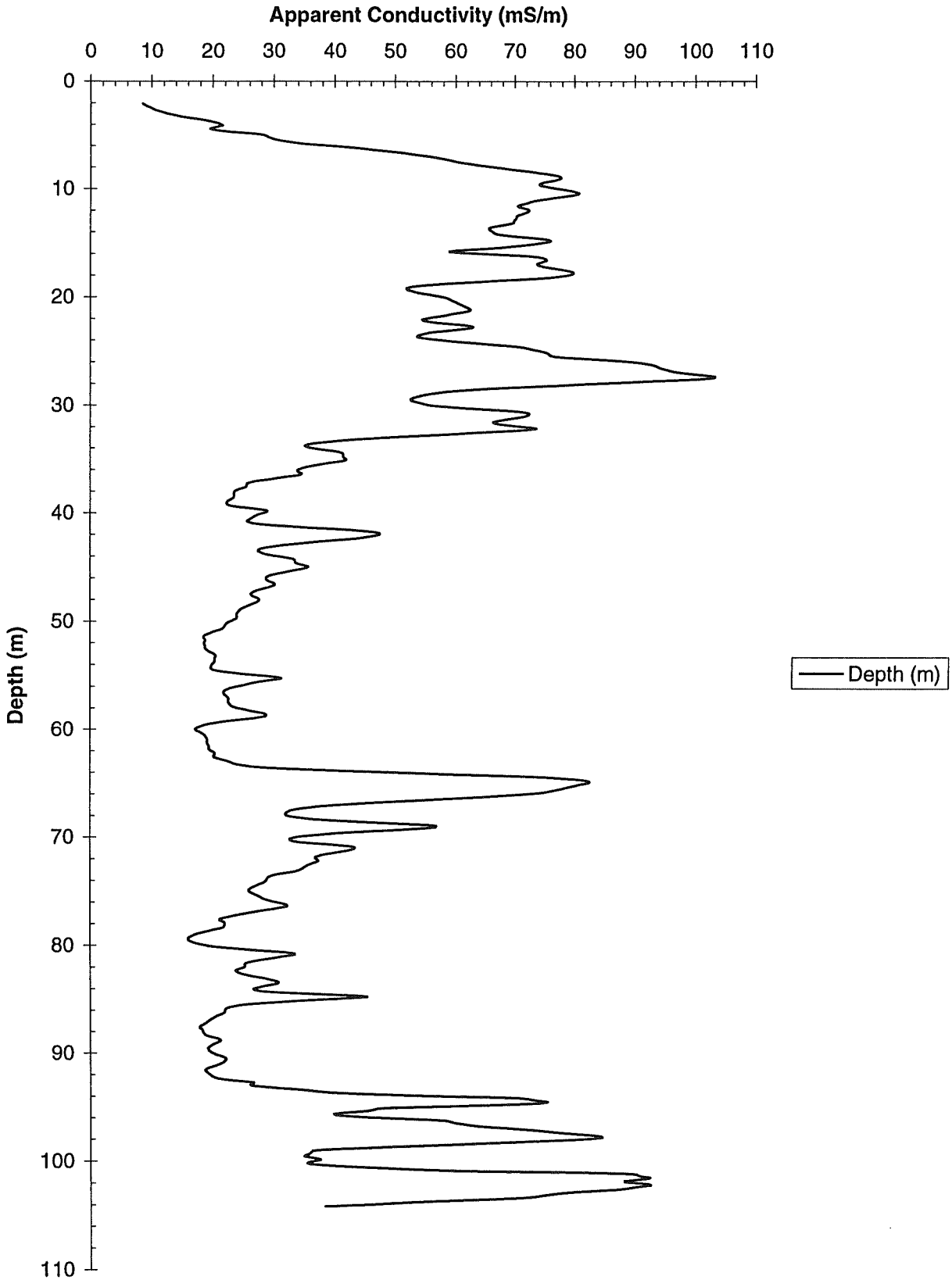

Figure 53: NFR 470 Apparent Resistivity in 2m block averages

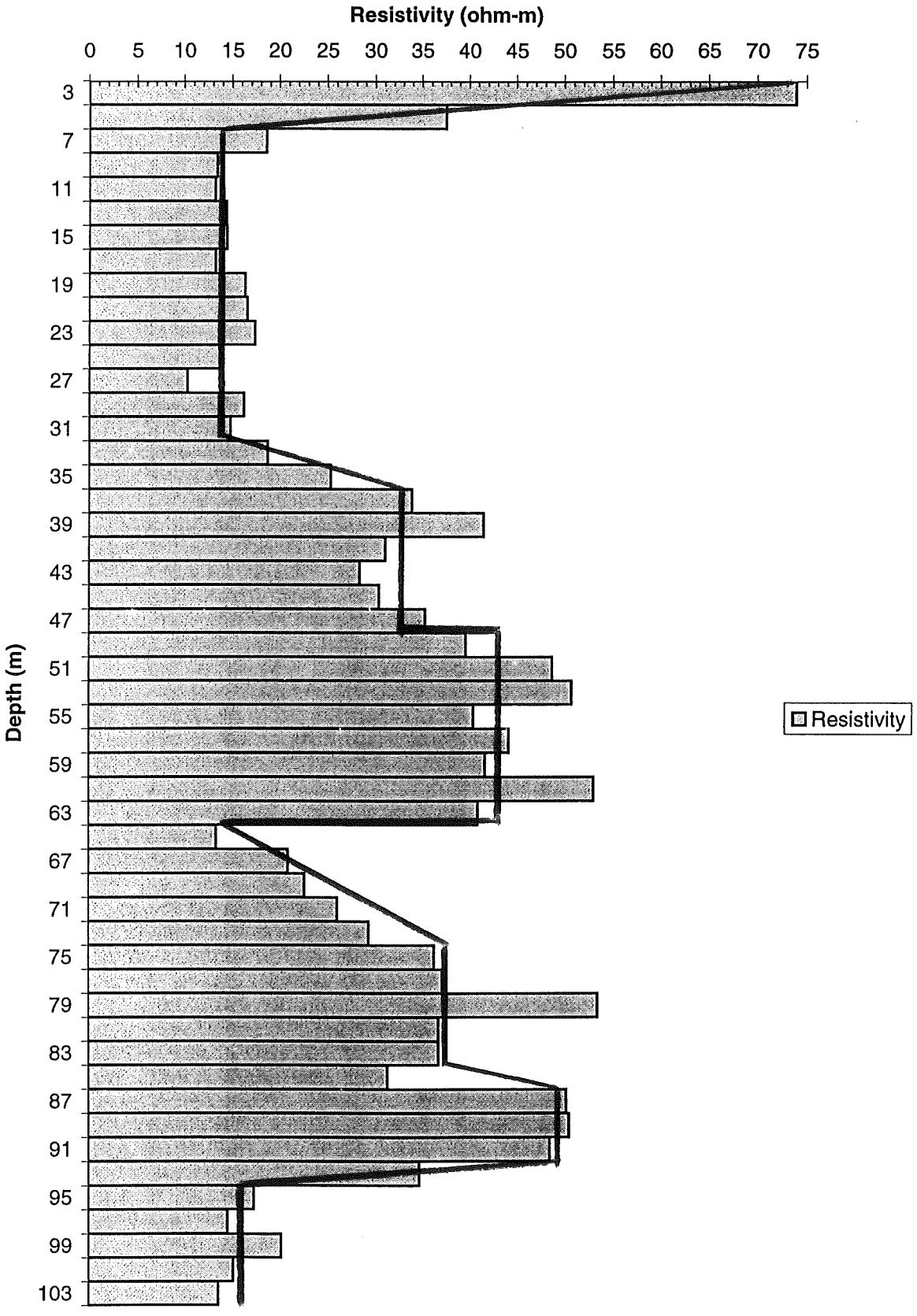

Figure 54: NFR 470 Density Logs

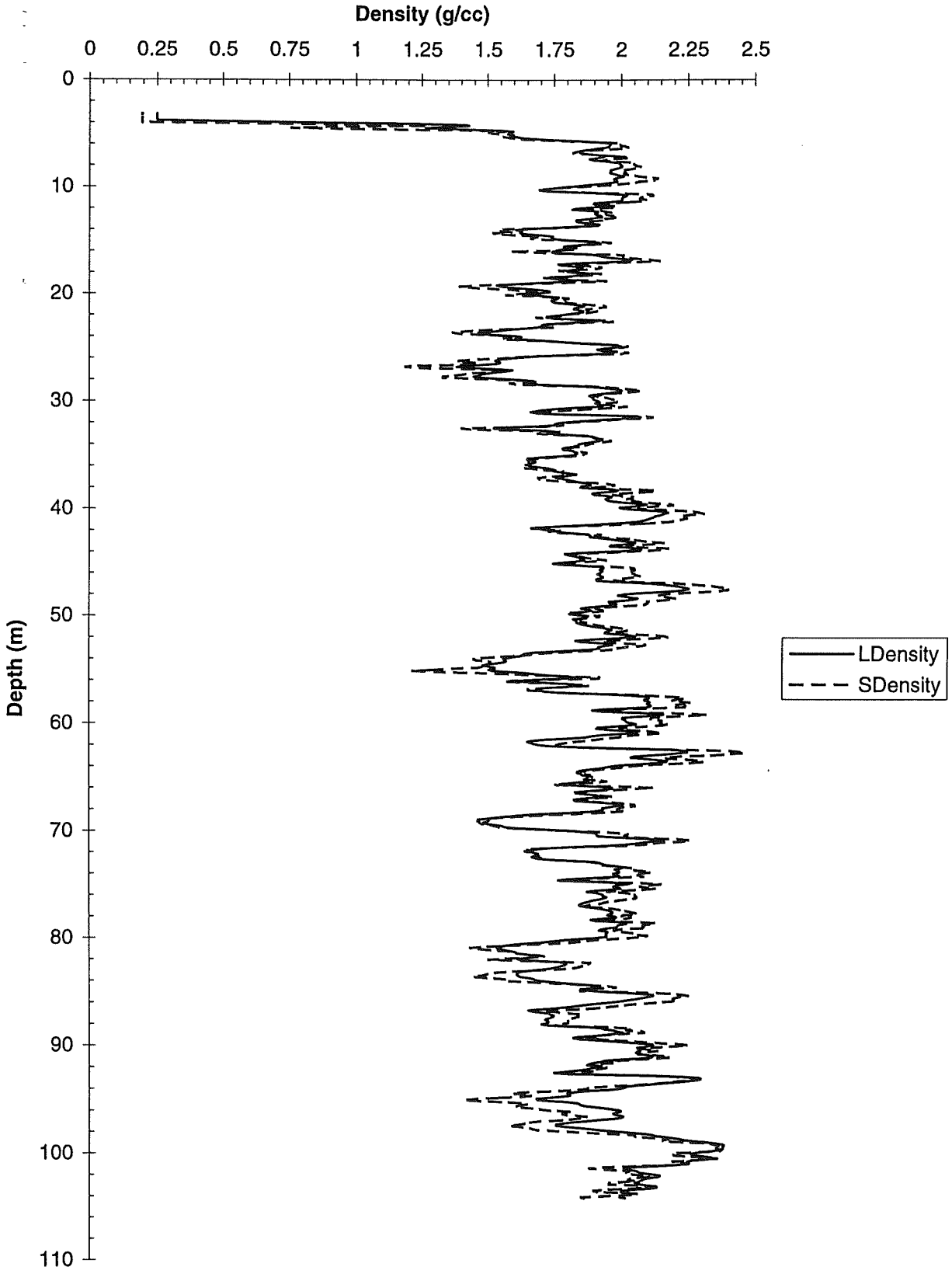

Figure 55: NFR 470 Magnetic Susceptability log

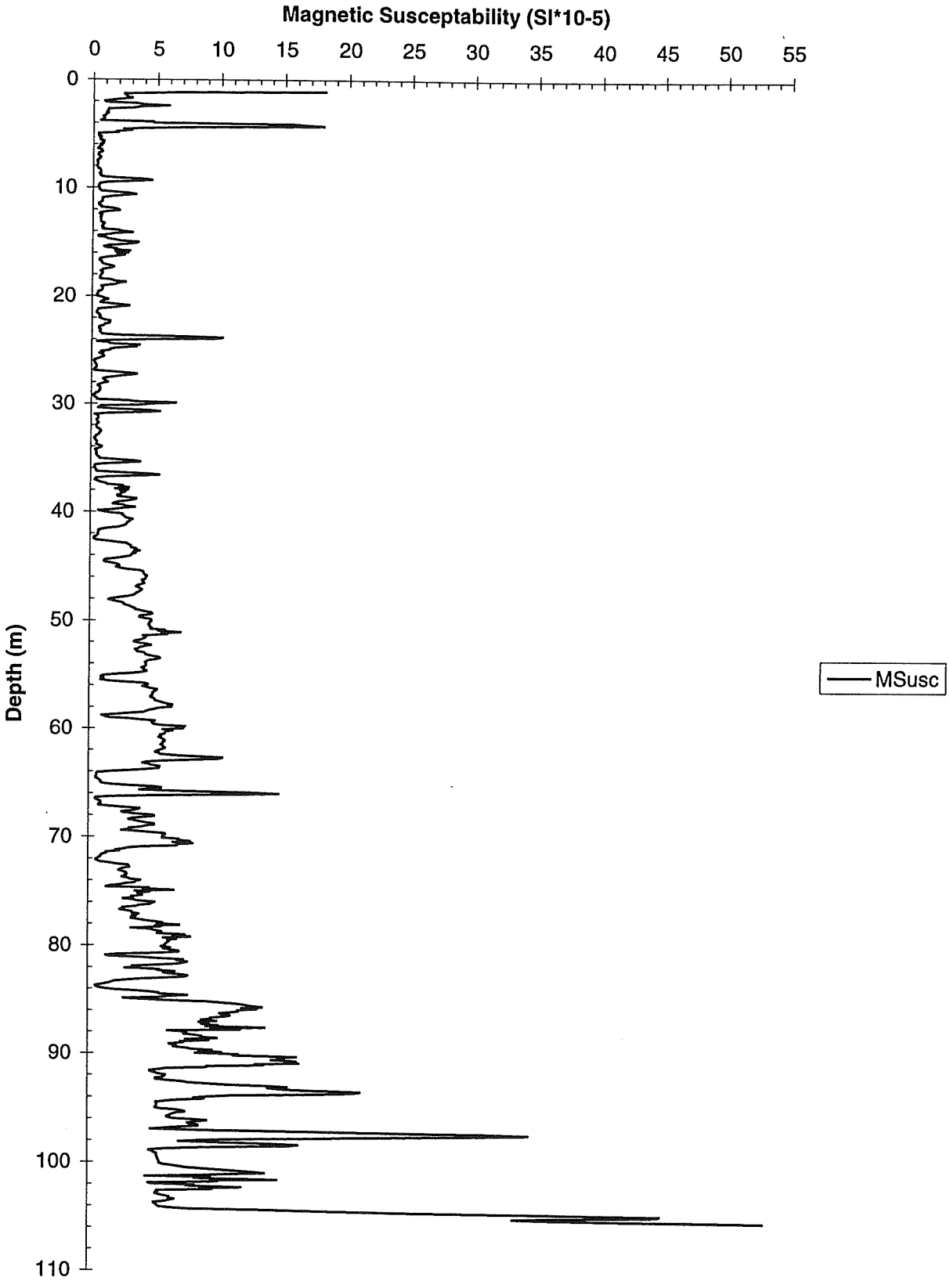

12.0 Airborne Magnetics

The total magnetic intensity (TMI) map (figure 56) is dominated by a strong regional trend, increasing towards the north-east. The regional magnetic trend increases in the same direction as the regional gravity decreases, though it is not known whether the two are related.

The TMI does show some visible higher frequency responses, which have been enhanced by a first vertical derivative (figure 57). The first vertical derivative acts as a high pass filter, effectively removing the regional trend. The derivative map features several linear magnetic highs cris-crossing the region, which are most likely maghemite concentrated in drainage channels. One maghemite channel runs across the southern and central lines (see arrow). There is also a broader magnetic high in the centre of the central line (underlying the maghemite channel). This is a very small magnetic high, localised in the area of the EM and resistivity response on the central line, but not extending to the northern line. Because of the TEM, resistivity and drilling results, a ground magnetic survey may have produced useful information. It is unlikely that the trough/conductor is being sensed by the airborne magnetics, as the response is more likely to be swamped by the overlying maghemite response. If a broad magnetic anomaly were found in the survey area, then a possible source could be pyrrhotite rich mineralisation, such as the Elura orebody. The Elura Zn-Pb-Ag mine is located twelve Kilometres south-southwest of Number Four Tank and was first detected by aeromagnetics in the 1970's (Emerson, 1980).

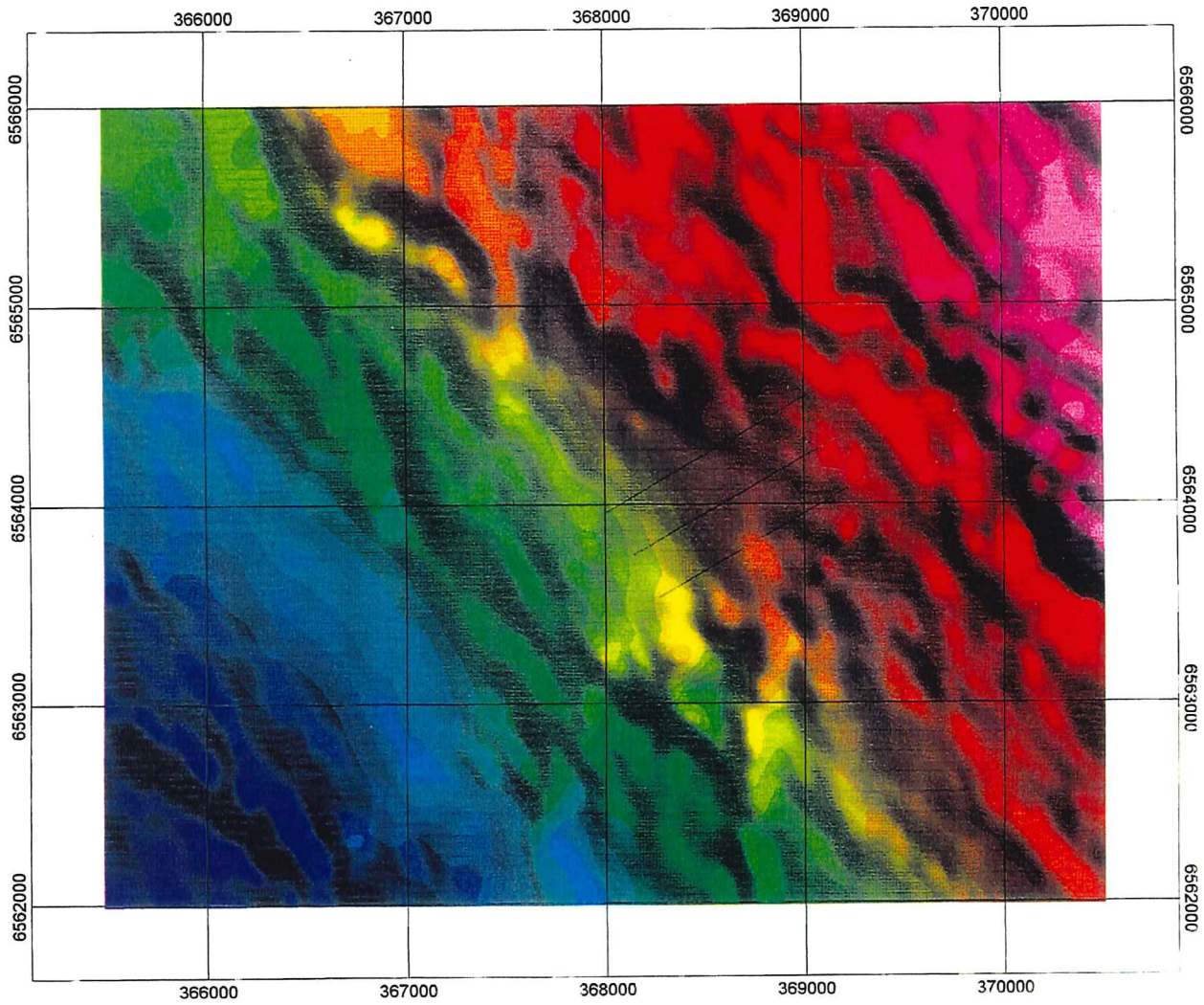

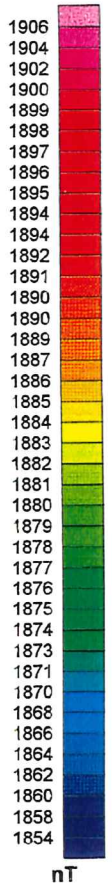

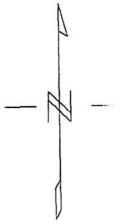

Scale 1:25000

250 0.0 250 500 750 1000 1250 1500

metres

AGD66 / AMG zone 55

Figure 56: Total magnetic intensity (TMI) map.

Pasminco Exploration
Number 4 Tank, Cobar, NSW **Airborne Magnetics** **TMI**
Sunshading : Inclination 60, Declination 45 Pixel Size : 50m

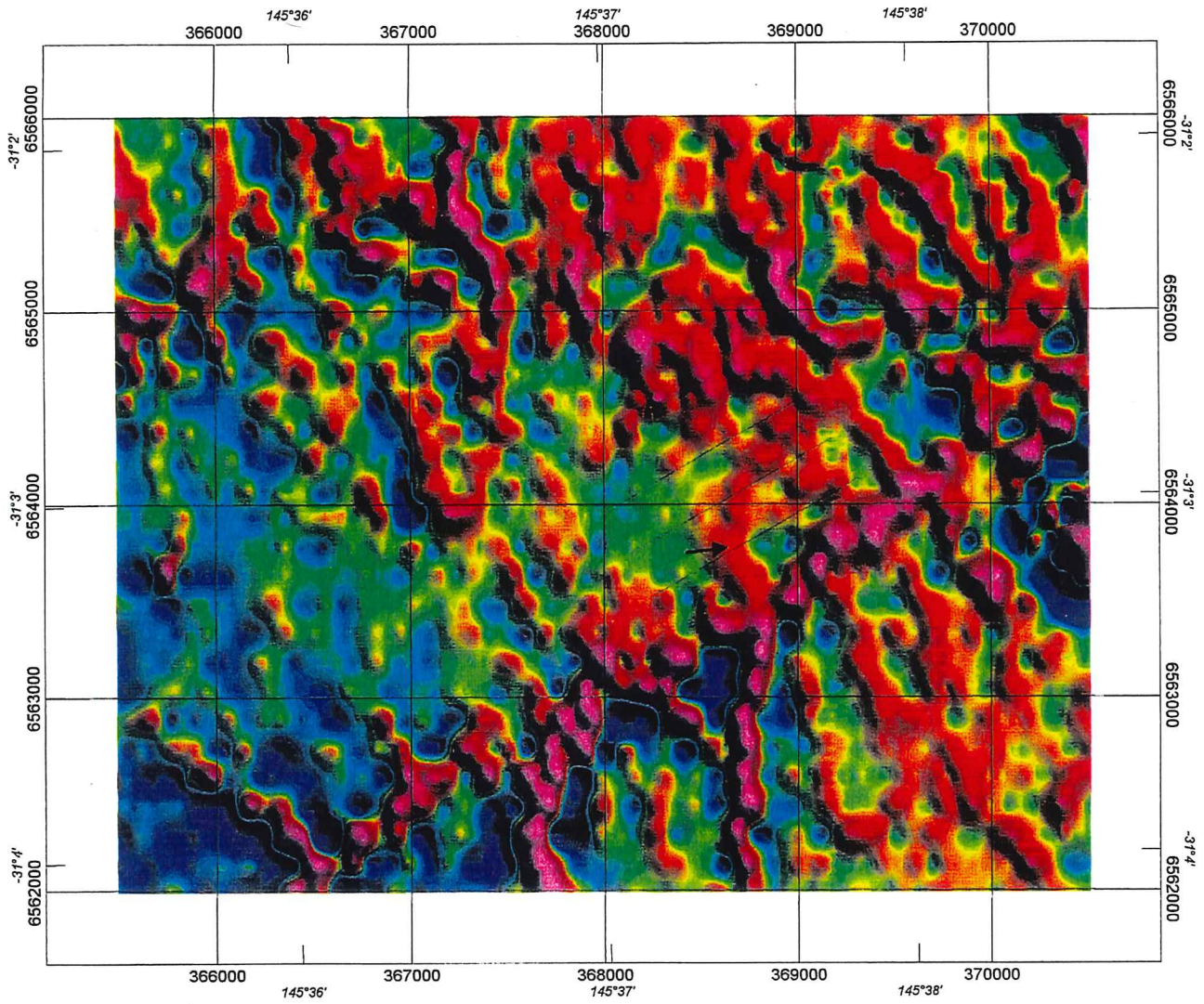

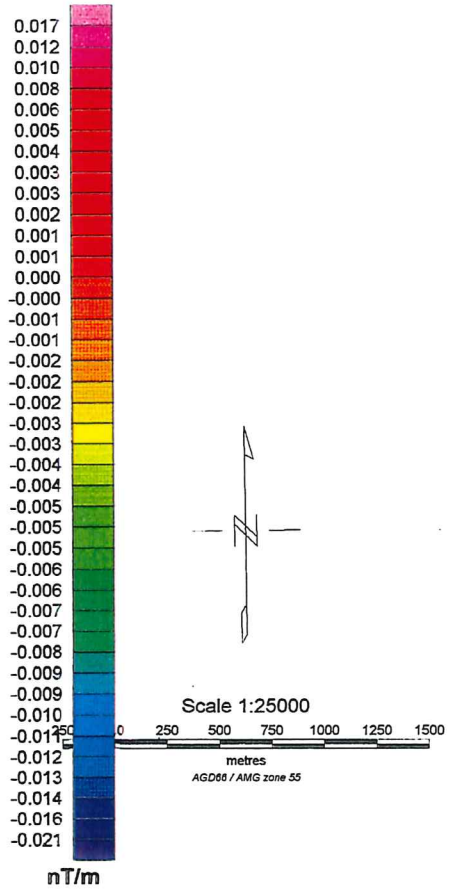

Figure 57: First vertical derivative of the TMI.

Pasminco Exploration
Number 4 Tank, Cobar, NSW **Airborne Magnetics** **VD1 of TMI**
Sunshading : Inclination 60, Declination 45 Pixel Size : 50m

13.0 Discussion

Several geophysical techniques were trialed, with the aim of interpreting conductivity structure of the weathered zone, depth to fresh rock, and identifying any underlying anomalies. Each technique used is now summarised below, along with suggestions for acquisition, processing and interpretation.

13.1 Vertical Electric Soundings

(i) Acquisition is slow. Surveys should be taken in two perpendicular directions.
(ii) Survey is centred on one point only (not a reconnaissance technique).
(iii) Very little processing required.
(iv) One dimensional inversions are quick and easy, inaccurate over trough.
(v) ***GRENDL*** is more reliable than ***VES*** because it calculates inversion statistics.
(vi) Best method for shallow work, but depth to fresh rock poorly constrained.
(vii) Not a good exploration technique but may be useful in follow up surveys.

13.2 Dipole-Dipole Resistivity / Induced Polarisation

(i) Fairly slow acquisition (but much faster than VES).
(ii) Processing relatively easy.
(iii) Two dimensional Zonge inversion gave best interpretation of trough and bedrock topography. Also gave best location for underlying conductor.
(iv) Very useful exploration technique. Use 50m dipoles for better lateral resolution.
(v) Depths and resistivities are not resolved. Use RAB/TEM to interpolate depths.
(vi) IP and resistivity targets will appear deeper in conductive terranes.
(vii) Time domain dipole-dipole IP minimises EM coupling, but some EM coupling is present.

13.3 SIROTEM MkIII In-loop Soundings

(i) Useful, fast and easy to perform. Good for reconnaissance.
(ii) Acquire as short time channels. 50 or 100m loops.
(iii) Processing is easy. Always do decay curve analysis.
(iv) Stripping is very good at isolating underlying targets.
(v) Stripping and decay curve analysis best identified underlying conductor.
(vi) ***GRENDL*** works well away from trough, best for depth to fresh rock.
(vii) Use 2 layer inversion only. ***GRENDL*** statistics should always be used.
(viii) ***GRENOCC*** gave similar results to ***GRENDL***. ***GRENOCC*** identified the trough.
(ix) Look for the top layer becoming thinner and more conductive as an indicator of interesting bedrock topography, such as a trough or conductor.

13.4 Exploration Strategy for the Cobar Basin

No single method could accurately define the conductivity structure, depth to fresh rock or properties of the underlying conductor. The best exploration technique is to use both dipole-dipole resistivity/IP and early time channel In-Loop SIROTEM MkIII soundings.

The electromagnetics can be used to identify anomalous areas, either from the raw traverses or as problems seen on ***GRENOCC*** or 2 layer ***GRENDL*** inversions. Decay curve analysis is necessary to determine the power law decay of the weathered zone, and to strip away the overburden response. Stripped electromagnetics is used to determine if any anomalies have exponential decays, and the time constants of any targets. Layered earth inversions performed away from anomalies can be used as a starting point for interpolating bedrock topography using the resistivity.

The double dipole resistivity can be inverted in two dimensions, giving a good approximation of bedrock topography (by interpolation). The Zonge resistivity inversion also gave the best constrained position of the underlying conductor. The n=1 and n=2 levels can be used to confirm the weathered zone resistivity, and to highlight lateral inhomogeneities within the weathered zone. Induced polarisation would be interpreted with emphasis on detecting chargeable bodies.

Any conductive anomalies found could be followed up with more detailed SIROTEM (smaller station spacing) or dipole-dipole resistivity (smaller dipoles and more stations), and also gravity, magnetics, magnetometric resistivity, fixed loop electromagnetics, CSAMT, RAB holes and downhole electromagnetics.

Drilling of any target must be carefully planned. When the locations of each method's anomalies are compared with the drill hole data, there are several points of conflict. SIROTEM defined the underlying conductor to be located between 1000E and 1300E. Dipole-dipole resistivity defined the trough as located between 1175E and 1350E, and the conductor to be between 1150E and 1300E (figure 58). The trough was defined from drilling as being between 1175E and 1250E.

Since the goal of these procedures is the finding of orebodies, drilling should aim to intersect the underlying conductive zone. Drill holes should be at least 150-200 metres long to best intersect a deep target. Figure 58 shows suggestions for drill hole locations for intersecting the Number Four Tank anomaly.

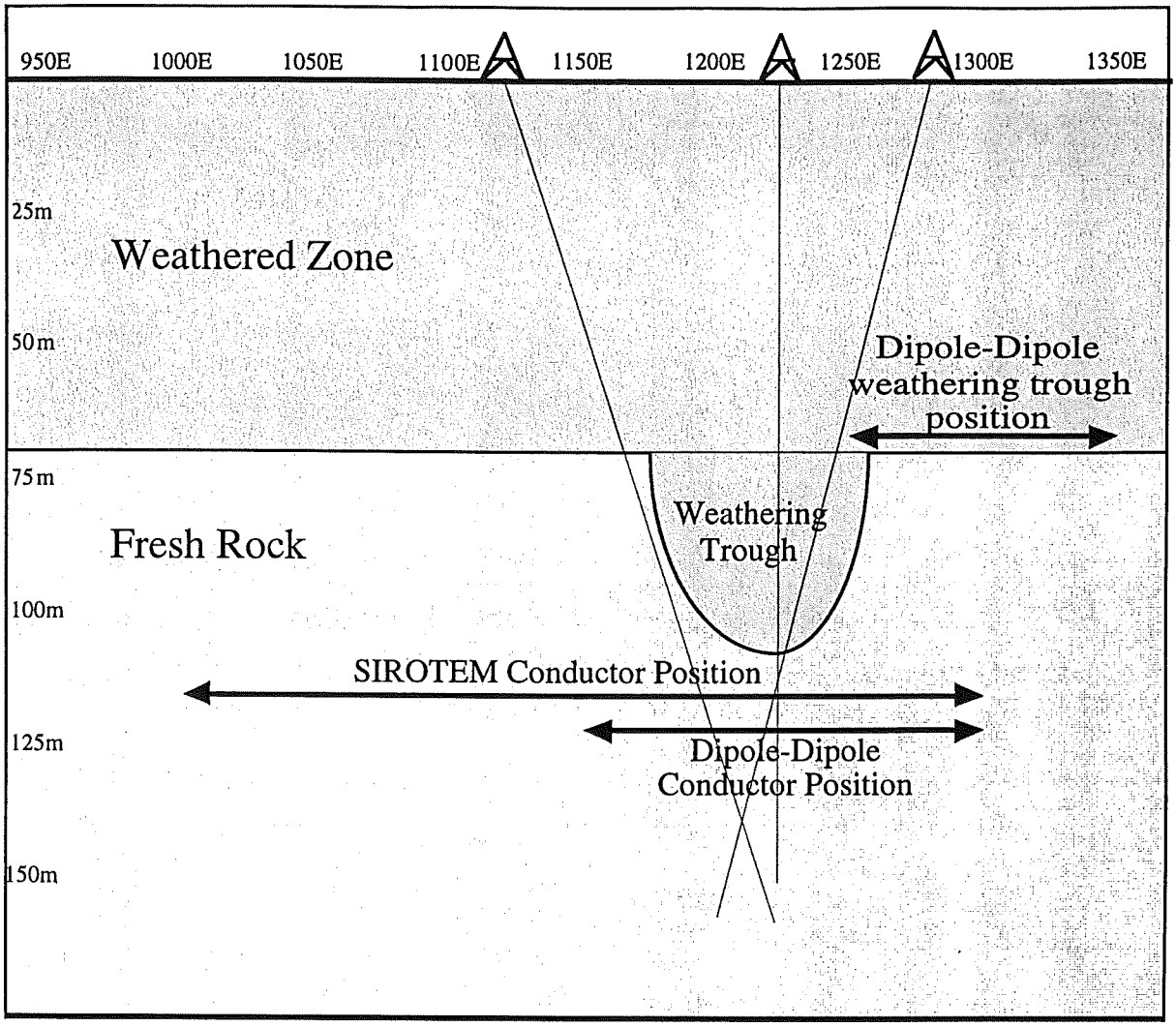

Figure 58: Known location of weathering trough with SIROTEM and dipole-dipole interpreted positions. Suggested methods for drilling anomalies, either one vertical drill hole, or two angled drill holes.

14.0 Conclusion

The conductivity structure in the Number Four Tank region can be interpreted as having three layers. The surface layer of alluvium is generally 3.3m thick, and has a resistivity of between 240 to 400 Ohm-m, as defined by the vertical electric soundings. The weathered zone, though having a complex internal structure, can be simplified as a single layer. The weathered zone is between 70 and 90 metres thick and of 20-30 Ohm-m resistivity. The weathered-fresh rock interface dips gently to the east. The fresh rock resistivity cannot be well constrained by any of the techniques used in this study, but must be greater than 500 Ohm-m. These results compare favourably with RAB drilling, and previous petrophysical results.

The weathering trough would be interpreted as being 100m across and 30m deep on the central line. The trough can only be interpreted confidently using the dipole-dipole resistivity. The trough was interpreted as being located between 1250E and 1350E, which is 75 metres east of the trough's actual location.

The underlying conductor is detected on the northern and central lines. Electromagnetics indicates a body with an exponential decay time constant of τ=0.45ms. The location of the conductor is best constrained by the double dipole resistivity as being between 1150E and 1300E.

The conductor is possibly a fault, through which copper-rich fluids have possibly been channelled. This would result in the weathering trough being formed, and also explain the copper geochemical anomaly within the weathering trough. A fault may be conductive due to hydrous minerals, and possibly metallic mineralisation. Without further drilling, the geology of the conductive zone cannot be positively defined.

Dipole-dipole resistivity and SIROTEM transient electromagnetics were the most useful and fastest methods used. Performing both of these techniques is probably the safest and most accurate survey technique for exploration in the Cobar Basin.

Weathered terranes pose many difficulties for exploration geophysics. By understanding the effects of a conductive weathered zone, we can design surveys, and use appropriate interpretation techniques, that will minimise, isolate and take into account these effects.

"If a man will begin with certainties he shall end in doubts; but if he will be content to begin with doubts he shall end in certainties." - Francis Bacon

Acknowledgments

I thank the many people who have generously supported my studies throughout the year, and I acknowledge with gratitude the following:-

My supervisors Dr Peter Brooker, Neil Hughes and Paul Basford for their excellent help and support throughout the year. They always took time to help me as needed.

Alex Copeland for performing the electrical and electromagnetic surveys.

Pasminco Exploration Elura office staff, especially Alan Neil, for their help with my survey.

Steve Busuttil of Mount Isa Mines, Mike Hatch of Zonge Engineering and Sandy Dodds of Primary Industries and Resources South Australia for all their time and support. The willingness of people and companies to help honours students is inspirational.

Professor Stewart Greenhalgh, Dr Richard Hillis and Dr Vic Gostin, as I could always stop them in the corridor with a question, and receive a profound response.

The 1998 Honours Geology and Geophysics class. We all helped each other as much as we could. Good luck in the future, as we all proceed along our separate ways.

Sarah Blackman who I could always talk to about my ideas.

Pasminco Exploration for the financial and technical support of my project.

I dedicate this thesis to my mother, my father and my grandfather. Their support and advice has carried me to this point. "Don't stop believing in what you can achieve".

References

Asten, M. W., 1992, Interpretation of Ground TEM Data from Conductive Terrains. *Exploration Geophysics*, **23**, 9-16.

Dobrin, M. B., Savit, C. H., 1988, *Introduction to Geophysical Prospecting*. McGraw-Hill Book Company.

Emerson, D. W., ed., 1980, *The Geophysics of the Elura Orebody*. ASEG Special Publication.

Fitterman, D. V., 1988, Equivalence Behaviour of Three Electrical Sounding Methods as Applied to Hydrogeological Problems. Presented at the 50th EAEG meeting in The Hague, Netherlands.

Hughes, N., 1998, Personal Communications on magnetometric resistivity and transient electromagnetic modelling.

Jupp, D. L. B., Vozoff, K., 1975, Stable iterative methods for geophysical inversion. *Geophysical Journal of the Royal Astronomical Society*, **42**, 957-976.

Kaufman, A., and Keller, G. V., 1983, Frequency and Transient Soundings. Elsevier, N.Y.

Kearey, P., Brooks, M., 1991, *An Introduction to Geophysical Exploration*. Blackwell Science Ltd. Publishers.

Lee, T., 1984, The transient electromagnetic response of a magnetic or superparamagnetic ground. *Geophysics*, **49**, 854-860.

Lowrie, W., West, G. F., 1965, The Effect of a Conducting Overburden on Electromagnetic Prospecting Measurements. *Geophysics*, **30**, 624-632.

McNeill, J. D., 1985, *The Galvanic Current Component in Electromagnetic Surveys*. Geonics Limited, Technical Note TN-17.

McNeill, J. D., 1995, *Optimal Detection of TDEM Anomalies under Conductive Overburden*. Geonics Limited, Technical Note TN-28.

Nabighian, M. N., 1979, Quasi-static transient response of a conducting half-space - An approximate representation. *Geophysics*, **44**, 1700-1705.

Nabighian, M. N., ed., 1991, *Electromagnetic Methods in Applied Geophysics*, volume 2, application, parts A and B, SEG Special Publication.

Raiche, A. P., 1984, The effect of ramp function turnoff on the TEM response of a layered ground. *Exploration Geophysics*, **15**, 37-41.

Raiche, A. P., Jupp, D. L. B., Rutter, H., Vozoff, K., 1985, The joint use of coincident loop transient electromagnetic and Schlumberger sounding to resolve layered structures. *Geophysics*, **50**, 1618-1627.

Schmidt B. L., 1990. Elura zinc-lead-silver deposit, Cobar. In: *Geology of the Mineral Deposits of Australia and Papua New Guinea*. (Ed., F. E. Hughes), 1329-1336. The Australian Institute of Mining and Metallurgy publication.

Smith, R. J., and Pridmore, D. F., 1989, Exploration in Weathered Terrains. *Exploration Geophysics*, **20**, 411-434.

Smith, R. S., and Keating, P. B., 1996, The usefulness of multicomponent, time-domain airborne electromagnetic measurements. *Geophysics*, **61**, 74-81.

Telford, W. M., Geldart, L. P., Sheriff, R. E., and Keys, D. A., 1976, *Applied Geophysics*. Cambridge University Press.

Vozoff, K., Jupp, D. L. B., 1975, Joint inversion of geophysical data. *Geophysical Journal of the Royal Astronomical Society*, **42**, 977-991.

Vozoff, K., Jupp, D. L. B., 1977, Effective search for a buried layer. *Bulletin of the Australian Society of Exploration Geophysicists*, **8**, 6-15.

Appendix 1
Brief Explanation of Electrical and Electromagnetic Techniques

Transient Electromagnetic Surveying

Electromagnetic (EM) methods are used to detect large, massive conductive bodies. EM methods are based on Faraday's law that a current is induced within a conductor when the conductor is exposed to a time varying magnetic field. The voltage induced within the conductor is proportional to the time rate of change of the magnetic field. The induced voltage is created to maintain the magnetic field that was present within the conductor before the time varying magnetic field was applied.

This is based on Lenz's law, and is best understood by visualising a small wire loop and a bar magnet. A wire loop next to a bar magnet will be sensing the magnetic field of the magnet. If the magnet is moved towards the loop, the magnetic field strength at the loop increases. The change in magnetic field strength induces a current within the loop, and the induced current has its own magnetic field. The current flowing in the loop is such that its associated magnetic field will cancel out the increase in magnetic field strength caused by moving the magnet.

Transient electromagnetic (TEM) methods work by passing a current through a wire loop on the surface. The current passing through the transmitter loop has an associated magnetic field, called the primary magnetic field. The primary magnetic field will be constant while a DC current is flowing in the loop. By rapidly reducing the loop current to zero, the primary magnetic field will also be changed, which will induce a voltage within the earth around the transmitter. Shortly after turn-off "currents will flow in the vicinity of the transmitter loop so as to maintain the magnetic field everywhere within the earth at a value that existed before the transmitter turn-off" (McNeill, 1995). This is, in essence, the same as the magnet and loop analogy earlier.

A change in the primary magnetic field will induce "eddy currents" within a nearby conductor. The eddy currents are such that their associated magnetic field, termed the secondary magnetic field, will attempt to maintain the magnetic field within the conductor before transmitter turn-off.

The eddy currents within a conductor decay over time at a rate proportional to the body's conductivity, and hence the secondary magnetic field will also vary over time. A receiver loop on the surface is used to detect time variations in the secondary magnetic field as they will induce a current within the receiver loop.

In TEM surveys the receiver loop measures the rate of decay of the secondary magnetic field. The slower the decay, the more conductive is the body or earth. The shape of the decay curve is diagnostic of the shape and conductivity of a conductor.

Resistivity Methods

In resistivity methods current is applied to the ground by a pair of current electrodes. One electrode is the source and the other is the sink. The applied current must flow through the earth between the two electrodes.

The voltage between two points on the surface is measured with a pair of potential electrodes and a voltmeter. "Deviations from the pattern of potential difference expected from homogeneous ground provide information on the form and electrical properties of subsurface inhomogeneities" (Kearey and Brooks, 1991).

Current will flow between the two current electrodes primarily along the path of least resistance. Hence if there is a conductive layer on the surface, current will flow near the surface, causing an decrease in potential difference between the two potential electrodes, and vice-versa for a resistive layer over conductive basement. The measured voltage and current can be used to determine the apparent resistance of the "circuit" using Ohm's law. The resistance is normalised by a geometric factor, indicating the relative positions of the potential and current electrodes, to yield the apparent resistivity. Two different resistivity surveys were carried out in the 1998 survey; Schlumberger vertical electric soundings and dipole-dipole resistivity.

The Schlumberger has the two current electrodes at some distance apart, and the potential electrodes very close together, directly in between the current electrodes (figure 6). As the current electrodes are spread further and further apart, the current passes through a larger volume of rock, effectively sensing down to greater depths.

The dipole-dipole array has the current dipole and the potential dipole separated by varying distances (figure 5). The further apart the two dipoles, the larger the volume of rock being sensed, and the greater the effective depth. The apparent resistivity is plotted as a pseudosection (figure 5), with the resistivity for a dipole spacing plotted at the intersection point of 45° lines between the two dipoles. The apparent resistivities plotted on a pseudo section are not the resistivities for that point, but are the bulk resistivity of the volume of rock being sensed by the two dipoles.

Induced Polarisation

Induced Polarisation (IP), in essence, measures the capacitance of the earth. When DC current is applied to the earth, current, in the form of ions, moves primarily along small conductive pathways such as through water filled pore spaces. At pore throats, these passageways become constricted, and ions cannot readily pass through, so positive ions become trapped on one side of the throat, while negative ions are trapped on the other side. Hence there exists a potential difference across the pore throat. This induced potential will slowly dissipate after current has been turned off (as with a capacitor). Polarisation also occurs across conductive grain boundaries where, ionic flow is transformed into electron flow.

Like TEM, the chargeability (similar to a normalised capacitance) is found by measuring the voltage decay after turn-off. The longer the decay, the more chargeable the ground.

Appendix 2
Summary of *GRENDL* inversion statistics

All of the statistics described here are adapted from *The use of statistical parameters as guides to an inversions merit* (notes from the MIM Exploration Ltd. TEM sounding user's meeting) and from discussions with Steve Busuttil of MIM.

Standard Error (σ)

Monitors the closeness of fit between the field and model data with respect to the inverse of the degree of freedom of the system. Standard error is a sum of the squared residual:

$$\sigma = \sqrt{\frac{1}{(n-p)} \times \sum_{i=1}^{n} (F_f - F_m)^2}$$

n = number of observations (channels)

p = number of parameters (2*layers - 1)

F_m = Modelled data

F_f = Field (observed) data

GRENDL attempts to minimise the standard error in its inversion. Note that for each extra layer that is added, the number of parameters increases by two. The squared residual will only marginally decrease when the model is made more complex, because large changes in the model only yield small changes in the calculated response. Because n > p, with increasing model complexity, larger standard errors are obtained for the same degree of fit.

Mean Percent Symmetric Error

This is calculated by first determining the Percent symmetric Error ($\%_s$) for each observed data point:

$$\%_s = \frac{F_f - F_m}{F_f + F_m} \times 200$$

The percent symmetric error is the error divided by the average of the observed and calculated values, multiplied by 100 to give a percentage. Thus, the mean percent symmetric error is:

$$\overline{\%_s} = \sqrt{\sum_{i=1}^{n} \frac{(\%_s^2)}{n}}$$

The individual percent symmetric errors should all be fairly equally distributed about zero. This would indicate a model which neither under or over estimates the observed data. This is an intuitive guide to the goodness of fit (termed the "CHI by EYE").

The mean percent symmetric error provides a representation of the amount by which the model over or under estimates the observed data. Large values of mean percent symmetric error represent an unbalanced inversion, which will require weighting of the data points.

Average Predicted Residual Error (APRE)

This is an estimate of the root mean squared predicted residual error. Simply put, the APRE is calculated in the following way:

(1) Remove one data point and invert using all of the other data points.
(2) Calculate difference between removed observation and the model calculated in (1).
(3) Do this for all n data points (perform n inversions each with n-1 observed values).
(4) Average the "predicted residual errors" calculated in (2) and (3).

GRENDL actually approximates the APRE to avoid the computing time involved in doing n inversions of n-1 data points. The APRE determines if a model is sufficiently complex. Models which have too few or too many layers will yield very large APRE values.

Confidence Limits

Note that the percent symmetric error is not affected by the number of parameters used (ie the complexity of the model). Hence it is possible to have a simple model which has a smaller standard error than a more complex model, but may have a larger percent symmetric error (ie not as good fit). A good degree of fit does not necessarily mean the model is acceptable.

The confidence limits are calculated mainly using the standard undamped singular values of the Jacobian and the standard error. The range of values within the 68% confidence range (one standard deviation of the normal distribution defined by the "ridge regression parameter") indicates how well a given parameter has been resolved. If a model has a low standard error and narrow confidence range then that parameter has been well defined.

It is very common in TEM inversions to have wide, or even unbounded confidence intervals for resistive layers. The effect of these poorly defined sections will be cumulative with depth. Hence depths to the top of deep conductive layers may be unreliable.

Appendix 3: *VES* Vertical Electric Sounding Inversion Statistics.

1500E					
No. of Layers=		3			
No. of Parameters=		5			
No. of Observations=		13		1/(n-p)=	0.125
Observed	Calculated	Residual Square	%s	%s^2	
369	388.9	396.01	-5.251	27.577	
417	367.5	2450.25	12.620	159.252	
308	308.2	0.04	-0.065	0.004	
185	192.2	51.84	-3.818	14.574	
79	87.2	67.24	-9.868	97.370	
45	38	49	16.867	284.512	
23	25.9	8.41	-11.861	140.682	
23	25.1	4.41	-8.732	76.244	
28	26.6	1.96	5.128	26.298	
36	31.3	22.09	13.967	195.086	
45	41.6	11.56	7.852	61.657	
63	66.2	10.24	-4.954	24.538	
93	102.6	92.16	-9.816	96.353	
	Sum Sq Res=	3165.21			
			Standard Error=	19.89	
			Mean %s=	9.624	

1500E					
No. of Layers=		4			
No. of Parameters=		7			
No. of Observations=		13		1/(n-p)=	0.1667
Observed	Calculated	Residual Square	%s	%s^2	
369	366.7	5.29	0.625	0.391	
417	377.8	1536.64	9.864	97.301	
308	330.2	492.84	-6.957	48.401	
185	198.9	193.21	-7.241	52.439	
79	84.2	27.04	-6.373	40.609	
45	36.4	73.96	21.130	446.486	
23	26.3	10.89	-13.387	179.223	
23	25.7	7.29	-11.088	122.950	
28	27.1	0.81	3.267	10.672	
36	31.6	19.36	13.018	169.462	
45	41.6	11.56	7.852	61.657	
63	65.7	7.29	-4.196	17.605	
93	102	81	-9.231	85.207	
	Sum Sq Res=	2467.18			
			Standard Error=	20.28	
			Mean %s=	10.124	

1500E					
No. of Layers=		5		1/(n-p)=	0.25
No. of Parameters=		9			
No. of Observations=		13			
Observed	Calculated	Residual Square	%s	%s^2	
369	389.6	424.36	-5.431	29.496	
417	370.5	2162.25	11.810	139.465	
308	311.4	11.56	-1.098	1.205	
185	191.6	43.56	-3.505	12.285	
79	85.1	37.21	-7.434	55.272	
45	37.2	60.84	18.978	360.168	
23	26.1	9.61	-12.627	159.448	
23	25.3	5.29	-9.524	90.703	
28	26.8	1.44	4.380	19.181	
36	31.5	20.25	13.333	177.778	
45	41.6	11.56	7.852	61.657	
63	66	9	-4.651	21.633	
93	102.3	86.49	-9.524	90.703	
	Sum Sq Res=	2883.42			
			Standard Error=	26.85	
			Mean %s=	9.68	

1200E					
No. of Layers=		3			
No. of Parameters=		5			
No. of Observations=		13		1/(n-p)=	0.125
Observed	Calculated	Residual Square	%s	%s^2	
270	232.3	1421.29	15.011	225.328609	
233	220.2	163.84	5.649	31.90804	
155	186	961	-18.182	330.578512	
107	117.3	106.09	-9.184	84.3482145	
53	52.8	0.04	0.378	0.14293831	
29	21.6	54.76	29.249	855.504695	
11	14.2	10.24	-25.397	644.99874	
15	15.3	0.09	-1.980	3.9211842	
23	20.5	6.25	11.494	132.117849	
29	30	1	-3.390	11.4909509	
39	44.5	30.25	-13.174	173.545125	
63	72.8	96.04	-14.433	208.311191	
141	113.5	756.25	21.611	467.035406	
	Sum Sq Res=	3607.14			
			Standard Error=	21.23	
			Mean %s=	15.61	

1200E					
No. of Layers=		4			
No. of Parameters=		7			
No. of Observations=		13		1/(n-p)=	0.16666667
Observed	Calculated	Residual Square	%s	%s^2	
270	231.4	1489.96	15.397	237.064182	
233	219	196	6.195	38.3741875	
155	184.2	852.64	-17.217	296.424439	
107	115.2	67.24	-7.381	54.4752945	
53	51.5	2.25	2.871	8.24156956	
29	21.2	60.84	31.076	965.698957	
11	14.2	10.24	-25.397	644.99874	
15	15.5	0.25	-3.279	10.7497984	
23	20.7	5.29	10.526	110.803324	
29	29.9	0.81	-3.056	9.33930203	
39	43.8	23.04	-11.594	134.425541	
63	71.4	70.56	-12.500	156.25	
141	111.4	876.16	23.455	550.129219	
	Sum Sq Res=	3655.28			
			Standard Error=	24.68	
			Mean %s=	15.73	

1200E					
No. of Layers=		3			
No. of Parameters=		5			
No. of Observations=		13		1/(n-p)=	0.125
Observed	Calculated	Residual Square	%s	%s^2	
270	243.3	712.89	10.403	108.228088	
233	228.2	23.04	2.082	4.33275237	
155	187.6	1062.76	-19.031	362.176672	
107	112.1	26.01	-4.655	21.6728282	
53	48.2	23.04	9.486	89.9873455	
29	20.8	67.24	32.932	1084.49864	
11	15.2	17.64	-32.061	1027.91213	
15	16.4	1.96	-8.917	79.5164104	
23	21.3	2.89	7.675	58.9047588	
29	29.9	0.81	-3.056	9.33930203	
39	42.7	13.69	-9.058	82.0388051	
63	68.6	31.36	-8.511	72.4309642	
141	106.7	1176.49	27.695	767.001509	
	Sum Sq Res=	3159.82			
			Standard Error=	19.87	
			Mean %s=	17.02	

Appendix 4: *GRENDL* Vertical Electric Sounding Inversion Statistics.

3 layer Schlumberger VES inversion at 1500E

THE INPUT DATA FOR THIS MODEL IS

I	AB/2	MN/2	APP.RES.
1	1.500	0.2500	369.0
2	2.500	0.2500	417.0
3	4.000	0.2500	308.0
4	6.500	0.2500	185.0
5	10.00	0.2500	79.00
6	15.00	0.2500	45.00
7	25.00	0.2500	23.00
8	40.00	0.2500	23.00
9	65.00	2.000	28.00
10	100.0	2.000	36.00
11	150.0	2.000	45.00
12	250.0	2.000	63.00

MAXIMUM ITERATIONS REACHED

```
********************************
* FINAL MODEL AFTER INVERSION *
********************************
```

Schlumberger VES inversion at 1500E

I	RESISTIVITY	THICKNESS	DEPTH
			0.0000
1	392.4	3.341	
			3.341
2	22.22	52.04	
			55.38
3	126.7		

STANDARD ERROR = 10.61 PERCENT

NOISE TO SIGNAL RATIO = 5.88 PERCENT

```
*****************************************************
* ERROR STRUCTURE OF THE FITTED MODEL FOR DC DATA *
*****************************************************
```

I	AB/2	MN/2	APPARENT RESISTIVITY DATA	APPARENT RESISTIVITY FINAL MODEL	WEIGHTED PERCENT SYMMETRIC ERROR
1	1.50	0.25	369.0	385.6	-4.4
2	2.50	0.25	417.0	365.5	13.2
3	4.00	0.25	308.0	309.4	-0.4
4	6.50	0.25	185.0	195.6	-5.6
5	10.00	0.25	79.00	89.18	-12.1
6	15.00	0.25	45.00	37.42	18.4

7	25.00	0.25	23.00	24.36	-5.7
8	40.00	0.25	23.00	24.32	-5.6
9	65.00	2.00	28.00	27.72	1.0
10	100.00	2.00	36.00	34.98	2.9
11	150.00	2.00	45.00	45.72	-1.6
12	250.00	2.00	63.00	62.90	0.2

MEAN PERCENT SYMMETRIC ERROR = 8.09
MAXIMUM PERCENT SYMMETRIC ERROR = 18.39
MAXIMUM SYMMETRIC ERROR OCCURED AT OBSERVATION 6

****
* LAYER THICKNESS PARAMETER SENSITIVITY ANALYSIS *
****

THE NUMBER OF EFFECTIVE PARAMETERS IS 4.998

****
* ERROR BOUNDS FOR LAYER THICKNESS *
****

LAYER RESISTIVITIES - 68 PERCENT CONFIDENCE INTERVAL (UNDAMPED)

LAYER	RES(I)	BOUND(1)	BOUND(2)	IMPORTANCE
1	392.4	367.7	418.6	1.00
2	22.22	20.29	24.34	1.00
3	126.7	71.09	225.9	1.00

LAYER THICKNESSES - 68 PERCENT CONFIDENCE INTERVAL (UNDAMPED)

LAYER	THK(I)	BOUND(1)	BOUND(2)	IMPORTANCE
1	3.341	3.186	3.503	1.00
2	52.04	37.78	71.67	1.00

****
* AVERAGE PREDICTED RESIDUAL ERROR (APRE) = 10.64 PERCENT *
****

4 layer Schlumberger VES inversion at 1500E

THE INPUT DATA FOR THIS MODEL IS

I	AB/2	MN/2	APP.RES.	WEIGHT
1	1.500	0.2500	369.0	0.500
2	2.500	0.2500	417.0	0.500
3	4.000	0.2500	308.0	
4	6.500	0.2500	185.0	
5	10.00	0.2500	79.00	0.500
6	15.00	0.2500	45.00	0.200
7	25.00	0.2500	23.00	
8	40.00	0.2500	23.00	
9	65.00	2.000	28.00	
10	100.0	2.000	36.00	
11	150.0	2.000	45.00	
12	250.0	2.000	63.00	
13	400.0	2.000	93.00	

CONVERGENCE ON PREDICTED DECREASE - 10 ITERATIONS

****
* FINAL MODEL AFTER INVERSION *
****

Schlumberger VES inversion at 1500E

I	RESISTIVITY	THICKNESS	DEPTH
			0.0000
1	405.3	3.171	
			3.171
2	21.53	55.56	
			58.73
3	260.1	11.88	
			70.62
4	173.5		

STANDARD ERROR = 5.45 PERCENT

NOISE TO SIGNAL RATIO = 2.99 PERCENT

****
* ERROR STRUCTURE OF THE FITTED MODEL FOR DC DATA *
****

I	AB/2	MN/2	APPARENT RESISTIVITY DATA	APPARENT RESISTIVITY FINAL MODEL	WEIGHTED PERCENT SYMMETRIC ERROR
1	1.50	0.25	369.0	397.1	-3.7
2	2.50	0.25	417.0	373.3	5.5
3	4.00	0.25	308.0	309.0	-0.3

4	6.50	0.25	185.0	186.2	-0.6
5	10.00	0.25	79.00	80.35	-0.8
6	15.00	0.25	45.00	33.78	5.7
7	25.00	0.25	23.00	23.35	-1.5
8	40.00	0.25	23.00	23.50	-2.1
9	65.00	2.00	28.00	26.94	3.9
10	100.00	2.00	36.00	34.54	4.1
11	150.00	2.00	45.00	46.44	-3.1
12	250.00	2.00	63.00	66.86	-5.9
13	400.00	2.00	93.00	89.36	4.0

MEAN PERCENT SYMMETRIC ERROR = 3.70
MAXIMUM PERCENT SYMMETRIC ERROR = 5.94
MAXIMUM SYMMETRIC ERROR OCCURED AT OBSERVATION 12

****
* LAYER THICKNESS PARAMETER SENSITIVITY ANALYSIS *
****

THE NUMBER OF EFFECTIVE PARAMETERS IS 5.000

****
* ERROR BOUNDS FOR LAYER THICKNESS *
****

LAYER RESISTIVITIES - 68 PERCENT CONFIDENCE INTERVAL (UNDAMPED)

LAYER	RES(I)	BOUND(1)	BOUND(2)	IMPORTANCE
1	405.3	383.1	428.7	1.00
2	21.53	19.97	23.22	1.00
3	262.1	UNBOUNDED		****
4	173.0	105.0	285.2	1.00

LAYER THICKNESSES - 68 PERCENT CONFIDENCE INTERVAL (UNDAMPED)

LAYER	THK(I)	BOUND(1)	BOUND(2)	IMPORTANCE
1	3.171	3.033	3.316	1.00
2	55.54	4.114	749.7	1.00
3	11.94	UNBOUNDED		****

****
* AVERAGE PREDICTED RESIDUAL ERROR (APRE) = 10.78 PERCENT *
****

5 Layer Schlumberger VES inversion at 1500E

THE INPUT DATA FOR THIS MODEL IS

I	AB/2	MN/2	APP.RES.	WEIGHT
1	1.500	0.2500	369.0	0.750
2	2.500	0.2500	417.0	0.500
3	4.000	0.2500	308.0	
4	6.500	0.2500	185.0	
5	10.00	0.2500	79.00	0.750
6	15.00	0.2500	45.00	0.750
7	25.00	0.2500	23.00	
8	40.00	0.2500	23.00	
9	65.00	2.000	28.00	
10	100.0	2.000	36.00	
11	150.0	2.000	45.00	
12	250.0	2.000	63.00	

MAXIMUM ITERATIONS REACHED

****
* FINAL MODEL AFTER INVERSION *
****

Schlumberger VES inversion at 1500E

I	RESISTIVITY	THICKNESS	DEPTH
			0.0000
1	412.0	2.789	
			2.789
2	55.47	5.218	
			8.007
3	15.92	20.85	
			28.85
4	46.92	62.10	
			90.95
5	144.3		

STANDARD ERROR = 7.57 PERCENT

NOISE TO SIGNAL RATIO = 7.05 PERCENT

****
* ERROR STRUCTURE OF THE FITTED MODEL FOR DC DATA *
****

I	AB/2	MN/2	APPARENT RESISTIVITY DATA	APPARENT RESISTIVITY FINAL MODEL	WEIGHTED PERCENT SYMMETRIC ERROR
1	1.50	0.25	369.0	401.8	-6.4
2	2.50	0.25	417.0	372.9	5.6

3	4.00	0.25	308.0	301.4	2.2
4	6.50	0.25	185.0	180.5	2.5
5	10.00	0.25	79.00	86.75	-7.0
6	15.00	0.25	45.00	42.00	5.2
7	25.00	0.25	23.00	23.65	-2.8
8	40.00	0.25	23.00	22.64	1.6
9	65.00	2.00	28.00	28.07	-0.2
10	100.00	2.00	36.00	35.74	0.7
11	150.00	2.00	45.00	45.56	-1.2
12	250.00	2.00	63.00	62.33	1.1

MEAN PERCENT SYMMETRIC ERROR = 3.79
MAXIMUM PERCENT SYMMETRIC ERROR = 7.02
MAXIMUM SYMMETRIC ERROR OCCURED AT OBSERVATION 5

****
* LAYER THICKNESS PARAMETER SENSITIVITY ANALYSIS *
****

THE NUMBER OF EFFECTIVE PARAMETERS IS 7.634

****
* ERROR BOUNDS FOR LAYER THICKNESS *
****

LAYER RESISTIVITIES - 68 PERCENT CONFIDENCE INTERVAL (UNDAMPED)

LAYER	RES(I)	BOUND(1)	BOUND(2)	IMPORTANCE
1	412.0	376.8	450.5	1.00
2	55.47	13.89	221.5	0.96
3	15.92	4.342	58.36	0.97
4	46.92	1.415	1556.	0.88
5	144.3	10.13	2055.	0.90

LAYER THICKNESSES - 68 PERCENT CONFIDENCE INTERVAL (UNDAMPED)

LAYER	THK(I)	BOUND(1)	BOUND(2)	IMPORTANCE
1	2.789	2.155	3.609	1.00
2	5.218	1.018	26.76	0.94
3	20.85	0.4420	983.3	0.77
4	62.10	0.4993	7724.	0.68

****
* AVERAGE PREDICTED RESIDUAL ERROR (APRE) = 12.01 PERCENT *
****

3 layer Schlumberger VES inversion at 1200E

THE INPUT DATA FOR THIS MODEL IS

I	AB/2	MN/2	APP.RES.	WEIGHT
1	1.500	0.3000	270.0	0.250
2	2.500	0.3000	233.0	
3	4.000	0.3000	155.0	0.250
4	6.500	0.3000	107.0	0.750
5	10.00	0.3000	53.00	0.900
6	15.00	0.3000	29.00	0.250
7	25.00	0.3000	11.00	0.250
8	40.00	0.3000	15.00	
9	65.00	1.000	23.00	0.500
10	100.0	5.000	29.00	
11	150.0	5.000	39.00	0.750
12	250.0	5.000	63.00	0.500
13	400.0	5.000	141.0	0.250

CONVERGENCE ON PREDICTED DECREASE - 4 ITERATIONS

****
* FINAL MODEL AFTER INVERSION *
****

3 layer Schlumberger VES inversion at 1200E

I	RESISTIVITY	THICKNESS	DEPTH
			0.0000
1	243.6	3.274	
			3.274
2	12.82	43.98	
			47.25
3	1024.		

STANDARD ERROR = 6.72 PERCENT

NOISE TO SIGNAL RATIO = 2.78 PERCENT

****
* ERROR STRUCTURE OF THE FITTED MODEL FOR DC DATA *
****

I	AB/2	MN/2	APPARENT RESISTIVITY DATA	APPARENT RESISTIVITY FINAL MODEL	WEIGHTED PERCENT SYMMETRIC ERROR
1	1.50	0.30	270.0	238.9	3.1
2	2.50	0.30	233.0	225.4	3.3
3	4.00	0.30	155.0	189.5	-5.0
4	6.50	0.30	107.0	117.2	-6.9
5	10.00	0.30	53.00	51.83	2.0
6	15.00	0.30	29.00	21.35	7.6

7	25.00	0.30	11.00	14.34	-6.6
8	40.00	0.30	15.00	15.24	-1.6
9	65.00	1.00	23.00	19.74	7.6
10	100.00	5.00	29.00	28.44	2.0
11	150.00	5.00	39.00	41.86	-5.3
12	250.00	5.00	63.00	68.04	-3.8
13	400.00	5.00	141.0	105.1	7.3

MEAN PERCENT SYMMETRIC ERROR = 5.25
MAXIMUM PERCENT SYMMETRIC ERROR = 7.63
MAXIMUM SYMMETRIC ERROR OCCURED AT OBSERVATION 9

****
* LAYER THICKNESS PARAMETER SENSITIVITY ANALYSIS *
****

THE NUMBER OF EFFECTIVE PARAMETERS IS 4.290

****
* ERROR BOUNDS FOR LAYER THICKNESS *
****

LAYER RESISTIVITIES - 68 PERCENT CONFIDENCE INTERVAL (UNDAMPED)

LAYER	RES(I)	BOUND(1)	BOUND(2)	IMPORTANCE
1	243.6	228.2	260.1	1.00
2	12.82	11.46	14.33	1.00
3	1024.	43.10	0.2434E+05	0.29

LAYER THICKNESSES - 68 PERCENT CONFIDENCE INTERVAL (UNDAMPED)

LAYER	THK(I)	BOUND(1)	BOUND(2)	IMPORTANCE
1	3.274	3.140	3.413	1.00
2	43.98	35.62	54.30	1.00

****
* AVERAGE PREDICTED RESIDUAL ERROR (APRE) = 6.51 PERCENT *
****

4 layer Schlumberger VES inversion at 1200E

THE INPUT DATA FOR THIS MODEL IS

I	AB/2	MN/2	APP.RES.	WEIGHT
1	1.500	0.3000	270.0	0.250
2	2.500	0.3000	233.0	
3	4.000	0.3000	155.0	0.250
4	6.500	0.3000	107.0	0.750
5	10.00	0.3000	53.00	0.900
6	15.00	0.3000	29.00	0.250
7	25.00	0.3000	11.00	0.500
8	40.00	0.3000	15.00	
9	65.00	1.000	23.00	0.500
10	100.0	5.000	29.00	
11	150.0	5.000	39.00	0.750
12	250.0	5.000	63.00	0.500
13	400.0	5.000	141.0	0.250

MAXIMUM ITERATIONS REACHED

****
* FINAL MODEL AFTER INVERSION *
****

3 layer Schlumberger VES inversion at 1200E

I	RESISTIVITY	THICKNESS	DEPTH
			0.0000
1	239.7	3.413	
			3.413
2	9.257	20.06	
			23.47
3	46.59	69.79	
			93.26
4	1088.		

STANDARD ERROR = 7.84 PERCENT

NOISE TO SIGNAL RATIO = 4.12 PERCENT

****
* ERROR STRUCTURE OF THE FITTED MODEL FOR DC DATA *
****

I	AB/2	MN/2	APPARENT RESISTIVITY DATA	APPARENT RESISTIVITY FINAL MODEL	WEIGHTED PERCENT SYMMETRIC ERROR
1	1.50	0.30	270.0	235.5	3.4
2	2.50	0.30	233.0	223.2	4.3
3	4.00	0.30	155.0	189.8	-5.0
4	6.50	0.30	107.0	119.6	-8.3

5	10.00	0.30	53.00	52.23	1.3
6	15.00	0.30	29.00	19.11	10.3
7	25.00	0.30	11.00	12.16	-5.0
8	40.00	0.30	15.00	14.96	0.2
9	65.00	1.00	23.00	20.98	4.6
10	100.00	5.00	29.00	29.07	-0.2
11	150.00	5.00	39.00	40.69	-3.2
12	250.00	5.00	63.00	64.58	-1.2
13	400.00	5.00	141.0	99.73	8.6

MEAN PERCENT SYMMETRIC ERROR = 5.29
MAXIMUM PERCENT SYMMETRIC ERROR = 10.28
MAXIMUM SYMMETRIC ERROR OCCURED AT OBSERVATION 6

****
* LAYER THICKNESS PARAMETER SENSITIVITY ANALYSIS *
****

THE NUMBER OF EFFECTIVE PARAMETERS IS 5.755

****
* ERROR BOUNDS FOR LAYER THICKNESS *
****

LAYER RESISTIVITIES - 68 PERCENT CONFIDENCE INTERVAL (UNDAMPED)

LAYER	RES(I)	BOUND(1)	BOUND(2)	IMPORTANCE
1	239.7	222.1	258.7	1.00
2	9.257	5.965	14.37	1.00
3	46.59	4.236	512.4	0.85
4	1088.	0.6795E-01	0.1743E+08	0.24

LAYER THICKNESSES - 68 PERCENT CONFIDENCE INTERVAL (UNDAMPED)

LAYER	THK(I)	BOUND(1)	BOUND(2)	IMPORTANCE
1	3.413	3.212	3.627	1.00
2	20.06	6.430	62.56	0.96
3	69.79	4.961	981.8	0.93

****
* AVERAGE PREDICTED RESIDUAL ERROR (APRE) = 8.49 PERCENT *
****

5 layer Schlumberger VES inversion at 1200E

THE INPUT DATA FOR THIS MODEL IS

I	AB/2	MN/2	APP.RES.	WEIGHT
1	1.500	0.3000	270.0	0.800
2	2.500	0.3000	233.0	
3	4.000	0.3000	155.0	0.750
4	6.500	0.3000	107.0	
5	10.00	0.3000	53.00	
6	15.00	0.3000	29.00	0.500
7	25.00	0.3000	11.00	0.300
8	40.00	0.3000	15.00	0.750
9	65.00	1.000	23.00	
10	100.0	5.000	29.00	0.900
11	150.0	5.000	39.00	
12	250.0	5.000	63.00	
13	400.0	5.000	141.0	0.800

****
* FINAL MODEL AFTER INVERSION *
****

Schlumberger VES inversion at 1200E

I	RESISTIVITY	THICKNESS	DEPTH
			0.0000
1	239.8	3.258	
			3.258
2	13.86	34.64	
			37.90
3	48.46	39.11	
			77.01
4	101.3	24.75	
			101.8
5	7521.		

STANDARD ERROR = 18.31 PERCENT

NOISE TO SIGNAL RATIO = 11.51 PERCENT

****
* ERROR STRUCTURE OF THE FITTED MODEL FOR DC DATA *
****

I	AB/2	MN/2	APPARENT RESISTIVITY DATA	APPARENT RESISTIVITY FINAL MODEL	WEIGHTED PERCENT SYMMETRIC ERROR
1	1.50	0.30	270.0	235.2	11.0
2	2.50	0.30	233.0	221.8	4.9
3	4.00	0.30	155.0	185.5	-13.4

4	6.50	0.30	107.0	115.7	-7.8
5	10.00	0.30	53.00	51.91	2.1
6	15.00	0.30	29.00	22.32	13.0
7	25.00	0.30	11.00	15.54	-10.3
8	40.00	0.30	15.00	16.61	-7.6
9	65.00	1.00	23.00	21.17	8.3
10	100.00	5.00	29.00	29.36	-1.1
11	150.00	5.00	39.00	42.30	-8.1
12	250.00	5.00	63.00	69.50	-9.8
13	400.00	5.00	141.0	110.5	19.4

MEAN PERCENT SYMMETRIC ERROR = 10.12
MAXIMUM PERCENT SYMMETRIC ERROR = 19.37
MAXIMUM SYMMETRIC ERROR OCCURED AT OBSERVATION 13

****
* LAYER THICKNESS PARAMETER SENSITIVITY ANALYSIS *
****

THE NUMBER OF EFFECTIVE PARAMETERS IS 4.996

****
* ERROR BOUNDS FOR LAYER THICKNESS *
****

LAYER RESISTIVITIES - 68 PERCENT CONFIDENCE INTERVAL (UNDAMPED)

LAYER	RES(I)	BOUND(1)	BOUND(2)	IMPORTANCE
1	239.8	209.4	274.6	1.00
2	13.86	6.819	28.17	1.00
3	48.46	UNBOUNDED		****
4	101.3	UNBOUNDED		****
5	7521.	UNBOUNDED		****

LAYER THICKNESSES - 68 PERCENT CONFIDENCE INTERVAL (UNDAMPED)

LAYER	THK(I)	BOUND(1)	BOUND(2)	IMPORTANCE
1	3.258	2.843	3.734	1.00
2	34.64	0.1154E-03	0.1040E+08	0.96
3	39.11	UNBOUNDED		****
4	24.75	UNBOUNDED		****

****
* AVERAGE PREDICTED RESIDUAL ERROR (APRE) = 40.80 PERCENT *
****